CORA Cork Open Research Archive
Cartlann Taighde Oscailte Chorcaí

Title	The study of a drug coating applied using a cold atmospheric plasma: everolimus coating properties
Authors	Frewen, Chloe
Publication date	2025
Original Citation	Frewen, C. 2025. The study of a drug coating applied using a cold atmospheric plasma: everolimus coating properties. MRes Thesis, University College Cork.
Type of publication	Masters thesis (Research)
Rights	© 2025, Chloe Frewen. - https://creativecommons.org/licenses/by-nc-nd/4.0/
Download date	2026-11-08 03:09:43
Item downloaded from	https://hdl.handle.net/10468/17940

UCC
University College Cork, Ireland
Coláiste na hOllscoile Corcaigh

Ollscoil na hÉireann, Corcaigh

National University of Ireland, Cork



The study of a drug coating applied using a Cold Atmospheric Plasma: Everolimus Coating Properties.

Thesis presented by

Chloe Frewen, BSc (Hons) Bioanalysis & Biotechnology

[https://orcid.org/0009-0004-5175-6892]

for the degree of

MASTER OF SCIENCE

University College Cork

School of Pharmacy

Head of School/Department: Professor Brendan Griffin

Supervisor(s): Professor Abina Crean, Dr. Katie Ryan and Dr. Liam O' Neill.

2025

Table of Contents

List of Tables v
List of Figures vii
Declaration xi
Acknowledgements xii
Abstract xiii
Research dissemination. xv
1 Literature Review 1
1.1 Introduction 1
1.2 Vacuum Plasma 4
1.3 Atmospheric plasma 6
1.3.1 Corona discharge 6
1.3.2 Dielectric barrier discharge (DBD) 7
1.3.3 Cold atmospheric plasma (CAP) 9
1.3.3.1 Cold Atmospheric Plasma (CAP) systems. 9
1.4 Plasma Applications 12
1.4.1. Deposition of Coatings using Plasma 15
1.4.2. Biodep™ system 17
1.5 Endovascular implants and their coatings 19
1.5.1 Cardiac implants 19
1.5.2 Anti-proliferative drugs as an endovascular device coating 22
1.5.3 Everolimus 24
1.6 Antioxidant used in pharmaceutical formulations- Butylated hydroxytoluene (BHT) 27
2. Thesis aim and objectives 29
3. Materials and Methods 30
3.1 Materials 30
3.2 Methods 31
3.2.1 Plasma deposition of everolimus 31
3.2.2 Characterisation of everolimus coating 35
3.2.2.1 Confocal and polarised white light imaging. 35
3.2.2.2 Water contact angle (WCA) 36
3.2.2.3 Fourier-transform infrared (FTIR) spectroscopy. 37
3.2.2.4 Raman spectroscopy. 37
3.2.2.5 Deep Ultraviolet (DUV). 38
3.2.2.6 Atomic force microscopy (AFM). 38

3.2.3 Quantification of everolimus recovered from titanium discs coated using 'Study 1' parameters. 39
3.2.4 Quantification of everolimus recovered from titanium discs coated using 'Study 2' parameters. 40
3.2.5 RP-HPLC methodology to detect and quantify everolimus using HPLC Method 1 and 2. 41
3.2.6 RP-HPLC method validation 42
3.2.7 Statistical analysis 43
3.2.7.1 One-way-ANOVA (significance level, α = 0.05) 43
3.2.7.2 Two-way-ANOVA (significance level, α = 0.05) 44
3.2.7.3 Paired t-test 44
3.2.7.4 Tukey post-hoc analysis 44
4 Results 46
4.1 Characterisation of everolimus coated titanium discs 46
4.1.1 Images acquired using polarised white light and confocal imaging 46
4.1.2 Water Contact angle (WCA) 47
4.1.3 Fourier-transform infrared (FTIR) spectroscopy 48
4.1.4 Raman spectroscopy analysis of coated samples 51
4.1.5 Deep Ultra-Violet mapping 52
4.1.6 Atomic force microscopy (AFM) 55
4.2 Coating Study 1: evaluating everolimus coated samples using HPLC Method 1. 56
4.2.1 (Method 1) Establishment of a RP- HPLC method for everolimus detection and quantification. 56
4.2.2 (Method 1) Quantification of everolimus deposited on coated discs. 58
4.3 Coating Study 2: evaluating everolimus coated samples using HPLC Method 2. 61
4.3.1 (Method 2) Establishment of a RP- HPLC method for everolimus detection, and quantification. 61
4.3.2 (Method 2) Quantification of everolimus mass eluted from wet coated discs (0 V) and plasma coated discs (90 V) 64
4.3.3 (Method 2) Analysis of everolimus degradation (tautomer peak ratio) eluted from wet coated discs (0 V) and plasma coated discs (90 V). 66
5 Discussion 70
6 Conclusions 76
7 Learning outcomes 77
8 References 79
9 Supplementary information. 88
9.1 Supplementary tables 88
9.1.1 HPLC Method 1: Inter- day and intra- day precision results. 88

9.1.2 HPLC Method 2 results. 89
9.1.3 Statistical analysis 90
9.2 Extended data and results 94
9.2.1 Quantum cascade laser analysis (QCL) 94
9.2.2 HPLC Method 2- Representative chromatograms for everolimus standards- study two. 95
9.2.3 HPLC Method 2- Representative chromatograms for everolimus coated samples- study two. 98

List of Tables

Table 1: Plasma coating methods discussed through literature, and their main features and uses. 3
Table 2: Traditional coating methods discussed through literature, and their main features and uses..... 4
Table 3: Key differences between CVD and PVD (58). 16
Table 4: Examples of drug eluting stents (DES), their manufacturers and coating methods. 23
Table 5: Key differences between sirolimus and everolimus in terms of half-life, potency, and uses (91). 25
Table 6: Details of materials, grade, and suppliers. 30
Table 7: Plasma deposition parameters employed in studies 1 and 2 to coat titanium discs with everolimus. 34
Table 8: Everolimus deposition calculations- Study 1 and Study 2. 35
Table 9: Summary of Raman acquisition parameters used to analyse everolimus-coated titanium discs.....38
Table 10: RP-HPLC parameters used to analyse everolimus samples in both Study 1 and Study 2. 42
Table 11: Tukey's test critical values for post-hoc analysis of WCA , and RP-HPLC results (k= number of groups in the analysis, df= degrees of freedom). 45
Table 12: Mean water contact angle (WCA) results for everolimus coated, everolimus/BHT coated and a blank titanium disc. Data represents mean ± standard deviation, n=5. 47
Table 13: Atomic force microscopy results of a blank titanium disc, everolimus coated disc without plasma (0 V) and with plasma (90 V). Data is expressed in nm and represents +/- standard deviation, n= 3. 56
Table 14: LOD calculation for HPLC method 1. 57
Table 15: LOQ calculation for HPLC method 1. 58
Table 16: Quantification of the average found concentration of everolimus (µg/disc) ± standard deviation of samples deposited with no plasma (0V), or with plasma at 90 V. The inclusion of BHT at 5% and 10% w/w was also investigated, n=3. 59
Table 17: LOD calculation for HPLC method 2. 62
Table 18: LOQ calculation for HPLC method 2. 63
Table 19: The improvement in LOD and LOQ in HPLC Method 2 in comparison to HPLC Method 1. 63
Table 20: Average everolimus mass (µg/ disc) ± standard deviation eluted from discs which were coated with everolimus and various levels of BHT (0%, 5%, 10%), via wet deposition (0 V) and plasma deposition (90 V) (n=3). 64
Table 21: Average percentage everolimus tautomer peak ± standard deviation, present in various everolimus samples and standards (500 µg/mL). 67
Table 22: HPLC Method 1-Inter-day precision (n=3) for method validation of the RP- HPLC used in study one, before issues arose with retention time. 88
Table 23: HPLC Method 1-Intra-day precision (n=3) for method validation of the RP- HPLC used in study one, before issues arose with retention time. 88
Table 24: RP-HPLC analysis of everolimus standards for the construction of a calibration curve 89
Table 25: Linear regression analysis, calculation of estimated concentrations, standard deviation, RSD and percent accuracy. 89
Table 26: One-way ANOVA test carried out on AFM surface roughness of blank titanium discs, everolimus coated discs without plasma (0V) and with plasma (90V) with a significance level of 0.05- study one. 90

Table 27: Two- way- ANOVA analysis of WCA results to assess the effect of deposition type, and use of BHT on WCA results of everolimus coated discs- study one. 90
Table 28: Two- way ANOVA carried out to analyse the effect of deposition type and use of BHT on average everolimus concentration found (µg/ disc)- study one. 90
Table 29: Tukey statistical test; Everolimus concentration recovered from samples coated by wet deposition (0 V), plasma deposition (90 V) and with various concentrations of BHT (0%, 5% 10%). Tukey critical value = 4.75 (k=6, df=12). 91
Table 30: Two- way ANOVA carried out to analyse the effect of deposition type and use of BHT on average everolimus concentration found (µg/ disc)- study two. 91
Table 31: One- way- ANOVA carried out to analyse the effect of degradation on the average percent tautomer peak (%) of an everolimus standard (500 µg/ mL)- study two. 91
Table 32: Two- way ANOVA carried out to analyse the effect of deposition type and use of BHT on average percent tautomer peak of everolimus samples (%)- study two. 92
Table 33: Tukey statistical test: Everolimus mass (µg/ disc) recovered from samples coated by wet deposition (0 V), plasma deposition (90 V) and with various concentrations of BHT (0%, 5% 10%). Tukey critical value = 4.75 (k=6, df=12), Table 29. 92
Table 34: One-way- ANOVA test carried out on the everolimus standard (1 mg/ mL) and degraded everolimus standard (1 mg/ mL) analysing average peak tautomer- study two. 93
Table 35: Tukey statistical test; Everolimus tautomer peak detected from samples coated by wet deposition (0 V), plasma deposition (90 V) and with various concentrations of BHT (0%, 5% 10%). Tukey critical value = 4.75 (k=6, df=12). 93

List of Figures

Figure 1: Three fundamental phases of matter, solid, liquid, and gas (vapour), along with the fourth state of matter, plasma (2). 1
Figure 2: Schematic of a typical vacuum plasma system (21). 5
Figure 3: Two examples of a low pressure plasma system, (l-r) small scale vacuum plasma and large scale vacuum chamber (23). 6
Figure 4: Schematic of a corona discharge illustrating the ionisation and drift region (26). 7
Figure 5: Dielectric Barrier Discharge (DBD) (31). 8
Figure 6: Schematic of a floating electrode dielectric barrier discharge (FE-DBD) reactor in protective housing (35). 10
Figure 7: Schematic of iontophoresis using acetylcholine (38). 11
Figure 8: Relationship between surface energy and surface tension in terms of wettability (50). 13
Figure 9: Examples of water droplet forming on surfaces with various surface energies (51). 14
Figure 10: Schematic of the sputtering process (56). 15
Figure 11: Schematic of chemical vapor deposition (CVD) (59). 17
Figure 12: Schematic of TheraDep Ltd.'s BioDep™ system using a computer numerically controlled (CNC) controller, illustration provided by Denis O' Sullivan (TheraDep Ltd). 18
Figure 13: Schematic of the plasma head in the BioDep™ system, provided by TheraDep Ltd. 18
Figure 14: An image of a drug eluting stent- XIENCE V everolimus- eluting coronary stent system used for the treatment of coronary artery disease (CAD) (67). 20
Figure 15: A schematic of a balloon angioplasty (69). 20
Figure 16: Schematics of various types of coating methods, A) Dip coating B) Electro-static spray coating C) Spray coating (88). 24
Figure 17: Chemical structures of everolimus isomers (95). 26
Figure 18: Chemical structure of everolimus and sirolimus, and their differing structure at position 40 (96). 27
Figure 19: Schematic representation of butylated hydroxytoluene (BHT) used to stabilise everolimus (98). 28
Figure 20:Schematic of the BioDep™ system used for the deposition of the everolimus coating (schematic designed by Denis O'Sullivan, Engineer at TheraDep Ltd). 31
Figure 21: An image of the syringe pump used in the BioDep™ plasma system, located in TheraDep Ltd, Clonmel, Ireland. 32
Figure 22: Image of the Biodep™ plasma deposition system located in TheraDep Ltd, Clonmel, Ireland. The white cable bringing the high-voltage power supply to the Teflon plasma head which contains two electrodes. The nebuliser is placed into this Teflon head and everolimus is deposited onto the titanium discs below. Pictured is during plasma deposition, as seen by two plasma jets (104). 33
Figure 23: KRUSS TVA 100 instrument in TheraDep Ltd, Clonmel, Tipperary, used for WCA analysis of the everolimus coated titanium discs. 36
Figure 24: Two titanium discs coated with each specific coating were placed into each well with 1 ml acetonitrile for elution of coating. Discs were coated with (i) everolimus (0% BHT), (ii) everolimus with 5% BHT (iii) everolimus with 10% BHT, through both wet chemical (0 V) and plasma deposition (90 V). 39
Figure 25: Polarised white light imaging results of (A) wet deposited everolimus (0 V), (B) plasma deposited everolimus (90 V), and (C) blank titanium disc. Red arrows in A and B indicates the presence of a ring. Scale bar indicates 50 μm in images A-C. 46

Figure 26:Confocal imaging of everolimus coated discs (A) wet deposit no plasma (B) plasma deposit (90 V). 47
Figure 27: Tukey Post- hoc analysis for water contact angle (WCA) with all groups surpassing the critical value, (* representing SSD. 48
Figure 28: Reference FTIR spectrum for analysis of everolimus reprinted from: (70).....48
Figure 29: Reference FTIR spectrum for analysis of BHT reprinted from:(113). 49
Figure 30: Representative FTIR spectra of everolimus deposited on NaCl discs. (Top) a wet deposit (0 V) and (Bottom) plasma deposited (90 V). Three independent replicates were analysed for each sample type. 50
Figure 31: Representative FTIR analysis of everolimus coating incorporating BHT, deposited on titanium using (Top) wet (0 V) and (Bottom) plasma (90 V) deposition. Three independent replicates were analysed for each sample type. 50
Figure 32: Raman spectrum of everolimus powder and coatings deposited by plasma and wet chemical process. 51
Figure 33: Magnified Raman spectrum (1000-1800 cm^{-1}) highlighting the areas containing peaks derived from (i) pure everolimus powder (ii) everolimus deposited by plasma (90 V) (iii) everolimus deposited via wet chemical process (0 V). 52
Figure 34: DUV map of everolimus coating deposited via plasma deposition (90 V) onto a titanium disc, green indicates presence of drug while red indicates no drug present (500 points of 100 µm measured)....53
Figure 35: DUV map of everolimus coating deposited via wet deposition (no plasma, 0 V) onto a titanium disc, green indicates presence of drug while red indicates no drug present (500 points of 100 µm measured)....54
Figure 36: Average DUV map comparisons (500 points of 100 µm spot size measured and averaged) between everolimus deposition using wet (0 V) and plasma deposition (90 V).....55
Figure 37: AFM scans of (A) wet deposited everolimus on a titanium disc and (B) plasma deposited (90 V) everolimus on a titanium disc. 56
Figure 38: Representative chromatogram for 1 mg/ mL everolimus standard run using the RP-HPPLC method for study 1, (Method 1). Elution of everolimus at 7.4 minutes.....57
Figure 39: Linear regression of HPLC peak area of everolimus standards against concentration over the range 5- 250 µg/mL. 58
Figure 40: Average everolimus mass eluted (µg/disc) ± standard deviation, deposited on samples coated by (i) wet deposition (0V) (ii) plasma deposition (90 V) and (iii) with the addition of 5% or 10% BHT. The theoretical everolimus mass per disc is represented by the red line (20 µg/disc). 59
Figure 41: Representative everolimus standard (500 µg/ mL) chromatogram, peak eluting at 12.2 minutes using HPLC Method 2. 61
Figure 42: Thermally degraded everolimus (500 µg/mL) with everolimus peak eluting at 12.5 minutes similar to everolimus standard which did not undergo thermal degradation. 62
Figure 43:HPLC Method 2 linear regression of everolimus standards in the range 5-500 µg/ mL used for analysis of samples in Study 2. Data represents the average peak area (mAU) and standard deviation of each standard, n=3. Note: the error bars are so small they are not visible. 63
Figure 44: Average everolimus mass eluted (µg/ disc) ± standard deviation, samples coated by (i) wet deposition (0V) (ii) plasma deposition (90 V) and (iii) with the addition of 5% or 10% BHT. The theoretical mass per disc is represented by the red line (105 µg/ disc).....66
Figure 45: Average everolimus (20 mg/mL) tautomer peak percent ± standard deviation, present in various eluted samples coated by (i) wet deposition (0V) (ii) plasma deposition (90 V) and (iii) with the addition of 5% or 10% BHT. A 500 µg/mL degraded everolimus control is also

present, while the average tautomer peak percent in an everolimus standard (500 µg/mL) is represented by the red line.....68
Figure 46: Flow-chart summarising the experimental methodology of this research. 71
Figure 47: QCL Spectral response of everolimus wet deposited (0 V) and Everolimus plasma deposited (90 V).....94
Figure 48: QCL image of everolimus deposited by (A) plasma 90 V and (B) wet deposition 0 V. 95
Figure 49: Representative chromatogram for the 500 µg/ mL everolimus standard run at the end of sequence to confirm retention time had not shifted, and also for comparison to 'degraded' everolimus. 95
Figure 50: Representative chromatogram for the 250 µg/ mL everolimus standard run at the end of sequence to confirm retention time had not shifted. 96
Figure 51: Representative chromatogram for the 100 µg/ mL everolimus standard run at the end of sequence to confirm retention time had not shifted. 96
Figure 52: Representative chromatogram for the 50 µg/ mL everolimus standard run at the end of sequence to confirm retention time had not shifted. 97
Figure 53: Representative chromatogram for the 25 µg/ mL everolimus standard run at the end of sequence to confirm retention time had not shifted. 97
Figure 54: Representative chromatogram for the 10 µg/ mL everolimus standard run at the end of sequence to confirm retention time had not shifted. 98
Figure 55: Representative chromatogram for the 5 µg/ mL everolimus standard run at the end of sequence to confirm retention time had not shifted. 98
Figure 56: Representative chromatogram for everolimus 0V coated sample, eluted after 2 hr in acetonitrile. Note, peak at 7 minutes was determined to be contamination due to polystyrene and acetonitrile interaction.....99
Figure 57: Representative chromatogram for everolimus 90 V coated sample, eluted after 2 hr in acetonitrile. Note, peak at 7 minutes was determined to be contamination due to polystyrene and acetonitrile interaction.....99
Figure 58: Representative chromatogram for everolimus 0 V + 5% BHT coated sample, eluted after 2 hr in acetonitrile. Note, peak at 7 minutes was determined to be contamination due to polystyrene and acetonitrile interaction.....100
Figure 59: Representative chromatogram for everolimus 90 V + 5% BHT coated sample, eluted after 2 hr in acetonitrile. Note, peak at 7 minutes was determined to be contamination due to polystyrene and acetonitrile interaction.....100
Figure 60: Representative chromatogram for everolimus 0 V + 10% BHT coated sample, eluted after 2 hr in acetonitrile. Note, peak at 7 minutes was determined to be contamination due to polystyrene and acetonitrile interaction.....101
Figure 61: Representative chromatogram for everolimus 90 V + 10% BHT coated sample, eluted after 2 hr in acetonitrile. Note, peak at 7 minutes was determined to be contamination due to polystyrene and acetonitrile interaction.....101
Figure 62: Representative chromatogram for acetonitrile left in a 6- -well plate. Note, peak at 7 minutes which was also observed in all coated samples which were eluted at 2 hours in a 6-well plate.....102
Figure 63: Representative chromatogram for acetonitrile left in a 6-well plate with a blank/ uncoated titanium disc. Note, peak at 7 minutes which was also observed in all coated samples which were eluted at 2 hours in a 6-well plate. It was confirmed that all coated samples eluted at 2 hours in 6- well plates had contamination form the interaction between the polystyrene plate and acetonitrile.....102

Figure 64: Representative chromatogram for everolimus coated disc, deposited with no plasma (0V). 103
Figure 65: Representative chromatogram for everolimus coated disc, deposited with no plasma (90V). 103
Figure 66: Representative chromatogram for everolimus coated disc with 5% BHT present, deposited with no plasma (0V). 104
Figure 67: Representative chromatogram for everolimus coated disc with 5% BHT present, deposited with no plasma (90V). 104
Figure 68: Representative chromatogram for everolimus coated disc with 10% BHT present, deposited with no plasma (0V). 105
Figure 69: Representative chromatogram for everolimus coated disc with 10% BHT present, deposited with no plasma (90V). 105

Declaration

This is to certify that the work I am submitting is my own and has not been submitted for another degree, either at University College Cork or elsewhere. All external references and sources are clearly acknowledged and identified within the contents. I have read and understood the regulations of University College Cork concerning plagiarism and intellectual property

The following work was conducted by Dr. Krishnakumar Chullipalliyalil, a researcher in the Centre for Advanced Photonics and Process Analysis (CAPPA) in Munster Technological University (MTU) Cork, and was subsequently interpreted by me:

- Confocal imaging,
- Polarised white light imaging,
- Raman spectroscopy, and,
- Deep ultraviolet (DUV) mapping.

Acknowledgements

I would like to express my sincere gratitude to all those who have supported me throughout the course of my research. First and foremost, I am deeply grateful to my employment manager and supervisor, Liam O' Neill, whose scientific insights and guidance were the foundation of this research. I would also like to thank Fiona O' Neill, our lab manager, for her unwavering support and assistance in the laboratory. My appreciation extends to my supervisors at University College Cork, Professor Abina Crean and Dr. Katie Ryan, for their invaluable advice, encouragement and support throughout my studies. I would also like to express my sincere gratitude to Dr. Krishnakumar Chullipalliyalil from the CAPPA centre MTU, for his invaluable assistance and expertise in conducting imaging and spectroscopy for my research. I am also thankful for the financial support provided by the Science Foundation Ireland (SFI) and the Synthesis and Solid State Pharmaceutical Centre (SSPC), without which this research would not have been possible.. I am deeply grateful to my family for their love, patience, and steady presence throughout this time. My grandparents, Marie, T.P, Noreen and Gerry, whom despite not fully understanding the specifics of my research, were always checking in and asking how I was doing. Their genuine concern and constant support have been a comforting presence throughout this journey. I want to thank my partner Andrew, for his constant encouragement and motivation, even on the toughest days, and for patiently listening to my endless rants about my thesis. I would also like to express my heartfelt thanks to my parents, Pat and Samantha, for their continued support, their listening ear during challenging times, and their unwavering encouragement. Their belief in me has been a source of strength and motivation throughout this journey. They should be immensely proud of the incredible parents they are and the values they have instilled in me.

Abstract

Coating medical devices with active pharmaceutical ingredients (APIs) such as everolimus is commonly used for therapeutic purposes such as reducing inflammatory responses and preventing restenosis in cardiovascular stents. Traditional coating methods like dipping and spraying require lengthy drying and curing steps, which may expose the API to heat and poses a risk of degradation. Cold atmospheric plasma (CAP) systems, which operate at low temperatures, offer a promising alternative by reducing thermal damage during deposition. The BioDep^{TM} unit, a custom-built CAP system developed by TheraDep Ltd has been used for depositing various biologics and therapeutics on different substrates.

In this study, the Biodep^{TM} system was used to deposit everolimus onto titanium discs. The deposition of everolimus through the Biodep^{TM} unit, with and without plasma and also the addition of butylated hydroxytoluene (BHT) was investigated. Everolimus is an anti-proliferative drug commonly used in drug-eluting stents. The coatings were characterised using a variety of analytical techniques, including water contact angle (WCA) analysis, Fourier-transform infrared (FTIR) spectroscopy, Raman spectroscopy, deep ultraviolet (DUV) mapping, and atomic force microscopy (AFM). A reverse-phase high performance liquid chromatography- ultra violet (HPLC/UV) method was developed to quantify the drug deposition and analyse the stability after deposition.

Imaging of the coated samples revealed the presence of everolimus rings attributed to the drying of the drug on the surface but no significant morphological changes. WCA analysis indicated a change in surface tension, indicating deposition of everolimus. Raman and FTIR spectroscopy confirmed the presence of everolimus, with lower peak intensities suggesting a low concentration was deposited. The addition of BHT during wet

deposition introduced a new FTIR peak, which was absent from the plasma deposited samples, potentially due to BHT oxidation. DUV mapping demonstrated non-uniform coverage of everolimus, while AFM revealed no significant differences in surface roughness between plasma and wet deposition methods. The HPLC/UV method showed no degradation of everolimus after deposition, however drug recovery was variable ranging from 36.9- 67.1 µg/ disc.

This study successfully demonstrated the use of CAP to deposit everolimus onto titanium discs, with no degradation of everolimus observed. Although the deposition was effective, further optimisation of the coating and elution processes is necessary to achieve more consistent drug loading and recovery. The findings suggest that the use of the CAP system for deposition holds promise for application in drug-eluting stent coatings.

Research dissemination.

A short oral presentation titled "*Investigation of the properties and performance of drug coatings applied using a novel plasma deposition process, known as Cold Atmospheric Plasma (CAP)*" presented at the SSPC Medicines and Materials meeting in University of Limerick on 7th June 2023.

A research poster titled "*Investigation of the properties and performance of drug coatings applied using a novel plasma deposition process, known as Cold Atmospheric Plasma (CAP)*" was presented in University of Limerick during the annual SSPC, SFI Research Centre for Pharmaceuticals symposium on 30th August 2023.

1 Literature Review

The following literature review introduces the plasma state of matter, with a focus on cold atmospheric plasma (CAP) and the BioDep™ CAP deposition system employed in this study. A background into the application of anti-proliferative drugs in drug eluting stents is provided. The pharmacological and chemical properties of everolimus, the anti-proliferative drug investigated in this study, are presented.

1.1 Introduction

Plasma is commonly understood as the liquid component of blood. However, it also refers to the 4th state of matter (Figure 1). In 1929, Irvin Langmuir applied the word 'plasma' for the first time to describe "a glowing ionised gas produced by electric discharge in a tube" (1). Depending on the "random kinetic energy" of the atoms or molecules in an object, it is determined to be found in one of the phases outlined in Figure 1.

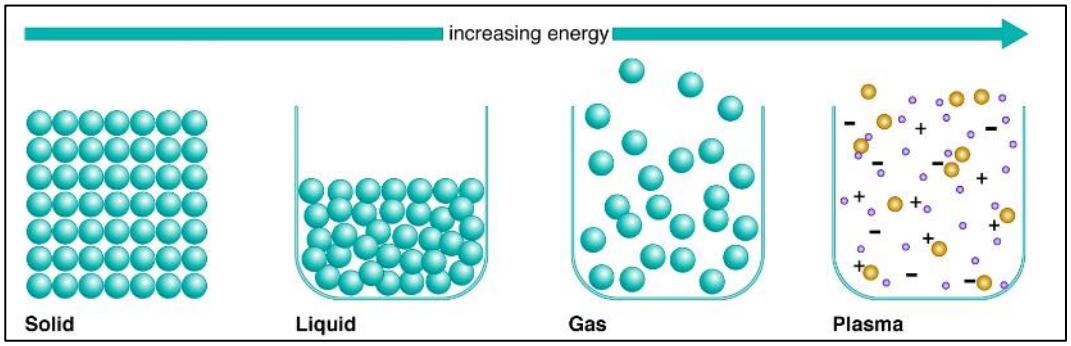


Figure 1: Three fundamental phases of matter, solid, liquid, and gas (vapour), along with the fourth state of matter, plasma (2).

Molecules become more energetic as temperature increases and transform matter in a sequence from solid to plasma (3). The equilibrium between the thermal energy of the particles and the "interparticle binding forces" determines the state of the object (1).

Atoms and molecules gain more thermal kinetic energy as they are heated, which enables them to overcome the “binding potential energy”, which can result in phase transitions. These phase transitions occur at a constant temperature for a specific pressure (1). Plasma or ‘ionised gas’ is a result of these phase transitions when a molecular gas dissociates into an atomic gas at elevated temperatures (1). When plasma is generated in a strong electric field, the ionised gas produced contains reactive species such as ions, and, electrons (4,5). To make plasma, energy is required to remove electrons from atoms, which can come from a variety of sources such as heat, light (ultraviolet or visible light from a laser source), electrical, radio frequency, high voltage, microwave frequencies, and atmospheric pressure (6).

Traditionally, plasma has been thought to be a harmful process due to the heat produced as a result of the high energy electrons colliding (1). However, the development of cold plasma at atmospheric pressure has paved the way for new applications, which are discussed in section 1.4 (Plasma applications).

The classification of plasma can depend on the pressure and temperature of the plasma (7). The pressure relates to the pressure of the gas being ionised, atmospheric or vacuum. Vacuum pressure is less than the surrounding atmospheric pressure, by definition, it is a negative pressure (8). Paschen’s Law is very important for vacuum plasma, as the lower the pressure is, the less voltage is needed for plasma production (9). The temperature relates to the final temperature of the gas, which can be thermal or non-thermal (cold).

Table 1 and

Table *2* provide a summary of the various plasma-based and traditional coating methods reported in the literature, highlighting their key features and applications.

Table 1: Plasma coating methods discussed through literature, and their main features and uses.

Plasma- based coating	**Description**	**Features**	**Applications**
Plasma enhanced CVD (PECVD)(10)	Plasma activated precursor gases resulting in film deposition at lower temps	• Non thermal plasma • Requires vacuum • Lower temperatures required	Used to coat temperature sensitive substrates
Dielectric Barrier Discharge (11,12)	Plasma generated between electrodes, which are separated by a dielectric barrier at atmospheric pressure	• Cold plasma • Atmospheric plasma • High concentration of reactive species	Used for surface modification, sterilisation, plasma polymerisation
Floating Electrode DBD (FEDBD) (11)	Uses target substrate as counter electrode to generate plasma at atmospheric pressure	• Cold plasma • Atmospheric pressure, • High concentration of reactive species • Requires consistent electrode distance	Used for surface treatment of irregular shapes, biomedical surfaces
Sputtering (13)	Ions bombarded of atoms which deposits onto substrate under vacuum	• Thin uniform coatings • Requires vacuum • Good adhesion • Controllable thickness	Used in semiconductor industry

Table 2: Traditional coating methods discussed through literature, and their main features and uses.

Traditional Coating	Description	Features	Applications
Dipping (14)	Substrate is immersed in drug/polymer and withdrawn	• Simple • Inexpensive • Can result in non-uniform coatings • Requires curing	Used for drug eluting stents (DES) such as Cypher™
Spraying (15)	Drug/polymer mixture is sprayed onto substrate in thin layers	• Can control coating thickness • Requires curing • Multiple layers possible • Uniform coatings	Used for DES and balloons such as Taxus™ and Endeavor™
Electrostatic spray (16)	Drug/polymer solution is charged electro-statically, which enhances attraction to substrate	• Has improved adhesion • Good uniformity • Controlled drug release • Requires curing	Used for DES such as Xience™
Physical vapour deposition (PVD) (17)	Vaporisation of solid/liquid to condense a thin solid film under vacuum	• Very thin uniform layers • Requires vacuum • Multiple layers needed	Used for semiconductor coatings
Chemical Vapour deposition (CVD) (18)	Gas phase chemicals deposit solid films through chemical reactions at elevated temperatures	• Corrosion resistant coatings • Requires high temperatures • Vacuum required	Used for mechanical part coatings

1.2 Vacuum Plasma

Vacuum plasma can also be referred to as “under pressure”, which is plasma generated at a pressure lower than atmospheric pressure. Absolute vacuum is 0 mbar. If the pressure has been indicated as a relative pressure, then the absolute vacuum is -1013 mbar and the atmospheric pressure is 0 mbar (19). The process by which vacuum plasma works involves a gas being ionised in a vacuum chamber, which forms a plasma (20).

There are two main reasons why plasma is created in a vacuum. Firstly, the gas introduced into the chamber will not ionise under pressure, therefore the vacuum must be introduced before the gas can ionise and as a result form plasma. Secondly, the gases present in the chamber can be controlled effectively under vacuum (20). The control of the gases introduced into the chamber plays a crucial part in the plasma process.

A schematic of the typical vacuum plasma system can be seen in Figure 2. Since the 1970s, plasmas such as oxygen and argon have been used to clean surfaces of organic impurities and contaminants as well as activate surfaces (20), which is discussed further in 1.4 (Plasma applications).

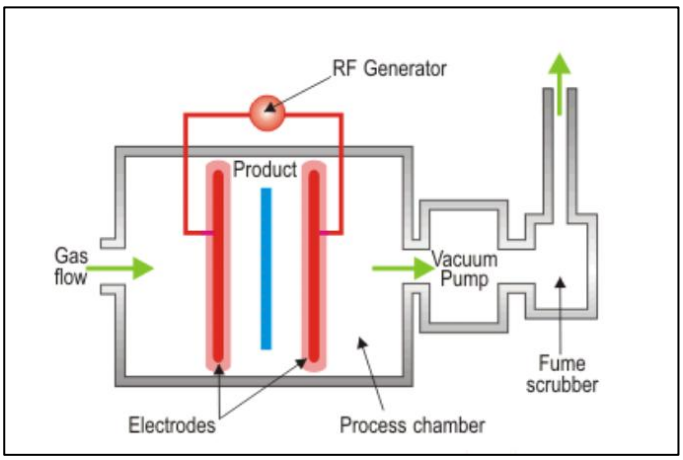


Figure 2: Schematic of a typical vacuum plasma system (21).

Low pressure plasmas have several disadvantages including issues with scaling and the need to ensure the materials being processed can withstand vacuum pressure. Scaling can be difficult when it comes to low pressure plasmas as the chamber needs to be very large as seen in Figure 3. Compared to atmospheric plasmas, low pressure plasmas are not as efficient in continuous mode. (22).



Figure 3: Two examples of a low pressure plasma system, (l-r) small scale vacuum plasma and large scale vacuum chamber (23).

1.3 Atmospheric plasma

Atmospheric plasmas have become an area of huge interest for a range of technologies such as deposition and surface treatment. A contributing factor to this is the avoidance of the huge costs associated with vacuum based plasma systems (24).

1.3.1 Corona discharge

Corona discharges are generated around atmospheric pressure with relatively low power electrical discharge (25). A corona discharge is produced when air or gas is exposed to ionisation inside a region of space which is exposed to high electric fields, caused by electrodes (26). A corona discharge is produced by strong electric fields. Corona discharge appears as a "faint filamentary discharge" which is emitted from the discharge electrode, this is depicted in the schematic in Figure 4 (26).

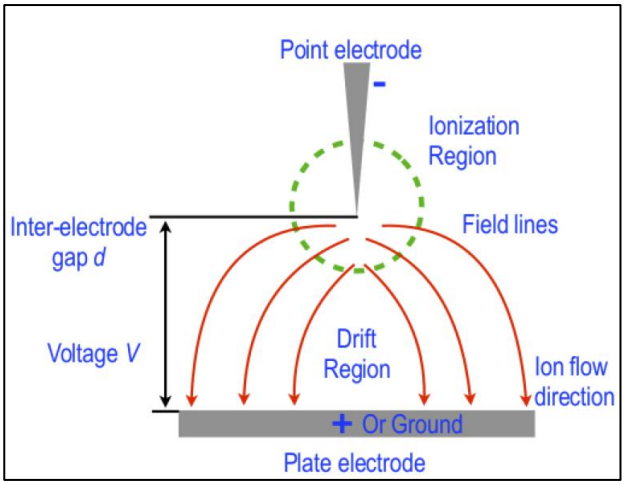


Figure 4: Schematic of a corona discharge illustrating the ionisation and drift region (26).

The polarity of the electrode dictates the type of corona produced. This can be unipolar (positive or negative), bipolar, alternating current (AC), direct current (DC) or high frequency (26). Despite the various types of corona, they all have an area where electrons collide with neutral molecules to cause ionisation and a drift region where these ions and electrons 'drift' towards ions with opposite polarity. High energy electrons collide with neutral molecules to break them up into electrons and ions inside the ionisation region. After the collision, if the electrons have lost their energy, no more new collisions occur which means the polarity of the corona is maintained. After ionisation, if high energy remains, then the electrons and ions are able to react with ionised particles to cause the production of plasma (26).

1.3.2 Dielectric barrier discharge (DBD)

DBD systems are similar to the corona plasma systems but have a dielectric barrier coating on the electrodes which prevents the "faint" filaments which occur with corona discharge (27,28). The development of DBD systems to produce CAP emerged from Siemens' investigations, which concentrated on the production of ozone (O_3). Ozone is made up of three oxygen atoms (29). When plasma is created, molecules are split into single oxygen atoms which then combine with O_2 to form O_3 (30). Siemens did this by

passing a flow of oxygen or air into a DBD and maintaining this in a narrow annular gap. The electrodes were positioned on the outside of the discharge chamber, meaning they were not in contact with the plasma (28).

These DBD systems are used in industry on a large scale. The advantages of non-equilibrium plasma are combined with the ease of atmospheric-pressure operation (28). Further research resulted in improved ozone generators as well as several new applications including surface modification, pollution control and in the last 20 years, flat plasma display panels used in television sets (31).

Dielectric-barrier discharge (DBD) reactors were designed by Werner von Siemens in 1857, a schematic of this process can be seen in Figure 5.

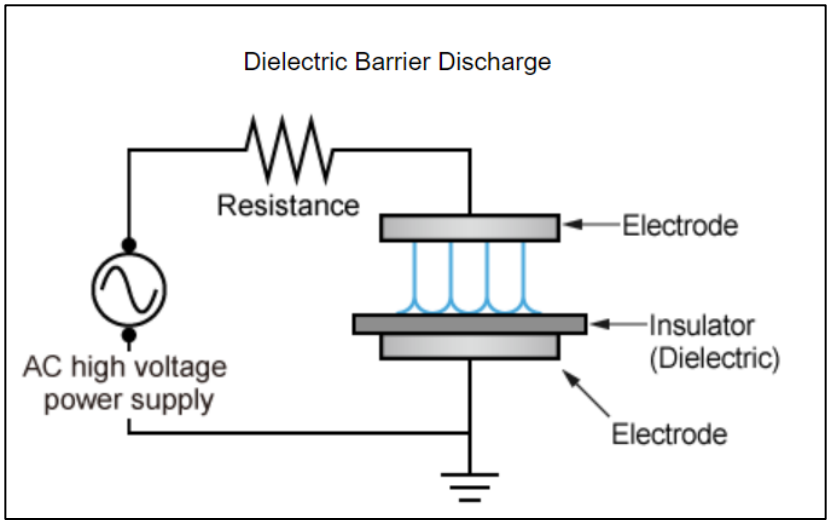


Figure 5: Dielectric Barrier Discharge (DBD) (31).

These atmospheric pressure DBD systems have unique features (32). These systems produce much higher electron energies than that of the ion and neutral species energy. A greater level of "dissociation, excitation and ionisation" occurs due to the collision of the high energy electrons with the gas. This encourages the plasma polymerisation. It is common in thermal plasmas for these reactions to result in an increase in the gas' internal energy. However, this is not the case in 'cold' plasma (31). Therefore, non-

thermal plasmas are not expected to cause thermal damage to thermolabile materials such as enzymes, antibodies, and therapeutics (31).

1.3.3 Cold atmospheric plasma (CAP)

Cold plasma created at atmospheric pressure is referred to as cold atmospheric plasma (CAP). When plasma is intended to interact with a substrate, damage to a substrate can occur when the temperature is high, which has been seen with traditional plasma processes (1). For this reason, some applications require low temperature plasma. This means that the plasma is not in thermal equilibrium, such as at atmospheric pressure. High energy electrons colliding, as well as the excitation, ionisation, and dissociation of the gas particles result in the production of heat (33). Low gas pressures can be used to produce these non-equilibrium plasmas, which have lower collision frequency (24). Low pressure, non-equilibrium plasma can be used in manufacturing and processes such as sputtering, plasma-enhanced chemical vapor deposition (CVD), plasma oxidation (anodization), planarization, and possible medical applications (33).

1.3.3.1 Cold Atmospheric Plasma (CAP) systems.

CAPs are produced under atmospheric conditions. CAP systems are ‘cold’, which means they will typically operate below 40˚C or will prevent heating by using a pulsed mode (34). CAP systems can be divided into three categories; direct, indirect and hybrid plasma sources (34).

An example of a direct CAP system is the floating electrode dielectric barrier discharge (FE-DBD). A schematic of this process can be observed in Figure 6.

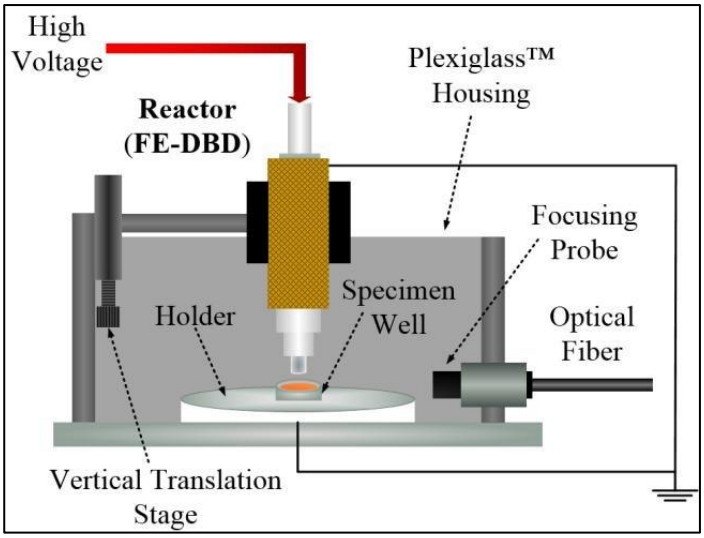


Figure 6: Schematic of a floating electrode dielectric barrier discharge (FE-DBD) reactor in protective housing (35).

This type of CAP system uses the target surface as a counter electrode and creates high concentrations of plasma-generated species. A limitation of this system is the need for a constant distance to the treatment area, which can be difficult when it comes to the human body which has a variety of curves and folds. Using a small treatment area can help eliminate this downfall (34).

When using DBD, the current which passes through the target area, must be monitored as there is strict safety regulations and limits which should not be exceeded (36). The current can also have positive effects on a desired area such as iontophoresis (36). Iontophoresis involves a weak electrical current being passed through the skin (37). Physical therapists may use plasma currents to treat several conditions such as tendonitis, tendinopathy, bursitis and to help manage scars (36). A schematic of the iontophoresis process can be observed in Figure 7.

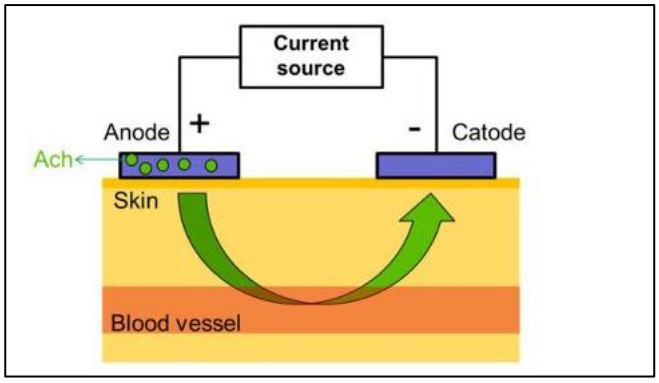


Figure 7: Schematic of iontophoresis using acetylcholine (38).

As mentioned above, DBD is used mainly as an ozoniser. These devices usually have two electrodes. A plasma discharge is formed between the two electrodes by applying an AC high voltage of varying kV and up to MHz frequency. Arcing is avoided by presence of the dielectric material on one or more of the electrodes. A non-thermal discharge is the resulting product (34).

Indirect plasma sources do not require the target source to be used as a counter electrode. A device is used which generates a plasma between two electrodes. After the generation of the plasma, it is transferred to the target area by a carrier gas or diffusion (39). By using a carrier gas, the plasma-generated reactive species can be modified and used to produce compositions for specific application. Indirect plasma sources vary in size from small thin plasma needles to multiple jet applications, up to plasma torches on a large scale. Indirect plasma is less controllable and also produces a lower concentration of plasma- generated species than DBD (34).

Hybrid plasma sources combine the benefits of both direct and indirect plasma sources. A technology known as surface micro-discharge is an example of a hybrid plasma technology. This generates a plasma using a multitude of nano and micro discharges on a grounded wire-mesh electrode. Since there is a smaller electrical resistance in the wired mesh, the current produced does not pass through the target area (34).

1.4 Plasma Applications

Plasma has evolved into an integral component across numerous industries. Plasma etching was first introduced in mid 1960s and more so in 1970s. In the 80s, plasma etching became a popular technique to etch layers and was then introduced for the production of integrated circuits (40). The ability to etch silicon, aluminium and silicon dioxide represented a breakthrough that allowed features of integrated circuits to decrease in size over the next 40 years (41). The semiconductor industry also uses plasmas for sputtering (40). Sputter deposition can also be referred to as physical vapour deposition (PVD). This is a technique used widely for depositing very thin layers of metals on semiconductor wafers (42).

Corona discharge has applications across a wide variety of processes as it is relatively easy to produce (25). Some applications include: air purification systems, surface treatment, electrostatic precipitators, printing, coating, waste-water treatment, and, textile treatment (43–45).

Plasma is also used for the surface modification of many materials in the biomedical field, both to enhance the surface properties of the substrate and biocompatibility (46). Vacuum plasma can also be used for activation of surfaces, which results in changes in the surface tension of the substrates. Vacuum activation works well for many surfaces including glass, plastics, ceramics, titanium, and nitinol. In a typical air or oxygen plasma, the bonds of the plastic polymer (non-polar hydrogen bonds) are replaced with oxygen bonds. This encourages water and polar liquid molecules to bond to the free valence electrons (19). Surface activation can be used to enhance wettability of the surface**.** One of the most notable examples includes surface treatment for cell culture applications. Many cell culture plates are made from plastic surfaces, meaning pre-

treatment is required as cells do not adhere well to plastics. Many different pre-coating steps have been investigated, including the addition of proteins such as collagen, fibronectin, and laminin, but all require a lengthy drying process before use (47). Prior to adding this coating, plates can be treated with vacuum plasma. The vacuum plasma 'activates' the plates, which causes a reduction in the contact angle of the surface and increases the hydrophilicity of the surface (48). The plasma exposure increases the number of OH groups on the surface which allows the pre-treating coatings to adhere effectively to the plastic surface (48). A visual representation of the relationship between surface energy, surface tension and wetting is shown in Figure 8 (49).

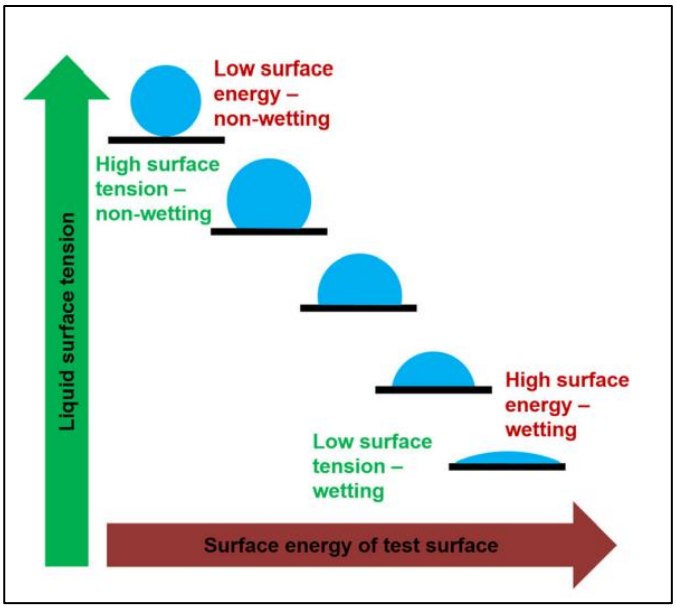


Figure 8: Relationship between surface energy and surface tension in terms of wettability *(50).*

When there is an interface between a solid and liquid, the angle between the surface of the liquid and the contact surface is called the contact angle (θ). This is a measure of the wettability of a solid by a liquid. Complete wetting or spreading of a liquid on a solid is 0º. Any contact angle between 0 º and 90 º is wettable (hydrophilic), while any value above 90 º is not wettable (hydrophobic). Ultra hydrophobic materials have a contact

angle that approaches 180 º (51). An example of bad wetting, good wetting and complete wetting of water droplets on a surface can be seen in Figure 9.

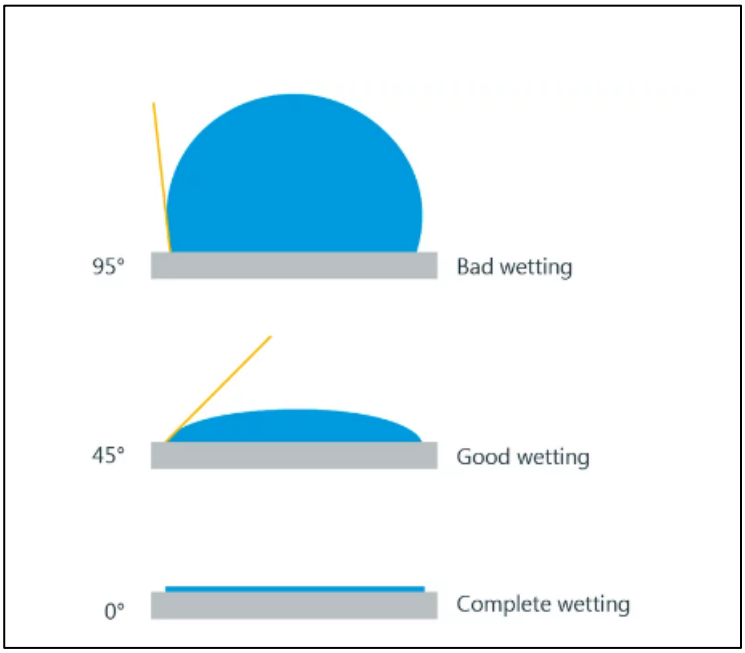


Figure 9: Examples of water droplet forming on surfaces with various surface energies (51).

Recent developments have seen approaches towards the application of CAP for medical applications (34). One key advantage of plasmas is their effectiveness to kill bacteria. Sterilisation and cauterisation procedures have used plasma for several years. The type of plasma used for sterilisation of equipment can be unsuitable for human tissue as it is either extremely hot or produced under a vacuum. Plasma processes can also be used for decontamination and disinfection purposes. Cold plasma has shown promising results in the non-thermal food processing process to inactivate contaminating micro-organisms on foods and packaging (52). Cold atmospheric plasma has also been proposed as an option for applications in the biological and medical sectors to reduce wound bacteria contamination and encourage wound healing (53).

1.4.1. Deposition of Coatings using Plasma

Plasma polymerisation is an significant engineering technique, capable of depositing thin functional films onto surfaces (54). The key advantage of this method is that it is entirely dry (54). Plasma polymerisation primarily involves converting monomers with functional groups into polymer-like layers, where these functional groups serve as anchor points and enhance adhesive interactions with other substrates (55). The process consists of two stages, plasma-assisted chemical vapor deposition (CVD) of a gaseous species (monomer) and polymerisation during deposition (55). The interaction between the gas phase molecules and plasma activates of the monomer, leading to its deposition on the substrate (55).

Other coating methods include physical vapor deposition (PVD), which occurs in a high vacuum. In PVD, the solid/liquid to be deposited is vaporised then condensed to form a thin solid layer. These coatings are typically very thin, often needing multiple layers. One common PVD method is sputtering, in which a target substrate is coated in a vacuum chamber, resulting in a thin film (56). A schematic of sputtering can be visualised in Figure 10.

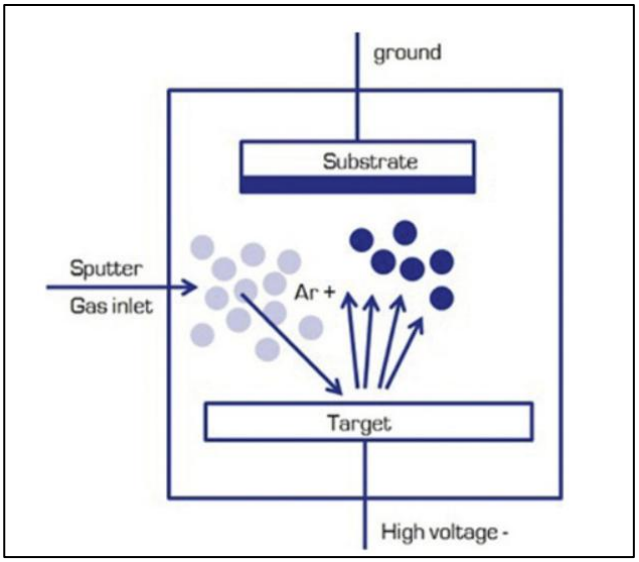


Figure 10: Schematic of the sputtering process (56).

Chemical vapor deposition (CVD) is a another method used for coating, particularly in semiconductor manufacturing . This process allows for a high quality, highly resistant coating of a wide variety of substrates. CVD is especially suitable when mechanical parts need protection against corrosion and wear (56). A schematic of the CVD process can be seen in Figure 11.

In plasma-enhanced chemical vapor deposition (PECVD), plasma replaces the thermal energy used in CVD A plasma is generated under vacuum when a high frequency electric field is applied to a gas, causing high energy electrons to collide with the precursor gas molecules and break them into reactive fragments (57). This process occurs at lower temperatures than compared to traditional CVD, which relies on heat to break chemical bonds. (57). Plasma enhanced CVD (PECVD) allows coating on substrates that cannot withstand high temperatures. (57). The various differences between CVD and PVD can be seen in the below table:

Table 3: Key differences between CVD and PVD *(58)*.

Parameter	PVD	CVD
Mechanism	Material is transferred as vapour	Chemical reaction of precursors on surface
Temperature	Lower than CVD	Higher than PVD, unless PECVD used
Atmosphere	Under vacuum	Can be vacuum or atmospheric
Material types	Mostly metals and oxides	Wide range including metals, ceramics, polymers
Film uniformity	Lower than CVD, but depends on geometry of substrate	Typically high with good conformity
Deposition rate	Moderate	Moderate to high
Adhesion	Moderate, may need pre-treatment	Generally excellent
Applications	Hard coatings optical films microelectronics	Semiconductor biomedical coatings MEMS

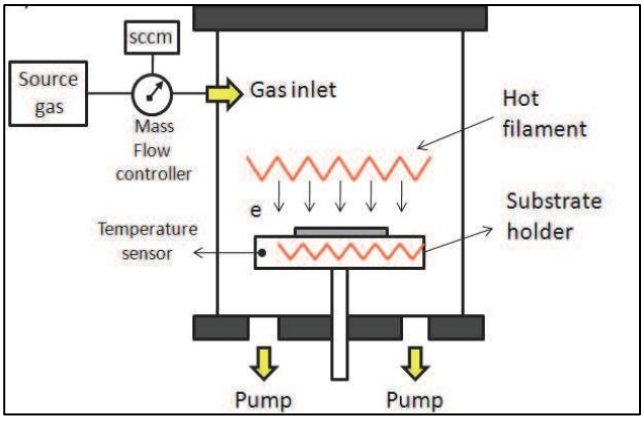


Figure 11: Schematic of chemical vapor deposition (CVD) (59).

In recent years, CAPs have emerged as a promising method for the deposition of biologics (33). The discharge type generated in CAP systems is influenced by factors such as power source, frequency, ambient gas pressure, and the shape and configuration of the electrodes. (4). This research will specifically focus on DBD and corona discharges produced by the proprietary BioDep™ system.

1.4.2. Biodep™ system

There is a wide choice of coating methods and materials used for various applications. In previous years, coatings have been applied by dipping, or spraying. These are often followed by a curing stage, which makes the entire coating process lengthy and time consuming. TheraDep Ltd have developed a process of depositing a coating using plasma that allows biologics and therapeutics to be adhered to various substrates. This is called the BioDep™ system. The BioDep™ system consists of a high voltage power supply (Redline G2000), which is connected to the deposition unit. Within this deposition unit, there are two metal electrodes that create the plasma (60). A schematic of the BioDep™ system can be observed in Figure 12.

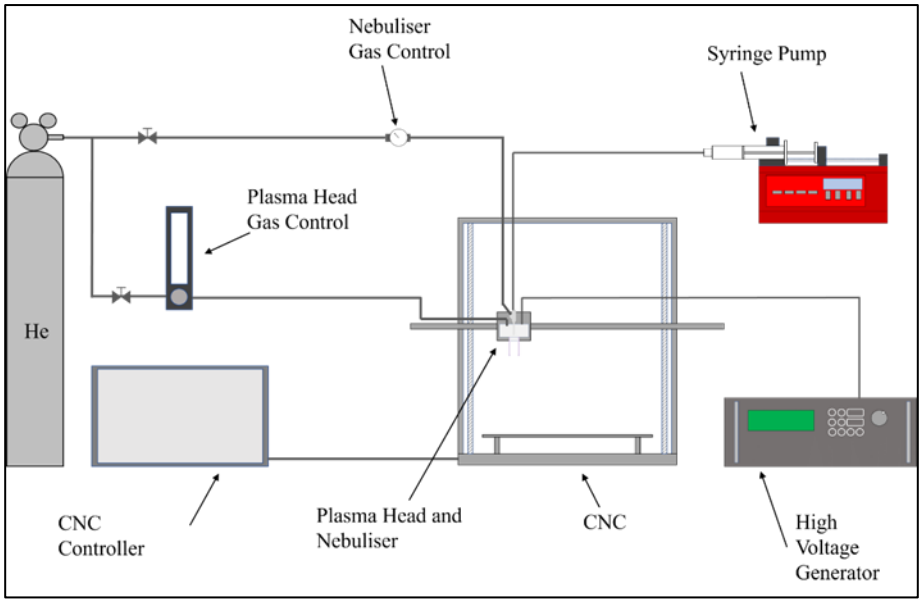


Figure 12: Schematic of TheraDep Ltd.'s BioDep™ system using a computer numerically controlled (CNC) controller, illustration provided by Denis O' Sullivan (TheraDep Ltd).

The patented plasma head used in the BioDep™ system is unique to this system. A schematic of this plasma head can be seen in Figure 13.

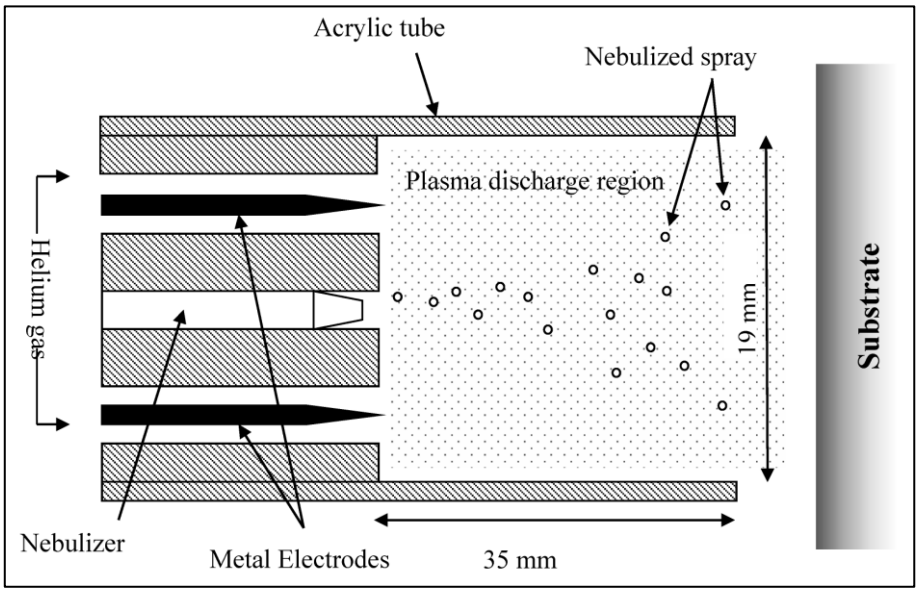


Figure 13: Schematic of the plasma head in the BioDep™ system, provided by TheraDep Ltd.

The BioDep™ coating process was adapted from a previous technology which was developed by Dow Corning. Coatings developed by Dow Corning were used in the textile industry (61). Dr. Liam O'Neill and John O' Donoghue discovered medical

applications for this technology when they passed red blood cells through the CAP and observed that the cells were still viable and unharmed by the plasma. This led to the development of TheraDep Ltd. TheraDep Ltd have carried out research looking at various applications of the BioDep^{TM} system to coat labware, and medical devices with a number of biologics and therapeutic drugs (62–64).

TheraDep Ltd has also researched and confirmed the possibility of using the BioDep^{TM} technology for wound healing, by depositing therapeutics such as collagen onto wounds and other tissue (65,66). TheraDep Ltd then developed the "Deposition Accessory" which can attach to the FDA approved Renuvion Handpiece from Apyx Medical. TheraDep now holds several patents associated with the deposition of biologics and therapeutics using CAPs.

The research in this thesis employs the BioDep^{TM} system, a custom-built CAP system that uses non-thermal helium plasmas that are produced at atmospheric pressure. This BioDep^{TM} unit was used to deposit a drug coating. As mentioned previously, non-thermal plasma can also be used under a vacuum to activate surfaces. The activation application is also used throughout this research as a pre-treatment of the titanium substrates prior to coating.

1.5 Endovascular implants and their coatings

1.5.1 Cardiac implants.

The most common cardiac implants include pacemakers, implantable cardioverter defibrillators (ICDs) and coronary vascular endoprosthesis (stents). An example of a cardiac implant can be visualised in Figure 14, this is known as a drug-eluting stent.



Figure 14: An image of a drug eluting stent- XIENCE V everolimus- eluting coronary stent system used for the treatment of coronary artery disease (CAD) (67).

Intravascular stents are delivered via balloon angioplasty and have been successful in the treatment of atherosclerotic occlusion, especially coronary arteries. The procedure involved in balloon angioplasty is represented in Figure 15. The reoccurrence of stenosis (restenosis) is the body's response to injury of the arterial walls (mechanical injury). Restenosis has two main processes, neointimal hyperplasia and vessel remodelling. Neointimal hyperplasia is when the smooth muscle cells migrate and proliferate (68). Restenosis has led to the advent of intravascular stenting. This involves deployment of an expandable tubular stent in the lumen of the vessel, which physically holds the vessel open (68).

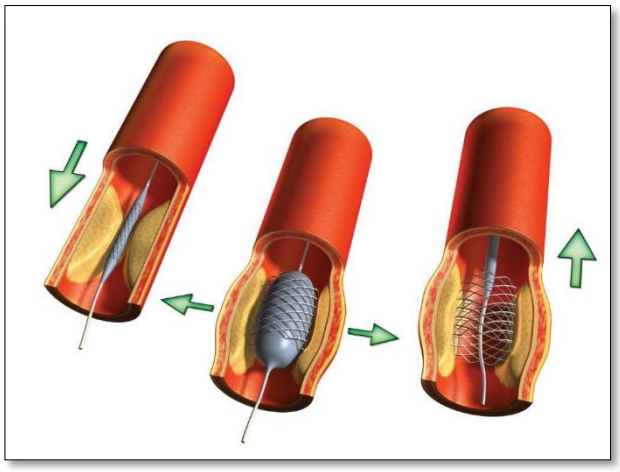


Figure 15: A schematic of a balloon angioplasty (69).

Stents have typically been made of stainless steel, nitinol (nickel-titanium alloy) or cobalt-chromium alloys. Suitable materials for a medical implant application should have desirable mechanical properties depending on the intended use and avoid undesirable host-tissue interactions (19). Materials should be non-toxic, non-carcinogenic, non-irritant and non-thrombogenic (70). The concept of biocompatibility refers to "the ability of a material to perform with an appropriate host response in a specific situation" (70). To understand the biocompatibility of specific implants, the chemical, biochemical, physiological, and physical mechanisms must be understood when they become operational under certain conditions.

It is very important to design and produce implantable devices which have properties to allow them to function and fit properly into the environment in the body (46). The ideal outcome varies depending on implant type and role. Bio-integration is desirable in many implant applications. However, exceptions include where the implant is a temporary device, or the implant is a pacemaker or neurostimulator and bio-integration would hinder the function. Bio-integration occurs at the interface between the host tissue and the implant. At this interface, no harmful effects are wanted, such as inflammatory responses. Implants can result in or be implicated in a variety of responses in the body, such as inflammation, coagulation, infection and fibrosis. After implantation of a device, the body recognises it as a foreign body and can trigger a series of responses known as the inflammatory response. The sequence of events follows the potential interaction between proteins and other physiological macromolecules with the material surface, initiation of inflammatory/immune response and finally repair/ regeneration process which may lead to an equilibrium between the host and implanted device (71). The formation of a fibrous capsule around the biomaterial can occur as a normal part of the inflammatory response, however, this can cause issues as the capsule contracts around

the implant. The inflammatory response can cause damage to the implant, implant failure, and also result in generation of toxic catabolites (72).

1.5.2 Anti-proliferative drugs as an endovascular device coating

Biocompatibility must be designed into the device. Medical devices are now requiring enhanced biocompatibility, which is being done by using bioactive coatings, pharmacological agents, nanotextures, or hybrid systems to have desirable biologic results. The term biocompatibility has moved from ‘do no harm’ to ‘do good’(73,74). The medical device and materials which it consists of need to meet biocompatibility requirements, as defined by ISO 10993 standards. In addition, under the European union medical device regulation (MDR, Regulation (EU) 2017/745, Annex 1 (General safety and performance requirements) specified that devices must be designed and manufactured in such a way that they do not pose unacceptable risks to substances or particles that may be released, and must minimise biological risks throughout their intended use. Compliance with MDR typically relies on the ISO 10993 series, especially ISO 10993-1, which provides a risk based framework for biological evaluation(75). These standards state that the device and materials must be nontoxic, non-thrombogenic, non-antigenic, non-carcinogenic, and non-mutagenic (73). The Food and Drug Administration’s Office of Combination Products (OCP) have responsibilities which cover the regulatory cycle of combination products such as drug-eluting stents, which determines the primary regulatory responsibility. Drug-eluting stents are mainly regulated by the Centre for Devices and Radiological Health, secondary responsibility is with Centre for Drug evaluation and Research, whom has responsible for drug content analysis (73)

Endovascular devices can benefit from the use of antiproliferative drugs. These drugs have consisted mainly of two classes of drugs, mammalian target of rapamycin (mTOR)

inhibitors and the Taxol® derivative, paclitaxel. The very first drug eluting stents used sirolimus, which is an mTOR inhibitor. Soon after the use of sirolimus became popular, paclitaxel was introduced as a device coating. Since then, the number of mTOR inhibitors has increased to become the most popular antiproliferative agents eluted from endovascular devices (76). Some examples of companies and the drug eluting stents they manufacture can be seen in Table *4*: Examples of drug eluting stents (DES), their manufacturers and coating methods.

Table 4: Examples of drug eluting stents (DES), their manufacturers and coating methods.

Company	Brand name	Drug eluted	Coating method	Reference
Cordis	*Cypher™* stent	Sirolimus	Dip coating	(77)
Medtronic	*Endeavor ™ Resolute ™ Onyx* stent (78)	Zotarolimus	Spray coating	(78,79)
Abbott Laboratories	*Xience ™* stent	Everolimus	Electro- spray coating	(67,80,81)
Boston Scientific	*Promus ™* stent	Everolimus	Spray coating	(82)
Boston Scientific	*Taxus ™* stent	Paclitaxel	Spray coating	(83,84)
Medtronic	*In. Pact Admiral ™*	Paclitaxel	Spray coating	(85)

The *Endeavor Resolute Ony ™* stent (Medtronic), *Promus™* and *Taxus™* (Boston Scientific), *Xience™* stent (Abbott Laboratories) and the *IN. PACT Admiral™* paclitaxel-coated percutaneous transluminal angioplasty (PTA) balloon catheter (Medtronic), all use a spray coating method (14,77–80). Prior to coating, the stents and balloons are cleaned and a primer layer applied to enhance adhesion of the drug. The coating is applied via spraying, which can involve multiple thin layers of a drug-polymer

mixture. Each of these layers needs to be carefully cured before the next is applied to ensure a uniform coating with controlled release (14). The *Xience*^{TM} stent manufactured by Abbott Laboratories is coated by electrostatic spray deposition. This means that the drug, everolimus, is mixed with a fluoropolymer, and this solution is then charged electrostatically (86). By charging this solution, it encourages the attraction of the solution to the surface of the stent when it is sprayed onto the surface (81). A curing step is still required to ensure the polymer is stable and adheres well to the surface and allows for controlled release of the drug (87). Schematics of dip coating, electro-static spray and spray coating can be visualised below in Figure 16.

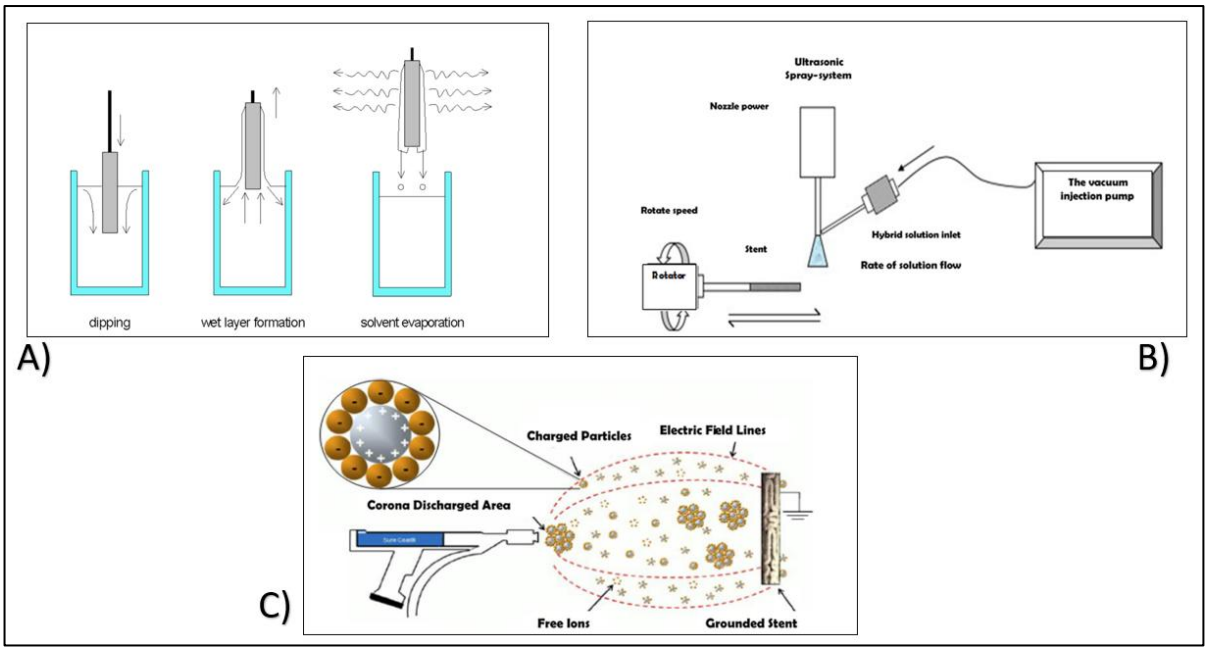


Figure 16: Schematics of various types of coating methods, A) Dip coating B) Electro-static spray coating C) Spray coating (88).

1.5.3 Everolimus

Everolimus is a derivative of rapamycin (also known as sirolimus). Everolimus is a small molecule drug with a molecular weight of 958 g/mol (89). Currently, everolimus is used as an immunosuppressant after organ transplants, and to treat various types of

malignancies (90). Both everolimus and sirolimus work similarly, but some of the differences are highlighted below in Table 5.

Table 5: Key differences between sirolimus and everolimus in terms of half-life, potency, and uses *(91)*.

Everolimus	**Sirolimus**
Shorter half-life than sirolimus	Longer half-life than everolimus
Higher potency than sirolimus	Less potent that everolimus
Higher bioavailability than sirolimus	Lower bioavailability than everolimus
Stimulates mitochondrial oxidation	Inhibits mitochondrial oxidation
Used in second generation DES like XIENCE V and Promus, reduces vascular inflammation to a greater extent	Some first generation eluting stents had issues with polymer biocompatibility and inflammatory response.

Everolimus is commonly used in drug eluting stents to prevent restenosis and rejection of stents by the body. Everolimus does this through several processes. Firstly, it has an antiproliferative effect. It inhibits the activity of the mTOR, which is a protein kinase that plays a vital role in cell proliferation and growth. Everolimus prevents smooth muscle cells from proliferating and migrating to the stent site by blocking the mTOR signalling pathway, thus inhibiting the formation of neointimal hyperplasia, which is a key contributor to restenosis. Everolimus also possesses anti-inflammatory properties, which also help suppress the immune response, that is triggered by the presence of the stent in the blood vessel. The reduction of inflammation minimises the risk of immune-mediated rejection against the stent (92). The mechanism of action involves the blocking of "growth-driven transduction signals in the T-cell response to alloantigen" (93). Everolimus is incorporated into a polymer coating on drug-eluting stents which allows for the controlled release of the drug. Some examples of these polymers include poly-n-butyl-methacrylate, vinylidene fluoride, and hexafluoro-propylene (94) . This ensures

the therapeutic levels of everolimus are maintained at the stent site for an extended period which provides continuous protection against restenosis and rejection (84).

Everolimus has two main isomeric forms, the predominant 6-member pyran and a less dominant 7-member oxepane, depicted in Figure 17 (95). These isomers are inter-convertible through the process of tautomerisation. Many degradation products of everolimus have been identified as isomers of everolimus. The 7-member oxepane also referred to as 501-95, is the only form which produces a tautomer peak during analysis via HPLC, so it represents a unique identification feature on a chromatogram.

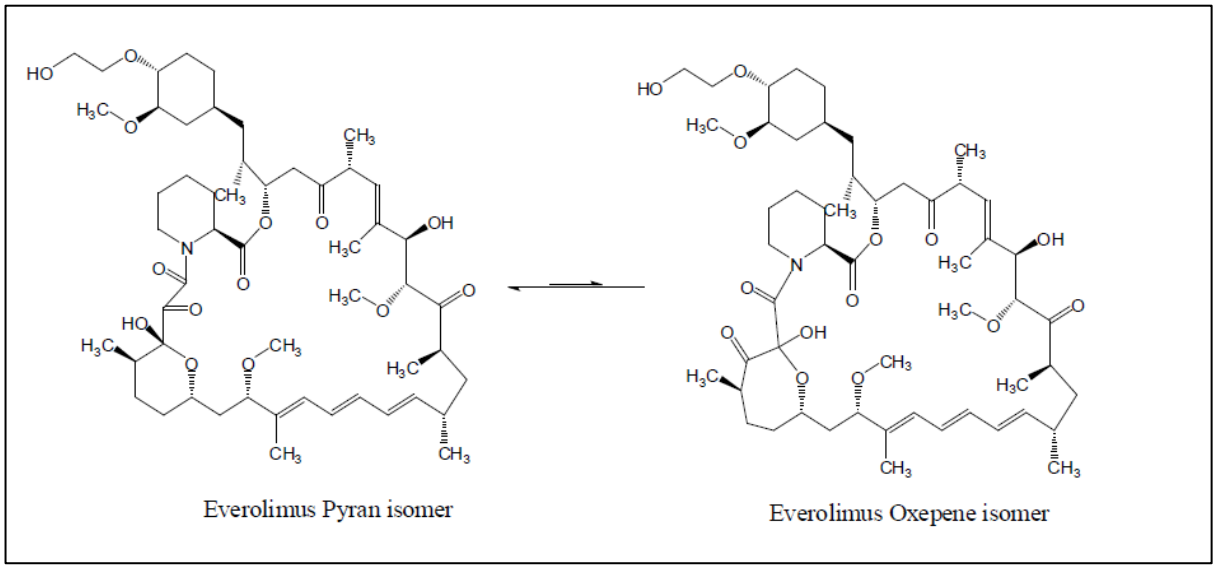


Figure 17: Chemical structures of everolimus isomers (95).

Everolimus and sirolimus differ structurally at position 40 where everolimus contains a stable 2-hydroxy-ethyl chain (93). This can be observed in Figure 18, where position 40 is highlighted in both everolimus and sirolimus.

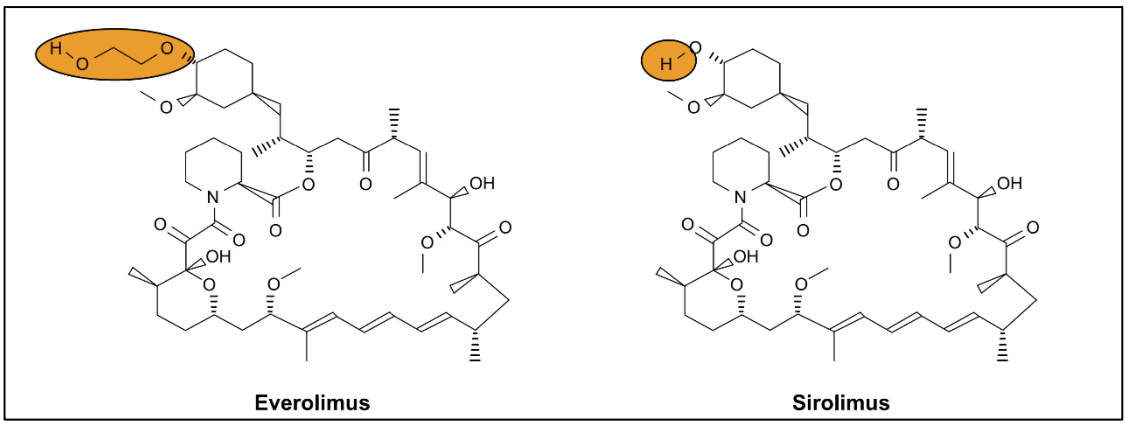


Figure 18: Chemical structure of everolimus and sirolimus, and their differing structure at position 40 (96).

Everolimus is a white to light yellow amorphous powder. It is almost insoluble in water. Everolimus is also unstable at temperatures above 25˚C and is also sensitive to light. Everolimus requires an antioxidant to stabilise it (97). Due to the complex structure of everolimus, several possible degradation pathways can occur at different positions in the molecule. On storage, it has been proven to be stable for 60 months at -25˚C. However, a correlation has been observed between increasing temperature and an increase in degradation products, which is caused by the reduction in antioxidant, butylated hydroxytoluene (BHT) levels. Everolimus was also observed to be hygroscopic, and sensitive to acid, base and hydrogen peroxide (97).

1.6 Antioxidant used in pharmaceutical formulations- Butylated hydroxytoluene (BHT)

Butylated hydroxytoluene (BHT) is commonly used as an antioxidant in pharmaceutical formulations. The structure of BHT is shown in Figure 19.

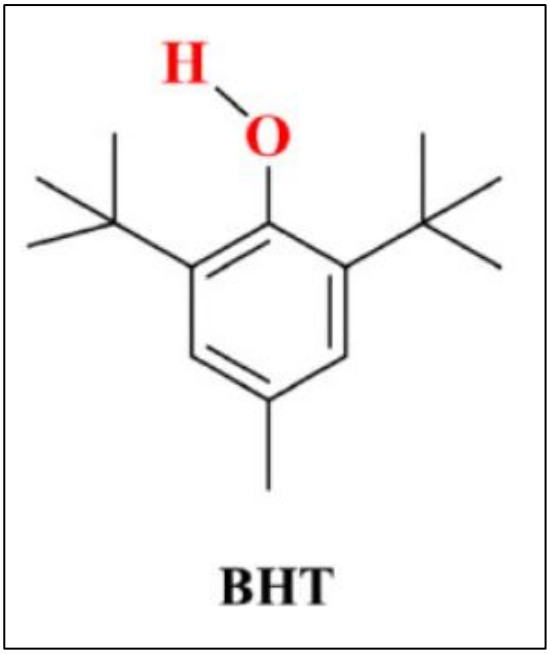


Figure 19: Schematic representation of butylated hydroxytoluene (BHT) used to stabilise everolimus (98).

BHT prevents degradation of sensitive compounds, including drugs such as everolimus. BHT is capable of stabilising everolimus by two key mechanisms. Firstly, BHT scavenges free radicals, which can cause chemical reactions that lead to drug degradation (99,100). Free radicals can be produced from a variety of processes, including exposure to light, oxygen, and increased temperatures. BHT is a chain-breaking antioxidant which means it interrupts the chain reaction of oxidation by donating hydrogen atoms to free radicals, stabilising them as a result (101). This prevents the propagation of oxidative reactions which can lead to the degradation of drugs, such as everolimus (101,102). Secondly, BHT has been reported to chelate metal ions such as copper and iron, which can catalyse oxidative reactions by generating reactive oxygen species. By forming a complex with these metal ions, BHT inhibits their activity and reduces the chances of oxidative degradation of drugs, such as everolimus (103). In this study, BHT will be included in the everolimus coating solutions at various concentrations to mitigate degradation.

2. Thesis aim and objectives

The aim of this research was to use the plasma coating process developed by TheraDep Ltd, known as BioDep™, to effectively deposit everolimus coatings onto titanium discs and to investigate the properties of the coatings. This aim is supported by three main objectives:

- To coat everolimus onto titanium discs using the BioDep™ plasma process and compare to wet deposition (no plasma).
- To characterise the everolimus coating using a range of analytical techniques; confocal and polarised white light imaging to visually inspect the coating on the substrate, water contact angle (WCA) to determine the hydrophobicity/ hydrophilicity of the coating, Fourier-transform infrared (FTIR) spectroscopy to determine the functional groups present when deposited with and without plasma, Raman spectroscopy to assess the presence of everolimus in the deposited coatings, deep ultraviolet mapping (DUV) to confirm the presence of the drug on the surface, and atomic force microscopy (AFM) to measure any changes in the surface roughness.
- To develop and validate an effective HPLC method to quantify everolimus loading onto titanium discs.

3. Materials and Methods.

3.1 Materials

Everolimus powder was purchased from Kemprotec Ltd. (Camforth, UK). Titanium discs were purchased from Lisnabrin Engineering Ltd (Cork, Ireland). All other reagents and chemicals were supplied by Merck Life Sciences Ltd. (Wicklow, Ireland) as detailed in Table 6.

Table 6: Details of materials, grade, and suppliers.

Material	**Form**	**Grade**	**Supplier**
Everolimus	Powder	>98%	Kemprotec Ltd.
Acetonitrile	Liquid	HPLC grade, >99.9%	Merck Life Sciences Ltd.
Methanol	Liquid	HPLC grade, >99.9%	Merck Life Sciences Ltd.
Water	Liquid	HPLC grade	Merck Life Sciences Ltd.
Ammonium formate	Powder	>99.995%	Merck Life Sciences Ltd.
Formic acid	Liquid	>95%	Sigma- Aldrich
Butylated hydroxytoluene	Powder	>99%	Merck Life Sciences Ltd.
NaCl Cards	Disc	N/A	Merck Life Sciences Ltd.
Titanium discs (15 mm diameter, area 3.54 cm^2)	Disc	II	Lisnabrin Engineering Ltd.

3.2 Methods

3.2.1 Plasma deposition of everolimus

The deposition of the everolimus was carried out using the Biodep^{TM} unit, which consists of a Redline G2000 high voltage (HV) power supply, and a helium supply that are both connected to Theradep's deposition module mounted on a CNC controller. It is a custom-built CAP system, used for deposition of APIs and other materials. A schematic of the nebuliser, chamber and substrate can be observed in Figure 20.

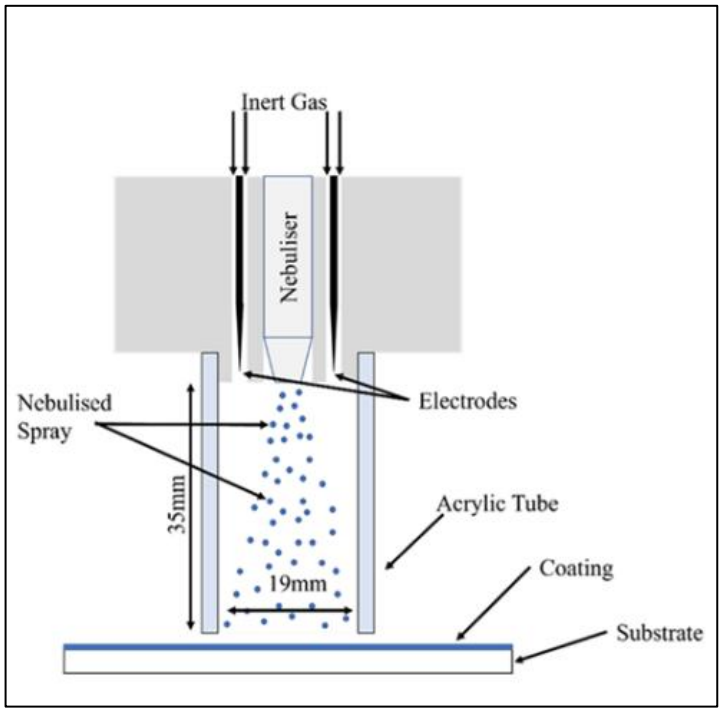


Figure 20:Schematic of the BioDep^{TM} system used for the deposition of the everolimus coating (schematic designed by Denis O'Sullivan, Engineer at TheraDep Ltd).

The Biodep^{TM} unit, has a 'plasma head' which consists of two electrodes, a gas port and a pneumatic nebuliser (T2100, Burgener), which is connected to a syringe pump. The syringe pump controls the flow rate of the solution to be deposited. The electrodes receive power from the Redline power supply which creates an electric field between the two electrodes and the substrate below to be coated. The substrate acts as a 'ground point'. The syringe pump allows the controlled flow of solution into the nebuliser. An image of

the syringe pump used in this specific system can be seen in Figure 21. A controlled flow of the nebuliser gas (argon) flows through the gas port on the nebuliser creating a fine mist that is sprayed into the electric field. The interaction between the plasma and the fine mist results in a plasma deposited, cured layer of the API on the substrate.



Figure 21: An image of the syringe pump used in the BioDep™ plasma system, located in TheraDep Ltd, Clonmel, Ireland.

To generate the plasma discharge, helium gas and the high voltage power were introduced into the Teflon head. Within this, the gas circulated around the electrodes, initiating plasma formation between them and the substrate. Both the nebulised spray and plasma discharge occurred within an acrylic tube, which can be observed in Figure 22.The dimensions of this tube were: width 28 mm and length 44 mm. The substrate to be coated was placed below the tube on a CNC table. This CNC table and plasma head are controlled by G-programming language, which can be referred to as ‘g-code’. This programme allows the control of the specific pattern and speed of the movement of the acrylic tube over the substrate.

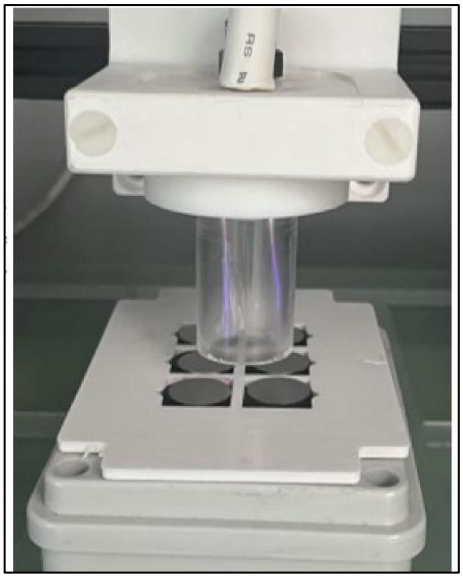


Figure 22: Image of the Biodep™ plasma deposition system located in TheraDep Ltd, Clonmel, Ireland. The white cable bringing the high-voltage power supply to the Teflon plasma head which contains two electrodes. The nebuliser is placed into this Teflon head and everolimus is deposited onto the titanium discs below. Pictured is during plasma deposition, as seen by two plasma jets (104).

Solutions of everolimus were prepared in ethanol. Pilot studies were carried out with an everolimus concentration of 7 mg/mL. However, for deposition Study 1, it was increased to 10 mg/mL to increase the mass deposited and to facilitate everolimus detection and more accurate analysis. In Study 2, the concentration of the everolimus solution was further increased to 20 mg/mL.

The substrate, titanium discs (15 mm diameter, area 3.54 cm^2), were sterilised with isopropanol (70%) prior to plasma activation. The discs were activated in a Diener Zepto vacuum activator (Ebhausen, Germany) for two minutes on either side using helium at a flow rate of 0.5 L/h and 100% power. After activation, the discs were coated with everolimus on both sides. The plasma deposition parameters used for depositing everolimus onto the titanium discs are shown in Table 7. Controls were also prepared, which were everolimus coated discs deposited through the Biodep™ unit without plasma (0 V), also referred to as 'wet deposit' or 'wet chemical process'. These served as controls to determine the effect of the plasma-everolimus interaction on everolimus stability.

Table 7: Plasma deposition parameters employed in studies 1 and 2 to coat titanium discs with everolimus.

	Study 1		**Study 2**	
Parameter	**Value/Unit**		**Value/Unit**	
Gas flow rate	6 L/min		6 L/min	
Precursor flow rate	100 µl/min		100 µl/min	
CNC speed	1000 mm/min		750 mm/min	
Step size	4.5 mm		2.25 mm	
Deposition type	**Plasma deposit**	**Wet deposit**	**Plasma deposit**	**Wet deposit**
Frequency	20.4 kHz	n/a	20.4 kHz	n/a
Voltage	90 V	0 V	90 V	0 V
Power	0.09 A 8W	n/a	0.09 A 8W	n/a

The two coating studies (Study 1 and Study 2) were carried out to deposit different theoretical masses of everolimus. The theoretical concentration of everolimus to be deposited onto titanium samples were calculated as shown in Table 8. Discs from coating Study 1 were analysed with HPLC Method 1, while discs from Study 2 were analysed with HPLC Method 2.

Table 8: Everolimus deposition calculations- Study 1 and Study 2.

Parameter	Study 1	Study 2
Everolimus liquid concentration	10 mg/ mL	20 mg/ mL
Liquid flow rate	100 µl/ min	100 µl/ min
CNC speed	1000 mm/ min	750 mm/ min
CNC step size	4.5 mm	2.25 mm
Coating efficiency	25%	25%
Number of passes	1	1
*Deposited weight/ minute	0.25 mg/ min	0.5 mg/ min
**Deposition time per cm^2	2 x 10^{-2} min/ cm^2	6 x 10^{-2} min/ cm^2
***Deposition rate	6 x 10^{-3} mg/ cm^2	3 x 10^{-2} mg/cm^2
Area of sample to be coated	3.54 cm^2	3.54 cm^2
****Deposited mass per disc	20 µg	105 µg
*****Deposited mass per cm^2	5.7 µg/cm^2	29.7 µg/cm^2

* Liquid concentration (mg/mL) x liquid flow rate/100 (mL/min) x efficiency of process
**Time per square cm= number of passes x 10 mm long/ number of steps per cm
*** Deposition weight per minute x time per square cm
****Deposition rate x area
*****Deposited mass per disc / area of disc

In the case of FTIR analysis, everolimus was deposited statically onto sodium chloride (NaCl) infrared (IR) cards at a flow rate of 100 µl/min, at a voltage of 90 V for the plasma deposited sample and at 0 V for the wet deposited sample. A Ti substrate was not used for FT-IR analysis as IR cannot penetrate Ti. The static deposit was carried out directly over the NaCl window for a duration of one minute, to ensure adequate drug deposition for analysis of functional groups in the drug.

3.2.2 Characterisation of everolimus coating

3.2.2.1 Confocal and polarised white light imaging.

Confocal laser scanning microscopy was used to assess the distribution of the everolimus coating on the surface of the titanium substrate. The samples were observed with a LSM710 upright confocal microscope (Zeiss, Oberkochen, Germany) using plan apochromat objective.

3.2.2.2 Water contact angle (WCA).

The water contact angle analysis of coated and uncoated samples was conducted using the Kruss TVA100 (Hamburg, Germany). The Kruss TVA100 uses a top-view method for the measurement of contact angle between a liquid and a solid. An image of the instrument used for this analysis is shown in Figure 23. Measurements were taken by pipetting a 5 µl water droplet onto the surface of the substrate using a micro-pipette. Methylene blue was added to the water prior to pipetting. An image of the droplet on the surface was captured from above using a high-resolution camera which is built into the Kruss TVA100 instrument. Software on the KRÜSS machine was used to analyse the image to determine the shape and size of the droplet, as well as the location of the three-phase contact line where the liquid, solid and vapour meet (49,105). The contact angle of the droplet was calculated based on the layout of the three-phase contact line. Each sample was measured in triplicate and average values reported.

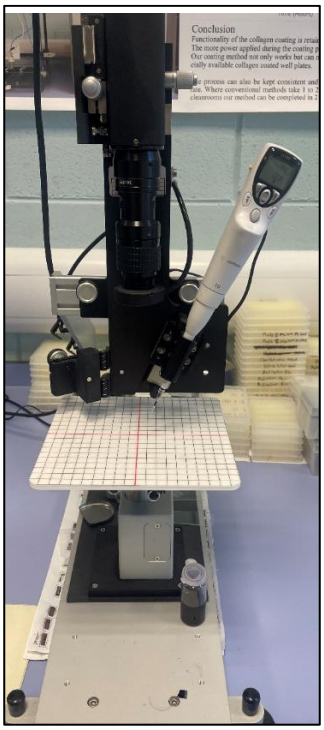


Figure 23: KRUSS TVA 100 instrument in TheraDep Ltd, Clonmel, Tipperary, used for WCA analysis of the everolimus coated titanium discs.

3.2.2.3 Fourier-transform infrared (FTIR) spectroscopy.

Fourier-transform infrared (FTIR) spectroscopy was used to analyse everolimus deposition on NaCl IR cards. The coated cards were analysed using a Perkin Elmer Spectrum One instrument (Waltham, USA), which operates in single beam mode. Each sample underwent 16 scans with a resolution 0.5 cm^{-1}.

3.2.2.4 Raman spectroscopy.

Raman spectroscopy measurements were carried out using a XploRA Raman spectrometer (Kyoto, Japan) equipped with the following parameters. The laser excitation sources utilised were wavelengths of 785 nm, 633 nm and 532 nm. Spectra were acquired with an acquisition time of 30 s per accumulation and a scan range of 250-3000 cm^{-1}. The binning function was set to 1. The grating employed had a resolution of 1200 lines per millimetre (l/ mm), ensuring high spectral resolution. A slit width of 100 µm was utilised to control the entrance of light into the spectrometer. Additionally, a hole diameter of 300 was employed to optimise signal-to-noise ratio. Spatial mapping was performed using a 100- point map configuration, with each map comprising a grid of 10 x 10 points. The step size along the X- axis was set to 3 µm, while along the Y- axis, it was set to 5 µm, ensuring comprehensive coverage of the sample surface. The detector used was a HJY/EM detector.

500 points were measured on different locations across the everolimus-coated titanium discs, with each point measuring 100 µm in area. The data was averaged. The data was baseline corrected to avoid Rayleigh scattering and normalised for comparison. Three different wavelengths were used 532 nm, 633 nm, and 785 nm.

Table 9: Summary of Raman acquisition parameters used to analyse everolimus-coated titanium discs.

Parameter	Setting
Range: 250- 3000cm^{-1}	Windows: 4
Autoscanning: Off	AutoFocus: Off
SWIFT: Off	AutoExposure: OFF
Spike filter: Off	Delay time (s): 0
Binning: 1	Readout mode: Signal
DeNoise: Off	ICS Correction: Off
Dark correction: Off	Instrument process: Off
Detector temperature: -60.09	Objective: 100
Grating: 1200	Filter: 100
Laser (nm): 785.12	Slit (µm): 100
Fiber: 0	Laser pol: 1
Raman pol: 2	StageXY: Marzhauser
StageZ: Marzhauser	Z (µm): 0

3.2.2.5 Deep Ultraviolet (DUV).

The DUV fluorescence was conducted using a fluorescence spectrometer (PL 200) (Photon systems Inc., Covina, USA). This was carried out with a 5X deep UV achromatic microscopic objective, and a Ne-Cu hollow cathode laser (PSI Ne-Cu 30, λ_{em}=248.6 nm) was focused directly on the sample. Spectra were taken between 250 nm to 620 nm using a 300 g/mm grating providing a 1.2 nm spectral resolution. A DUV map (8 mm^2, 500 points) was measured and averaged.

3.2.2.6 Atomic force microscopy (AFM).

Atomic force microscopy was carried out using a Nanosurf Easy Scan unit (Nano Surf AG, Switzerland) under the following conditions: the voltage of the tip was set at 0 V, the z height of scans was set to 4.9 µm, the scan range was 50 µm, with overscan enabled at 10%. The scans were analysed using Nanosurf ^{TM} Easy Scan software. Everolimus

coated titanium discs deposited by wet deposition (0 V) and plasma deposition (90V) were analysed. Each sample type was analysed in triplicate and averages reported.

3.2.3 Quantification of everolimus recovered from titanium discs coated using 'Study 1' parameters.

Everolimus coated titanium discs prepared in coating Study 1 (section 3.2.1) underwent elution in acetonitrile (ACN). Two coated discs were placed in each well of a polystyrene 6-well plates (Sarstedt), Figure 24, to which 1 mL of ACN was added. The plates were wrapped in parafilm to prevent solvent evaporation, and left for 2 h at room temperature, with regular gentle swirling of the plate. Two factors were evaluated, (i) comparison of plasma and wet deposition and (ii) the impact of BHT addition at three concentration levels, 0%, 5% and 10%, Figure 24.

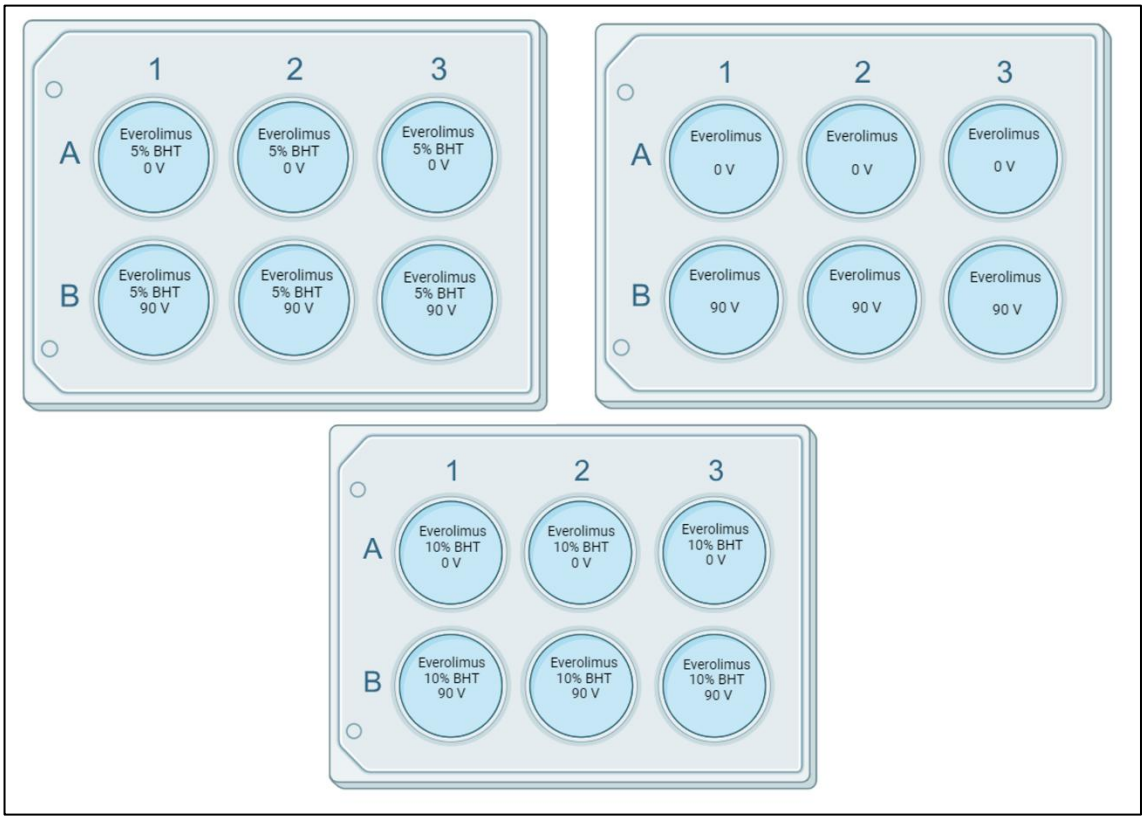


Figure 24: Two titanium discs coated with each specific coating were placed into each well with 1 ml acetonitrile for elution of coating. Discs were coated with (i) everolimus (0% BHT), (ii) everolimus with 5% BHT (iii) everolimus with 10% BHT, through both wet chemical (0 V) and plasma deposition (90 V).

Considerable evaporation occurred which affected the accuracy of the results obtained and therefore a new method for elution was determined. Capped-glass vials were used instead of 6-well plates and ethanol was used as solvent instead of ACN. Two coated-titanium discs were added to each vial with 1 ml ethanol. Parafilm was placed around the lids as a secondary precaution and the drug was allowed to elute at room temperature for a duration of 2 hours, with regular gentle swirling of the vials to ensure the liquid fully covered the discs. After elution, the 1 ml eluent was removed via pipette and the concentration and stability of everolimus was determined by RP-HPLC. Again, everolimus discs evaluated included a comparison of plasma and wet deposition and the impact of BHT addition at three concentration levels, 0%, 5% and 10% (6 coating types). Each sample type was evaluated in triplicate and averages reported.

3.2.4 Quantification of everolimus recovered from titanium discs coated using 'Study 2' parameters.

Due to difficulties quantifying the mass of everolimus deposited in Study 1, the deposition method was adjusted. The revised method is referred to as Study 2 and parameters are detailed in section 3.2.1.

Titanium discs were coated with an increased everolimus concentration (20 mg/mL). Any issues related to the evaporation of ACN were avoided by using glass jars with lids and 6-well plates, which were covered in parafilm during the test phase. One coated titanium disc was placed in each well of a polystyrene 6-well plate (Sarstedt) and 1 mL of ACN was added. Initial scoping experiments involved a 2 h elution process at room temperature with regular gentle swirling. This was then switched to a 24 h elution process in glass jars due to the presence of a contaminant from the interaction of the polystyrene plate and acetonitrile, see supplementary information, section 0, Figure 56-Figure 63. The coated discs were placed in capped glass vials containing 1 mL of ACN and left on a plate shaker

for 24 h at room temperature. Blank discs were also incubated in 1 mL ACN for a duration of 24 h in glass vials.

3.2.5 RP-HPLC methodology to detect and quantify everolimus using HPLC Method 1 and 2.

The RP-HPLC method employed for everolimus quantification was based on a European Pharmacopeial method employing a reverse phase C18 column (106). The composition of mobile phase A was altered to reduce polarity. The RP-HPLC parameters employed for method 1 are outlined in Table 10. After method validation was carried out on HPLC method 1, issues arose with the retention time drifting during sample analysis. This together with characterisation studies which showed a low and variable coating prompted a 2nd study to be undertaken. Study 2 involved changing the RP-HPLC method to enhance reproducibility during sample analysis. The samples measured using HPLC Method 2 were coated using the parameters outlined in Study 2 (Table 7). The RP-HPLC parameters employed for both methods are outlined in Table 10. A forced degradation sample of everolimus was prepared by placing 500 µg everolimus in a glass jar and placing it in a water bath at 60ºC for 4 hours, and then exposing the vial to room temperature and light for 24 hours before pipetting 1 ml ethanol into the vial.

Table 10: RP-HPLC parameters used to analyse everolimus samples in both Study 1 and Study 2.

Parameter	**Details HPLC Method 1**			**Details HPLC Method 2***		
Instrument	Agilent 1120			Agilent 1220		
Column	Kinetex® 2.7 µm C18 150 x 2.1 mm					
Mobile phase A*	Formic acid/ methanol/ 0.7g/L ammonium formate/ ACN Volume ratio (0.05/100/450/450)			HPLC Grade water		
Mobile phase B	Formic acid/ methanol/ 0.96g/L ammonium formate/ ACN Volume 0.05/100/330/570)			HPLC Grade ACN		
Gradient	Time	% A	% B	Time	% A	% B
	0	20	80	0	70	30
	10	100	0	10	30	70
	15	100	0	15	30	70
	20	20	80	20	70	30
Flow rate	0.3 mL/ min			0.9 mL/ min		
Temperature	60°C			40°C		
Detector	UV detection at 278 nm					
Injection	10 µl					

*Note the changes to the mobile phases, the gradient, flow rate and temperature but also a new HPLC instrument was used in comparison to Method 1.

3.2.6 RP-HPLC method validation

For the HPLC Method 1, the stock solution of everolimus was prepared by dissolving the drug in ethanol (96%) at a concentration of 10 mg/mL. Everolimus standards ranging from 5- 1000 µg/mL were prepared in ethanol. For HPLC Method 2, the stock solution of everolimus was prepared by dissolving the drug in ethanol (96%) at a concentration of 20 mg/mL. Everolimus standards ranging from 1- 500 µg/mL were prepared in ethanol.

For Method 1, everolimus standards (5- 250 µg/mL) were freshly prepared daily and analysed on three separate days. Each day these standards were analysed in triplicate by the HPLC method previously described above and parameters outlined in Table 10. The peak area of the everolimus standards were plotted against concentration to create a calibration curve, which was used to determine everolimus concentration recovered from the coated discs. Limit of detection and limit of quantitation were calculated using the following equations:

Equation 1: Limit of detection (LOD)

$$\boldsymbol{LOD = \frac{3.3\ x\ \sigma}{S}}$$

Equation 2: Limit of quantitation (LOQ)

$$\boldsymbol{LOD = \frac{3.3\ x\ \sigma}{S}}$$

3.2.7 Statistical analysis

In this study, several statistical methods were employed to analyse the data and determine the significance of the results.

3.2.7.1 One-way-ANOVA (significance level, α = 0.05)

Statistical analysis was conducted using one-way ANOVA to determine whether there were statistically significant differences between the means of three or more independent groups. A null hypothesis was defined, stating no significant difference between groups. If the p-value was less than 0.05, the null hypothesis was rejected, indicating significant difference between group means (107).

3.2.7.2 Two-way-ANOVA (significance level, $\alpha = 0.05$)

Statistical analysis using two-way ANOVA was conducted on everolimus concentrations and tautomer peak percents found after deposition with and without plasma to determine if any statistically significant main or interaction effects occurred. The assumptions included normality, homogeneity of variances, and independent observations. A hypothesis was defined, stating no significant difference between the main effects and interaction, and if the p-value for any factor or interaction was less than 0.05, the null hypothesis for the factor was rejected (108).

3.2.7.3 Paired t-test

The t-test was used to compare the means of two paired groups, in this case the mean percent tautomer peak of the everolimus sample that underwent degradation in comparison to the everolimus standard. This test assumes normally distributed data. The null hypothesis stated that there was no difference between group means, and if the p-value was less than 0.05, the null hypothesis was rejected, indicating a significant difference (94)

3.2.7.4 Tukey post-hoc analysis

After conducting ANOVA, Tukey's post-hoc analysis was applied to identify which specific group were statistically significantly different. Using critical values, the test compared multiple group means, If the test statistic (q) exceeded the critical value, the null hypothesis for that comparison was rejected, indicating a significant difference between the groups (110).

Table 11: Tukey's test critical values for post-hoc analysis of WCA , and RP-HPLC results (k= number of groups in the analysis, df= degrees of freedom).

k	df	Critical value	Post-hoc analysis test
4	16	4.05	Water contact angle results
6	12	4.75	RP-HPLC results for Study 1 and 2.

4 Results

4.1 Characterisation of everolimus coated titanium discs

4.1.1 Images acquired using polarised white light and confocal imaging

Images acquired using polarised white light in Figure 25 show that the wet deposited everolimus, plasma deposited everolimus and blank titanium disc are all similar in appearance, except for the presence of rings formations on both samples with everolimus coatings. The presence of the rings on both the wet deposit and plasma deposit, are indicative of the everolimus coating on the substrate. As the drug is nebulised and deposited, it is cured instantly on the surface which can result in 'rings' as it hits the surface. This appearance was noted for other materials deposited employing the BioDep^{TM} system including collagen (65).

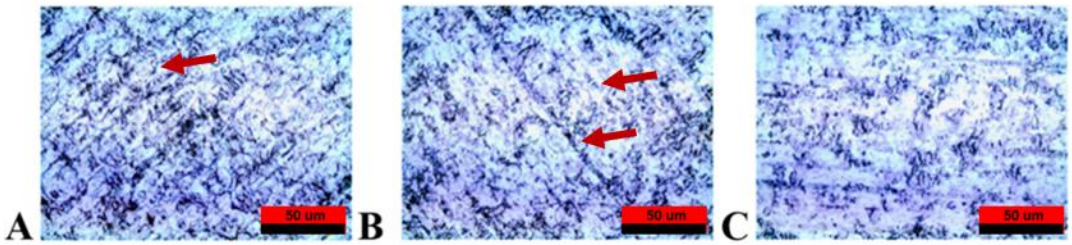


Figure 25: Polarised white light imaging results of (A) wet deposited everolimus (0 V), (B) plasma deposited everolimus (90 V), and (C) blank titanium disc. Red arrows in A and B indicates the presence of a ring. Scale bar indicates 50 µm in images A-C.

The everolimus coating deposited on titanium discs using both the wet and plasma deposition were also visualised using confocal imaging, Figure 26. Again both the wet and plasma deposited everolimus coatings appear visually similar with both images showing rings, which again are indicative of the coating on the surface as previously noted

(65). The plasma process did not alter the appearance of the everolimus coating on the titanium disc, which further supports the polarised white light imaging.

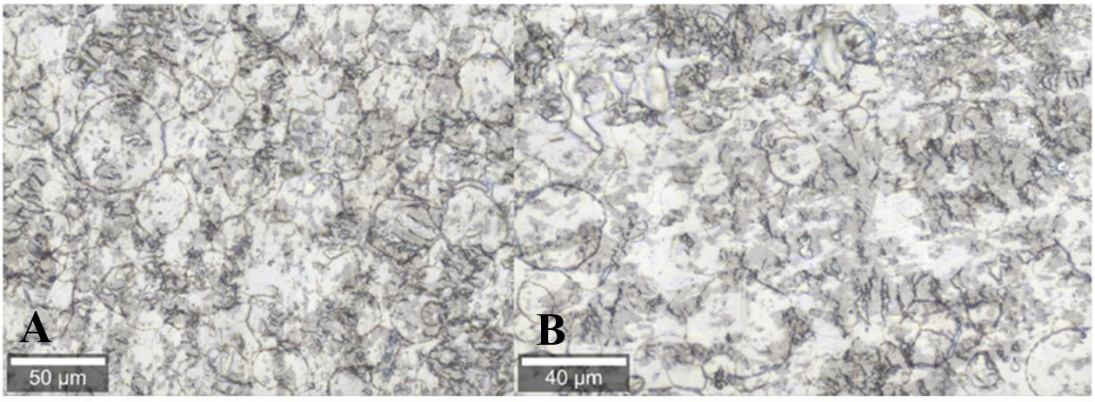


Figure 26:Confocal imaging of everolimus coated discs (A) wet deposit no plasma (B) plasma deposit (90 V).

4.1.2 Water Contact angle (WCA)

The results presented in Table 12 demonstrate that the surface chemistry of the titanium disc was significantly changed by the everolimus coating. Initially, the blank titanium disc exhibited a WCA of 95º, which was then reduced to 60º with the wet deposit of everolimus. Plasma deposited everolimus showed a slightly higher WCA of 64º. The addition of BHT further reduced the WCA, for the wet deposit (50 ± 3º) compared to plasma deposition (60º). Statistical analysis using two-way ANOVA showed significant effects of both plasma treatment ($p = 0.0125$) and BHT ($p = 0.025$) on WCA. An increase in hydrophilicity of the titanium disc was observed for all coatings, with WCAs ranging between 50 ± 3º and 64 ± 8º, compared to 95 ± 7º for the blank disc.

Table 12: Mean water contact angle (WCA) results for everolimus coated, everolimus/BHT coated and a blank titanium disc. Data represents mean ± standard deviation, n=5.

Coating solution deposited	**Wet deposit (0 V)**	**Plasma deposit (90 V)**
Blank titanium disc- control	95 ± 7º	
Everolimus 10 mg/ mL	60 ± 4º	64 ± 8º
Everolimus 10 mg/ mL + 10% BHT	50 ± 3 º	61 ± 4 º

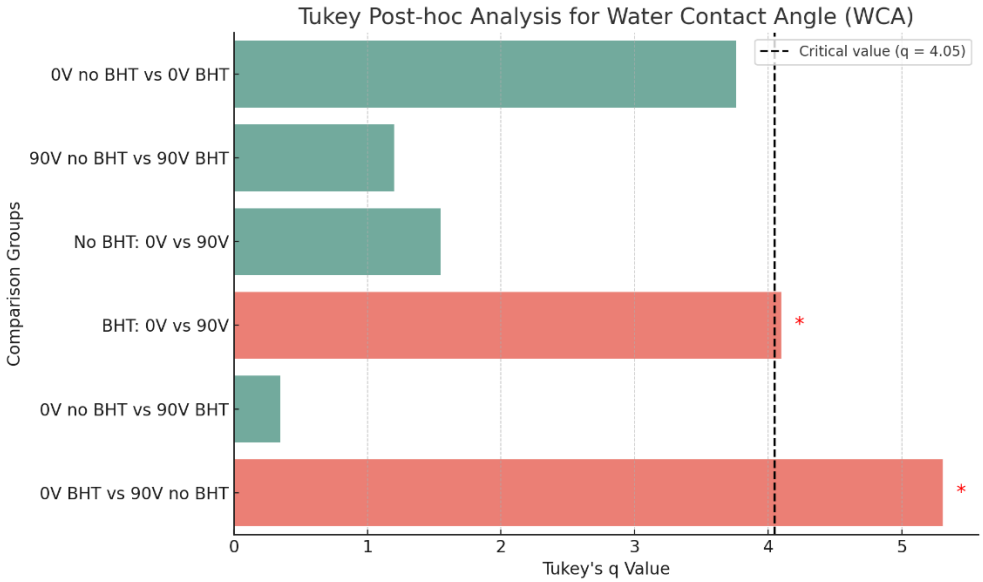


Figure 27: Tukey Post- hoc analysis for water contact angle (WCA) with all groups surpassing the critical value, (representing SSD.*

4.1.3 Fourier-transform infrared (FTIR) spectroscopy

The reference FTIR spectra of everolimus and BHT can be seen in Figure 28 and Figure 29**.** Everolimus characteristic bands seen at 3400cm^{-1} and 2900 cm^{-1}, which are representative of O-H stretching and C- H stretching, as well as bands at 1725 cm^{-1}, which are representative of C = O stretch are present in all coated samples (97,111) .

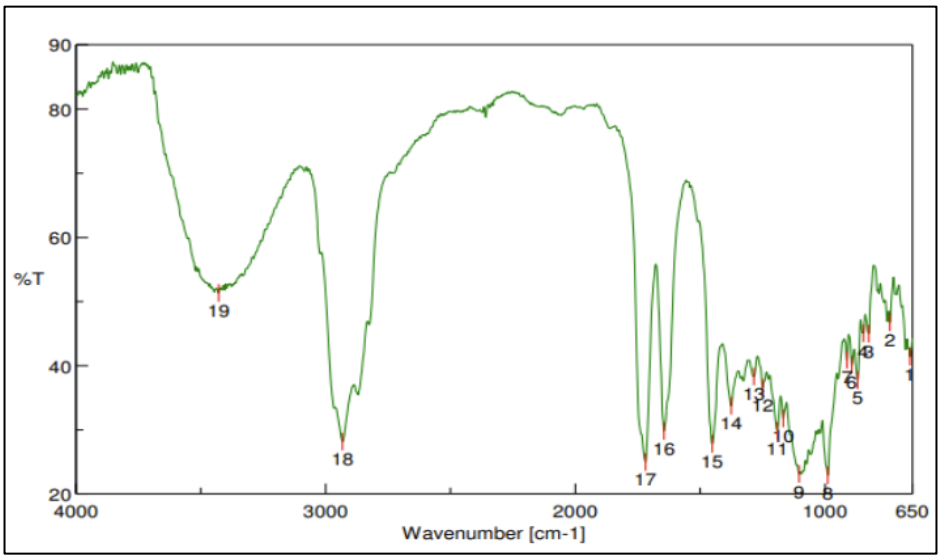


Figure 28: Reference FTIR spectrum for analysis of everolimus reprinted from: (70).

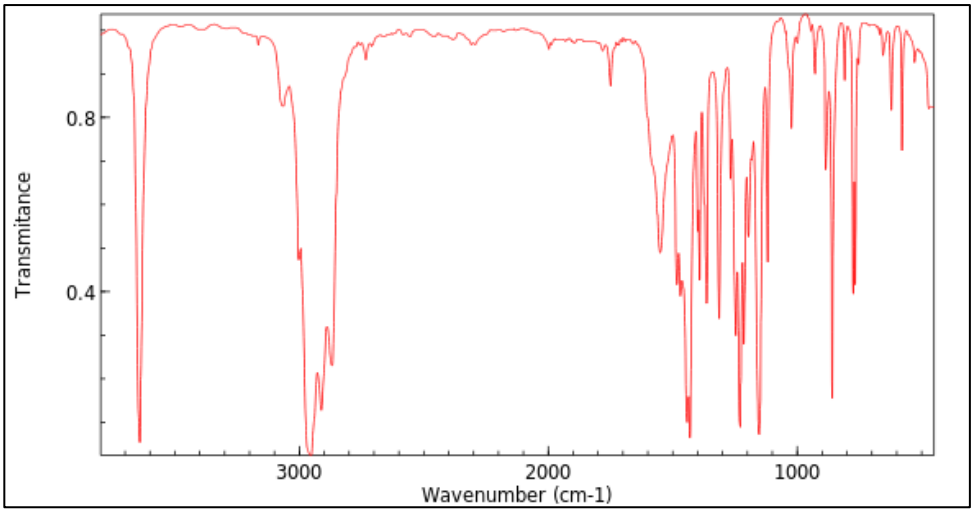


Figure 29: Reference FTIR spectrum for analysis of BHT reprinted from:(113).

The everolimus coatings on the NaCl discs, deposited with and without plasma (90 V and 0 V), were analysed using FTIR spectroscopy (Figure 30). NaCl cards were chosen as IR cannot penetrate titanium. The spectra revealed no additional peaks or changes in peak ratios, indicating that plasma treatment did not alter the everolimus chemistry. Key features included a broad band (3700-3100 cm^{-1}), carbonyl peaks (~ 1722 cm^{-1}), and C-O stretching (~ 1090 cm^{-1})(111) . Adding 10% BHT (Figure 31) to the coatings led to minor changes, with a sharp peak 3622 cm^{-1} in wet deposits which is also present in the BHT reference spectrum (Figure 29), but not in plasma-treated samples, possibly due to BHT oxidation in plasma. Further studies are required to confirm this

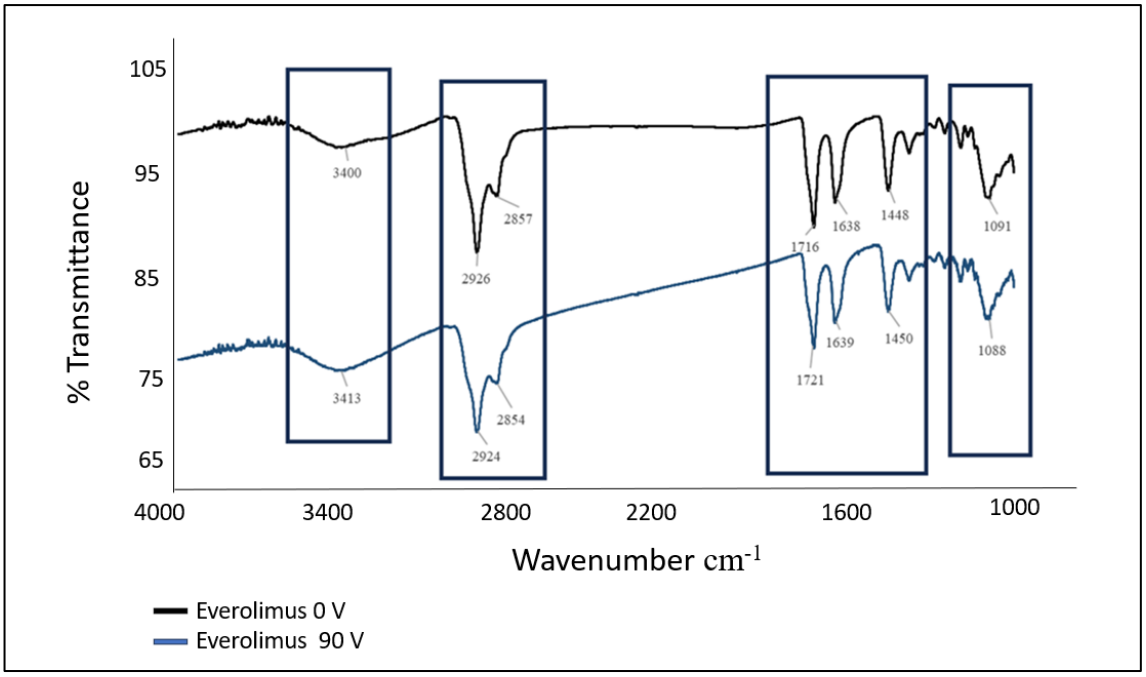


Figure 30: Representative FTIR spectra of everolimus deposited on NaCl discs. (Top) a wet deposit (0 V) and (Bottom) plasma deposited (90 V). Three independent replicates were analysed for each sample type.

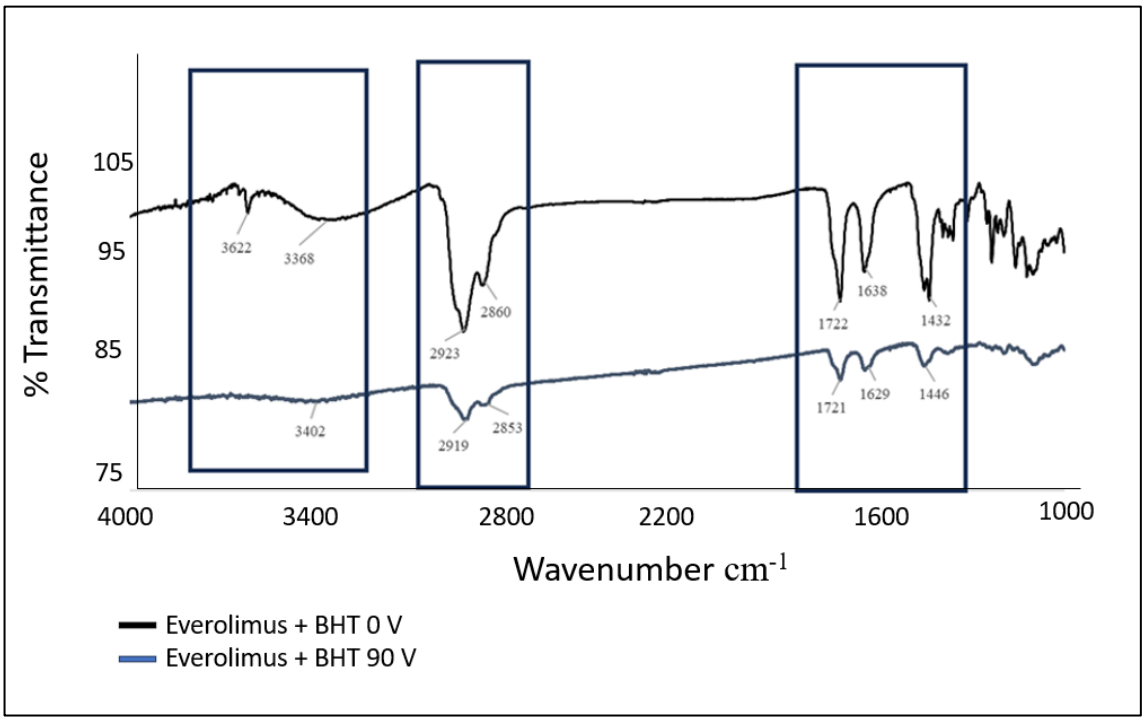


Figure 31: Representative FTIR analysis of everolimus coating incorporating BHT, deposited on titanium using (Top) wet (0 V) and (Bottom) plasma (90 V) deposition. Three independent replicates were analysed for each sample type.

4.1.4 Raman spectroscopy analysis of coated samples

An ultra-wide Raman scan revealed several features within the range 400-1800 cm^{-1}, Figure 32. The peaks at the lower wavenumbers are most likely due to the various forms of titanium dioxide (TiO_2) on the surface of the discs. Titanium dioxide exists in two forms, rutile and anatase (114). The anatase form is reported to demonstrate a dominant peak at 516 cm^{-1} (115), while the rutile phase has two peaks, one at 446 cm^{-1} and the other at 610 cm^{-1} (116) . This mixture of oxides can contribute to a peak at 300 cm^{-1} (117). The spectra collected exhibits broad overlapping peaks between 300 cm^{-1} and 650 cm^{-1} which suggests the oxide surface may consist of a mixture of oxide phases.

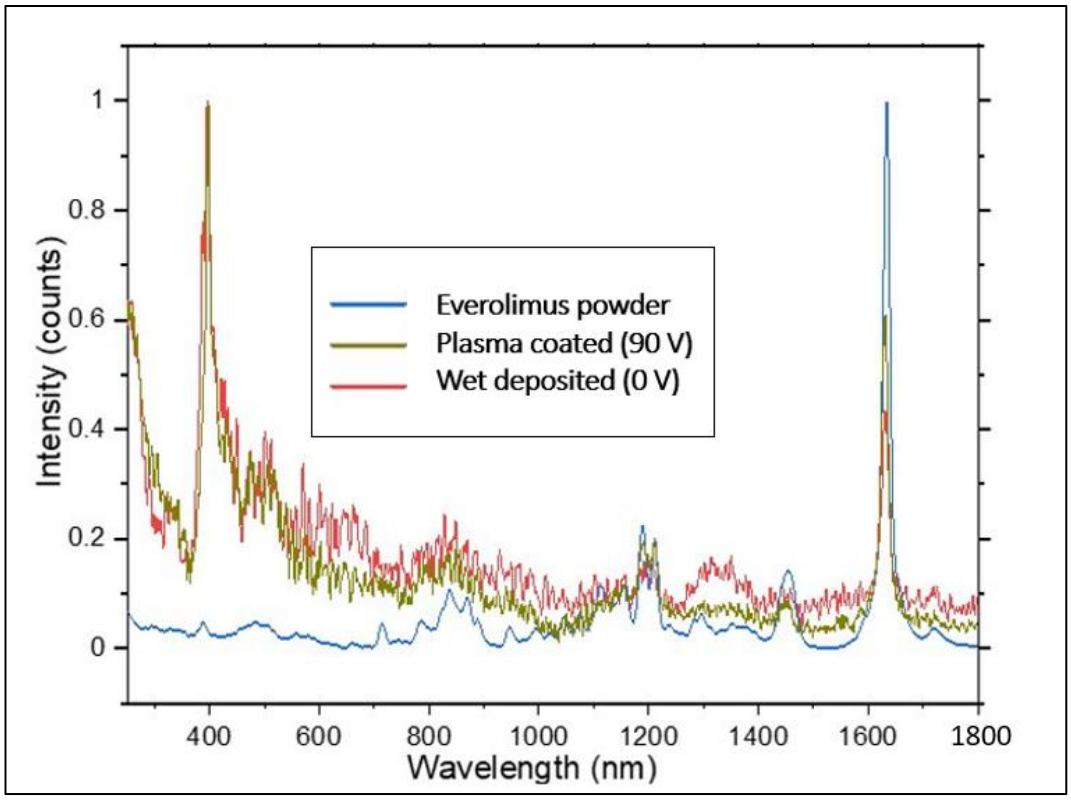


Figure 32: Raman spectrum of everolimus powder and coatings deposited by plasma and wet chemical process.

A focused analysis of the 1000- 1800 cm^{-1} region, Figure 33, which is free from background interference from the titanium surface, highlights key everolimus peaks. The spectrum of pure everolimus shows a dominant carbonyl peak at 1640 cm^{-1}, along with

weaker C-H, C-O and C-C/C-H peaks at 1450 cm^{-1}, 1220 cm^{-1}, and 1180 cm^{-1}, respectively (118). Both the wet and plasma deposited everolimus coatings exhibit these features, though with lower intensity, especially in the wet deposit, suggesting a low concentration of everolimus on the titanium surface. Additionally, the C-O and C-H peaks are more pronounced in the plasma deposited sample, while they appear broader and less resolved in the wet deposit. This confirms the presence of everolimus on both substrates.

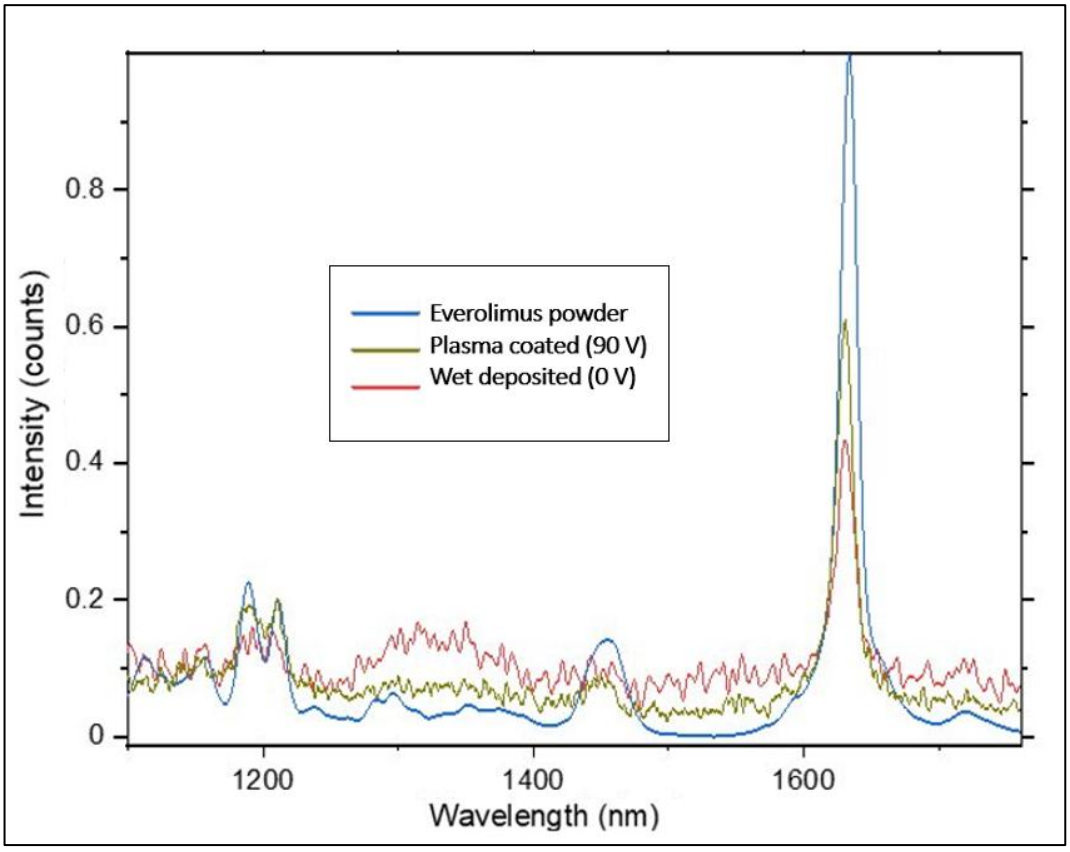


Figure 33: Magnified Raman spectrum (1000-1800 cm^{-1}) highlighting the areas containing peaks derived from (i) pure everolimus powder (ii) everolimus deposited by plasma (90 V) (iii) everolimus deposited via wet chemical process (0 V).

4.1.5 Deep Ultra-Violet mapping

The distribution of everolimus on the titanium substrate was determined by mapping the DUV fluorescence spectral response and comparing it to the spectral response of controls (positive control- everolimus powder, negative control- uncoated titanium substrate). To visualise the distribution, mapped regions with a spectral response similar to everolimus

powder were displayed as green, while red indicated the uncoated titanium substrate. The gradient from green to red in the DUV fluorescence map revealed a heterogeneous distribution of the everolimus coating, with areas of higher concentration and regions with little to no coating.

Figure 34 shows the DUV map of a plasma deposited (90 V) everolimus coating, confirming the presence of everolimus on the surface, but with a low and uneven concentration.

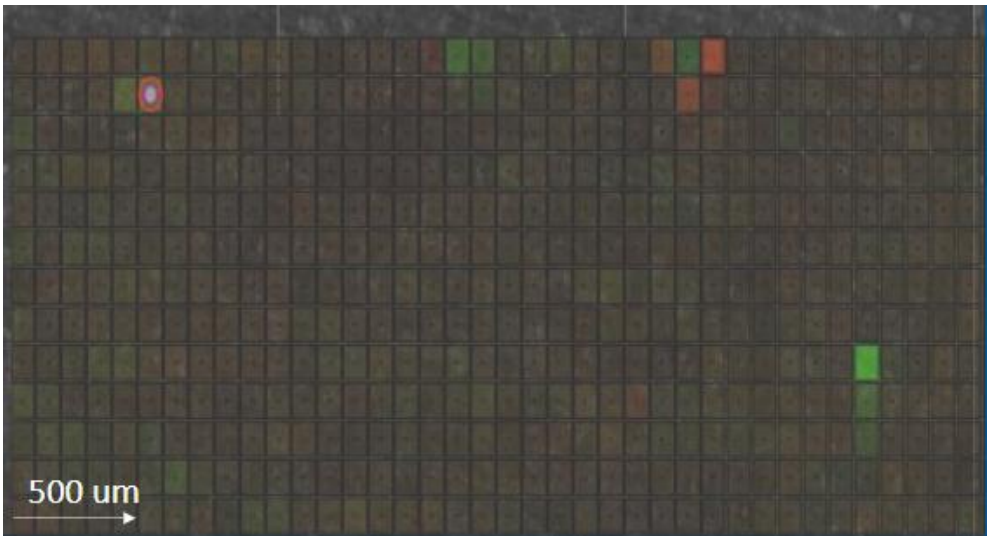


Figure 34: DUV map of everolimus coating deposited via plasma deposition (90 V) onto a titanium disc, green indicates presence of drug while red indicates no drug present (500 points of 100 µm measured).

In Figure 35, the DUV map of the everolimus coating deposited via wet chemical process (0 V) shows more green squares in comparison to the plasma deposited map in Figure 34, indicating a larger coated area. The green to red gradient observed confirms a low concentration of everolimus across the surface, similar to the plasma deposited sample. Additionally, the DUV map supports the findings from confocal and polarised white light imaging, showing ring-like formations of everolimus, where the coating has cured, this further illustrates the non-uniformity of the coatings.

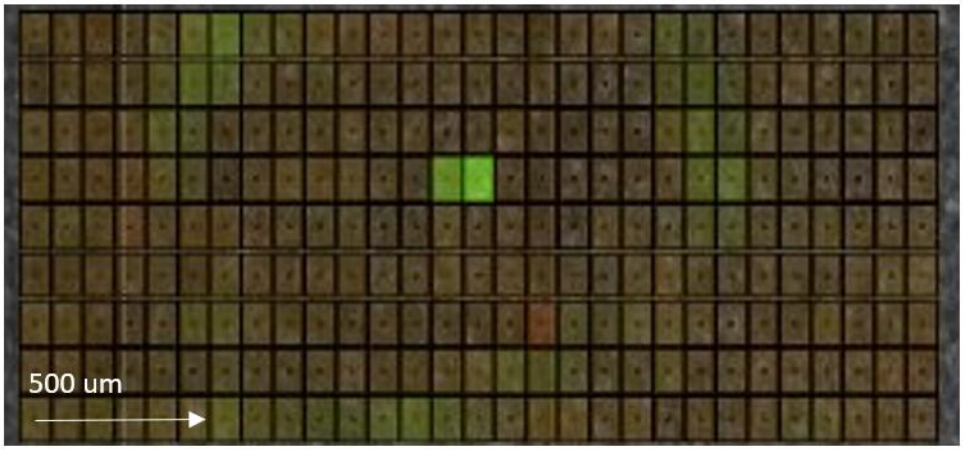


Figure 35: DUV map of everolimus coating deposited via wet deposition (no plasma, 0 V) onto a titanium disc, green indicates presence of drug while red indicates no drug present (500 points of 100 μm measured).

The DUV analysis data summarised in Figure 36, compared the plasma deposited everolimus with the wet deposited coating. The wet deposited everolimus exhibited a higher mean intensity which indicates a greater concentration of the drug on the surface in comparison to the plasma deposited everolimus. However, despite this increased intensity, both samples still show a relatively low concentration of everolimus across the surface, highlighting the overall limited deposition.

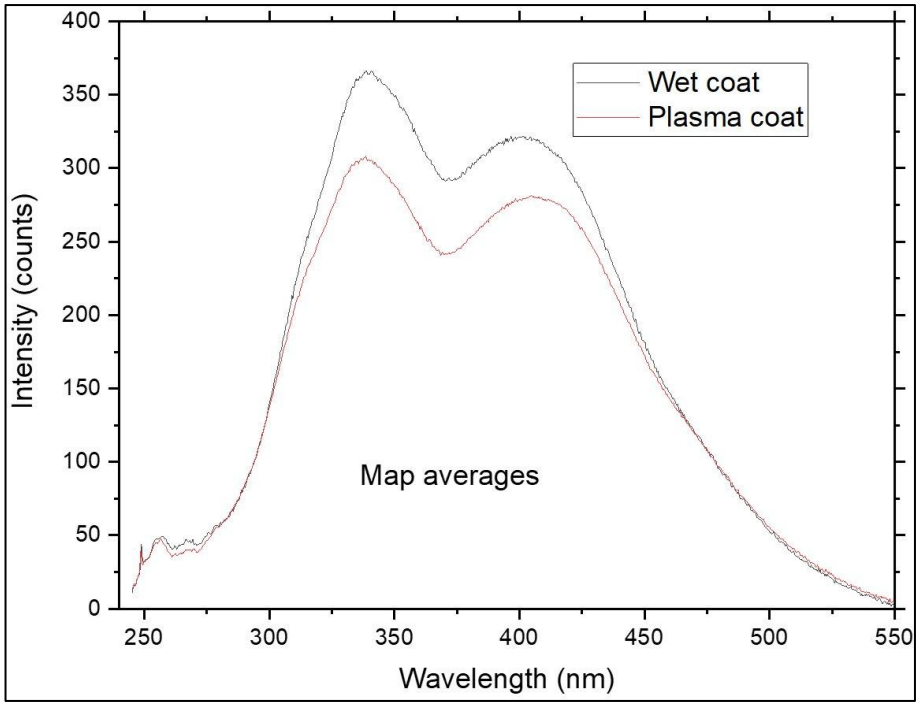


Figure 36: Average DUV map comparisons (500 points of 100 µm spot size measured and averaged) between everolimus deposition using wet (0 V) and plasma deposition (90 V).

4.1.6 Atomic force microscopy (AFM)

The surface properties of the everolimus coating deposited with and without plasma (0 V and 90 V) were compared to a blank titanium disc using AFM, representative AFM scans of each can observed in Figure 37. In Table 13, the difference in surface roughness between the blank titanium disc and everolimus coated discs is shown. The AFM results showed that the deposition of everolimus with and without plasma, did not significantly affect the surface roughness of the titanium disc. There is no statistically significant difference between the average surface roughness of an everolimus coated disc with no plasma (0 V) and everolimus coated disc with plasma at 90 V ($p = 0.126$), indicating that the morphology was not affected by the deposition of the everolimus coating.

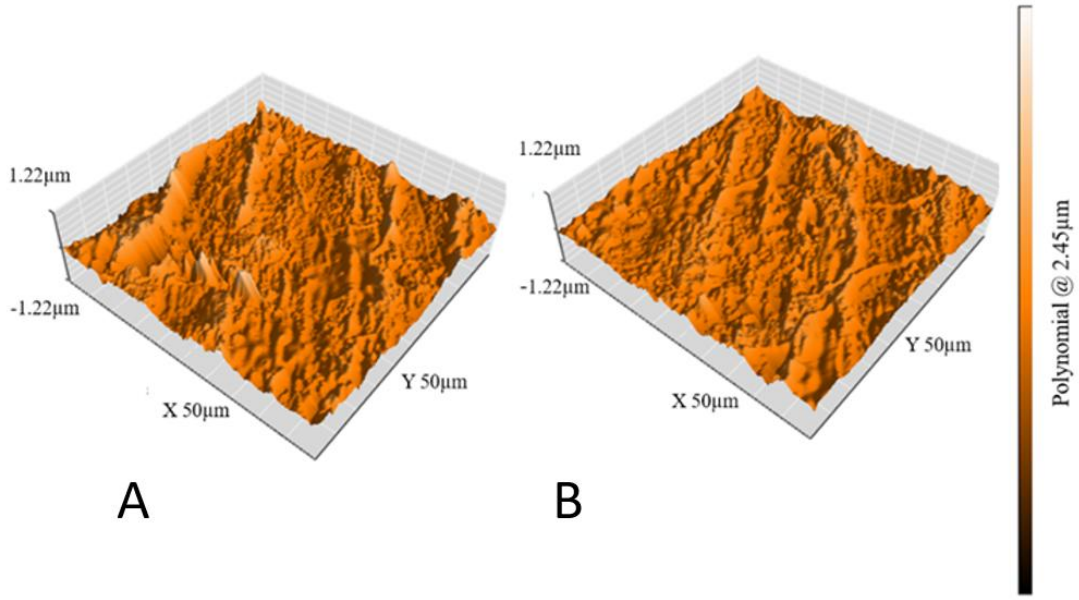


Figure 37: AFM scans of (A) wet deposited everolimus on a titanium disc and (B) plasma deposited (90 V) everolimus on a titanium disc.

Table 13: Atomic force microscopy results of a blank titanium disc, everolimus coated disc without plasma (0 V) and with plasma (90 V). Data is expressed in nm and represents +/- standard deviation, n= 3.

	Blank Ti disc	**Everolimus 0 V**	**Everolimus 90 V**
Average surface roughness	72 ± 9 nm	77 ± 11 nm	90 ± 7 nm

4.2 Coating Study 1: evaluating everolimus coated samples using HPLC Method 1.

4.2.1 (Method 1) Establishment of a RP- HPLC method for everolimus detection and quantification

The RP-HPLC method 1 is described in Table 10. This method was evaluated for its ability to detect and quantify everolimus. The everolimus standard (1 mg/mL) eluted at approximately 7.5 minutes, displaying its characteristic tautomer peak (Figure 38).

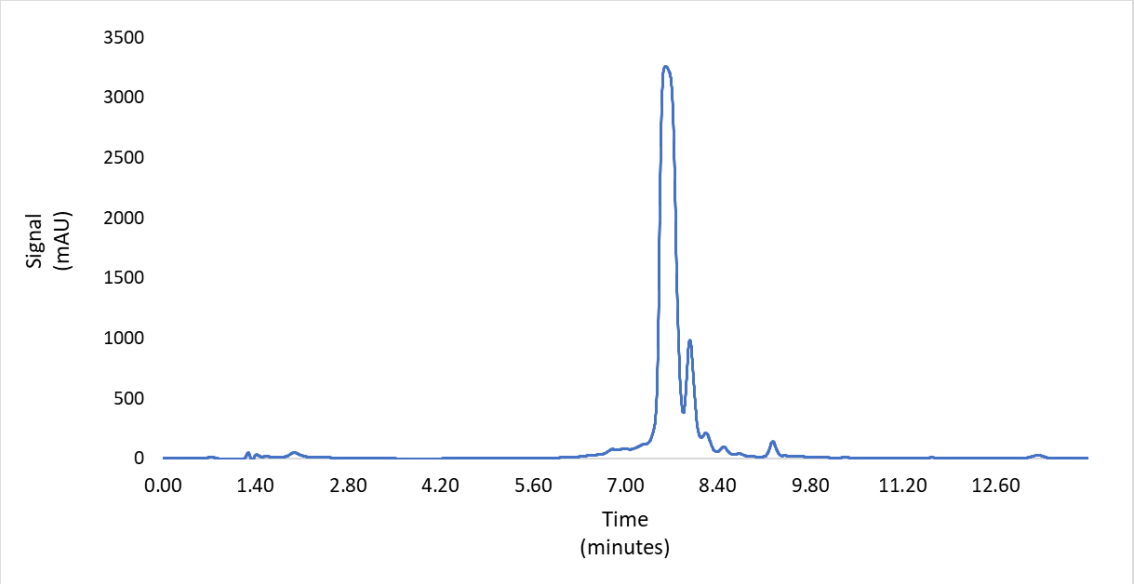


Figure 38: Representative chromatogram for 1 mg/ mL everolimus standard run using the RP-HPPLC method for study 1, (Method 1). Elution of everolimus at 7.4 minutes.

Next, the linearity of the UV response with changes in everolimus concentration was determined. A linear regression analysis of everolimus standards over the concentration range of 5 µg/ mL -250 µg/ mL showed an excellent linearity with an R^2 value of 0.9998 (Figure 39). This method had a limit of detection (LOD) of 3.01 µg/mL and a limit of quantification (LOQ) of 9.11 µg/mL. This method was applied to analyse the eluted everolimus from titanium discs, which were coated according to the parameters in Study 1 (Table 7).

$$\boldsymbol{LOD = \frac{3.3\ x\ \sigma}{S}}$$

Table 14: LOD calculation for HPLC method 1.

LOD		Value in calculation
3.3	Constant	3.3
σ	Standard deviation of response	9.55
S	S = Slope of the calibration curve	10.487

$$LOQ = \frac{10\ x\ \sigma}{S}$$

Table 15: LOQ calculation for HPLC method 1.

LOQ		Value in calculation
10	Constant	10
σ	Standard deviation of response	9.55
S	S = Slope of the calibration curve	10.487

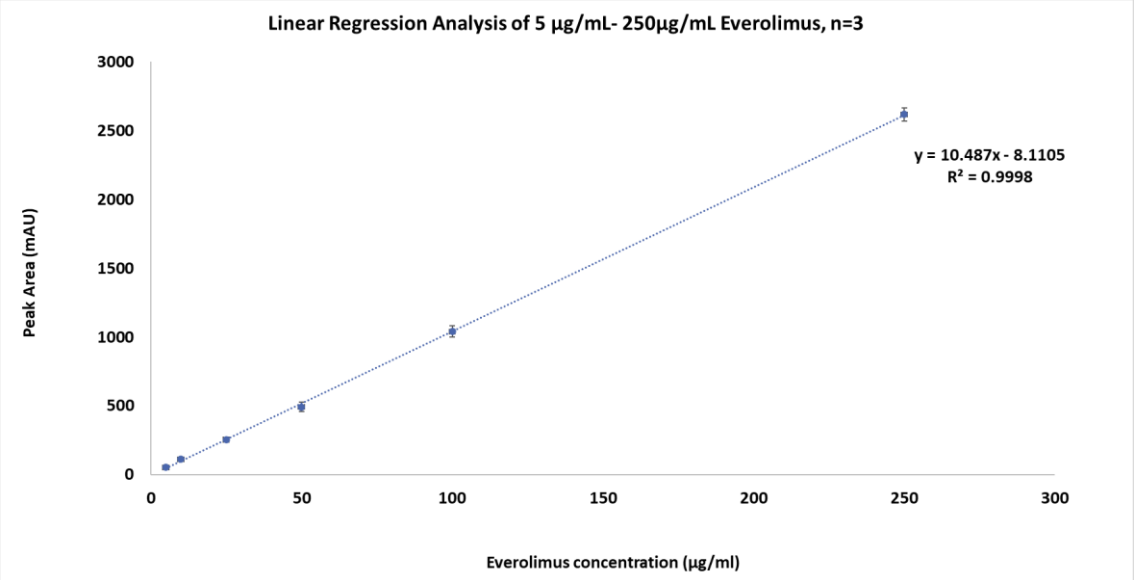


Figure 39: Linear regression of HPLC peak area of everolimus standards against concentration over the range 5- 250 µg/mL.

4.2.2 (Method 1) Quantification of everolimus deposited on coated discs.

Titanium samples were coated with a 10 mg/mL everolimus solution using two methods: wet deposition without plasma (0 V) and plasma deposition at 90 V. The effect of adding BHT at 5% and 10% to the everolimus coatings was also studied. Table 16 shows the everolimus concentration recovered from both sides of the titanium discs (3.54 cm^2 surface area). The expected concentration per 1 mL sample was 40 µg based on two discs, i.e. 20 µg per disc. The deposition rate calculations for the BioDep™ plasma unit are outlined in Table 8. Recovered concentrations ranged from 10 ± 2 µg to 19 ± 2 µg per disc.

Table 16: Quantification of the average found concentration of everolimus (µg/disc) ± standard deviation of samples deposited with no plasma (0V), or with plasma at 90 V. The inclusion of BHT at 5% and 10% w/w was also investigated, n=3.

Everolimus coating solution 10 mg/ mL	**Average mass calculated (µg/disc)**	**RSD %**	**Percentage theoretical mass**
0 V	14 ± 2	13%	72% ± 9%
90 V	14 ± 2	15%	69% ± 10%
5% BHT 0 V	19 ± 1	8%	93% ± 6%
5% BHT 90 V	10 ± 2	24%	50% ± 12%
10% BHT 0 V	12 ± 6	49%	58% ± 28%
10% BHT 90 V	13 ± 4	27%	66% ± 18%

A visual representation of the everolimus mass (µg/disc) detected in each sample can be seen in Figure 40, with the red line representing the theoretical concentration expected (20 µg/disc). Variability in the deposition efficiency of the BioDep™ unit explains the error bars extending above this theoretical value.

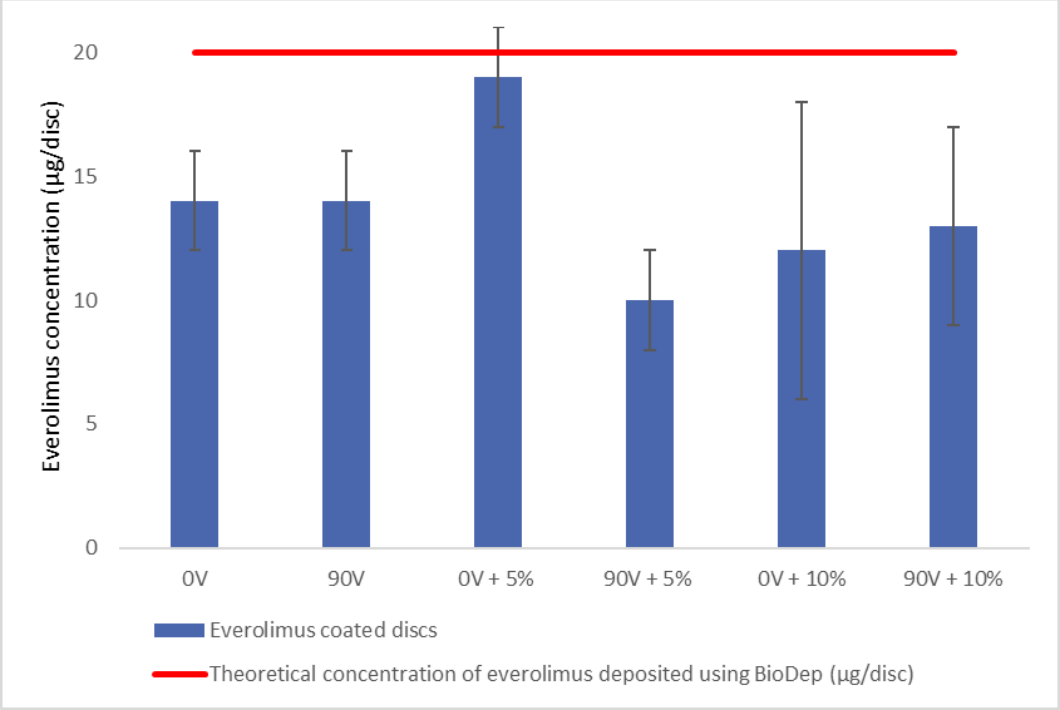


Figure 40: Average everolimus mass eluted (µg/disc) ± standard deviation, deposited on samples coated by (i) wet deposition (0V) (ii) plasma deposition (90 V) and (iii) with the addition of 5% or 10% BHT. The theoretical everolimus mass per disc is represented by the red line (20 µg/disc).

Each sample was compared to the theoretical mass per disc. The highest recovery (94%) was observed for wet deposited everolimus with 5% BHT (19 ± 2 μg/disc). However, recovery from the plasma deposited (90 V) sample dropped 50% (10 ± 2 μg/ disc). Wet deposited everolimus with 10% BHT had a lower recovery than without BHT (58%, 12 ± 6 μg/ disc). Plasma deposition (90 V) with 10% BHT had an improved recovery (66%, 13 ± 4 μg/ disc). Everolimus without BHT had high recoveries for both wet deposited (71%) and plasma deposited (69%). High variability indicated by the error bars, especially for 5% BHT, suggests inconsistent coating efficiencies. No statistically significant effects were found for deposition method ($p = 0.119$) or BHT concentration ($p = 0.54$). However, an interaction between plasma voltage and BHT concentration was significant ($p = 0.033$), prompting further analysis with Tukey post-hoc analysis. Tukey tests concluded there was no statistically significant effect between voltage and concentration on BHT. There was no overall effect of either factor, but there is a crossover effect, which means the effect of the BHT on the concentration of everolimus found is opposite, depending on the voltage used for deposition (119).

During sample analysis, the retention time of the drug gradually shifted with each run, which had not occurred during method validation. Although there was no sample carryover and injection washes were effective, the retention time still shifted, with everolimus eluting earlier each time. Despite this, the peak shape remained consistent. However, issues arose when the proposed drug peak started eluting between 3-4 minutes, as smaller peaks were present here. As a result, a second HPLC method (Method 2) was developed and used in Study 2, with adjusted coating parameters (Table 8).

4.3 Coating Study 2: evaluating everolimus coated samples using HPLC Method 2.

4.3.1 (Method 2) Establishment of a RP- HPLC method for everolimus detection, and quantification.

A second HPLC method was implemented due to the lack of reliability of the RP-HPLC method in Study 1 (Method 1), which resulted a drift in retention times during sample analysis. To address this, the RP-HPLC method was modified to improve reliability. Additionally, it was also decided to increase the concentration of everolimus deposited (to 20 mg/mL), as well as adjusting the coating parameters to optimise drug loading onto the discs. Further, with adjustments to the BioDep^{TM} coating parameters (Table 7), Study 2 resulted in improved changes in the everolimus concentration deposited (Table 8). Samples were analysed using HPLC Method 2 (Table 10).

Employing the amended RP-HPLC method the everolimus standards eluted between 12.04 and 12.95 minutes and had the tautomer peak shape, Figure 41.

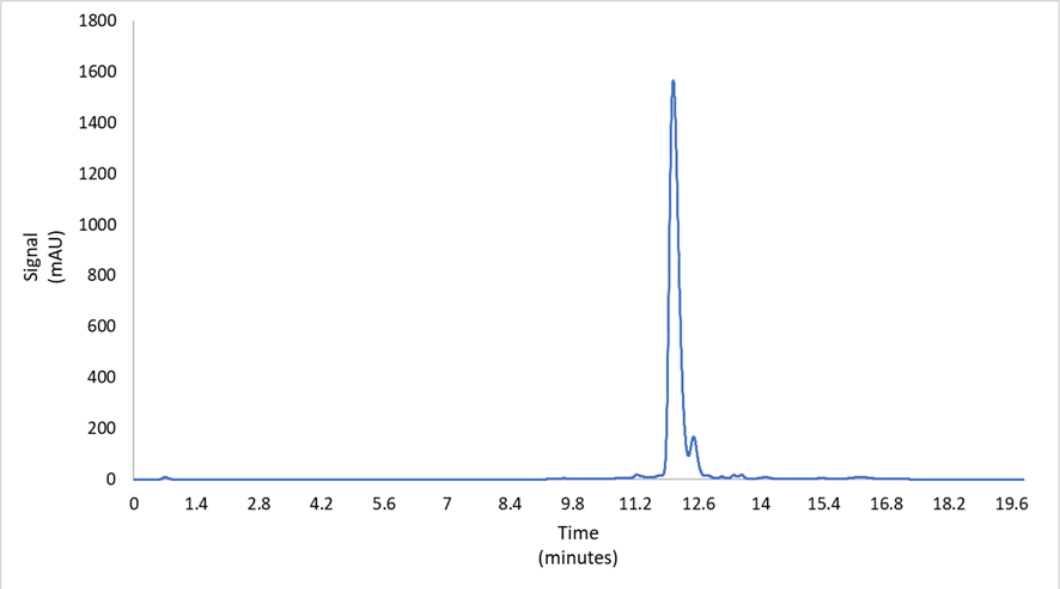


Figure 41: Representative everolimus standard (500 µg/ mL) chromatogram, peak eluting at 12.2 minutes using HPLC Method 2.

The everolimus sample subjected to thermal degradation eluted at 12.5 minutes without the formation of new peaks or the loss or alteration of existing ones (Figure 42). This suggests that the 'degraded' sample was not actually degraded, and that everolimus is more stable than initially anticipated.

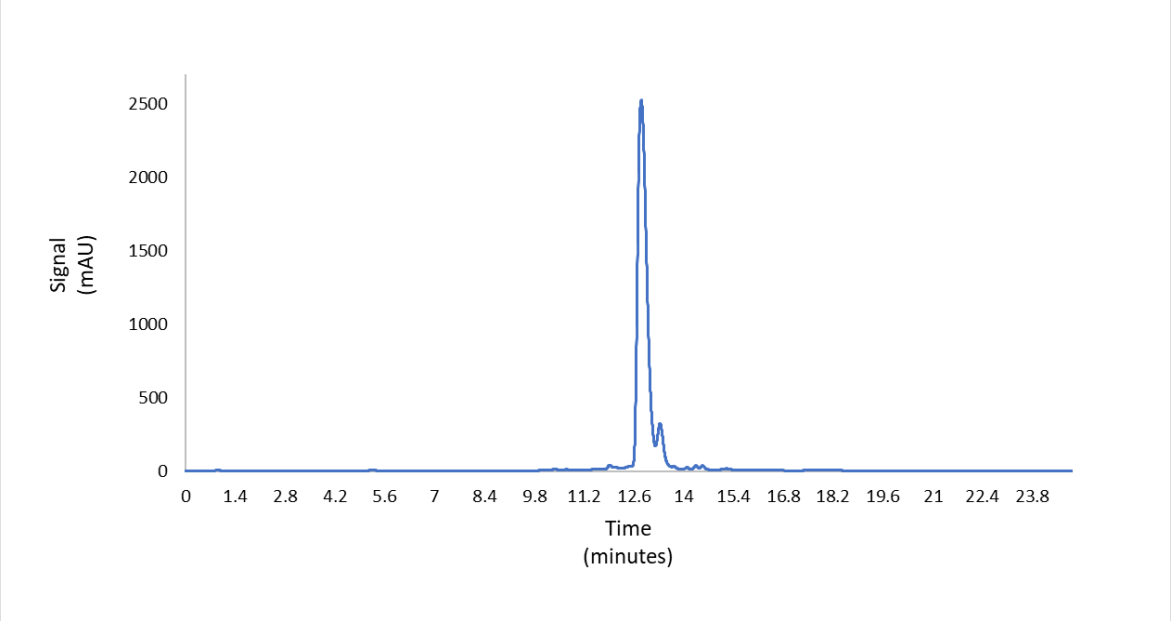


Figure 42: Thermally degraded everolimus (500 µg/mL) with everolimus peak eluting at 12.5 minutes similar to everolimus standard which did not undergo thermal degradation.

A calibration curve for determining everolimus concentration in samples was prepared over the range of 5- 500 µg/mL, and yielded an R^2 value of 0.9999 (Figure 43). It is important to note the differences in the limits of detection (LOD) and quantification (LOQ) compared to HPLC Method 1, as outlined in Table 19.

$$\boldsymbol{LOD = \frac{3.3\ x\ \sigma}{S}}$$

Table 17: LOD calculation for HPLC method 2.

LOD		**Value in calculation**
3.3	Constant	3.3
σ	Standard deviation of response	2
S	S = Slope of the calibration curve	67.221

$$LOQ = \frac{10\ x\ \sigma}{S}$$

Table 18: LOQ calculation for HPLC method 2.

LOQ		Value in calculation
10	Constant	10
σ	Standard deviation of response	2
S	S = Slope of the calibration curve	67.221

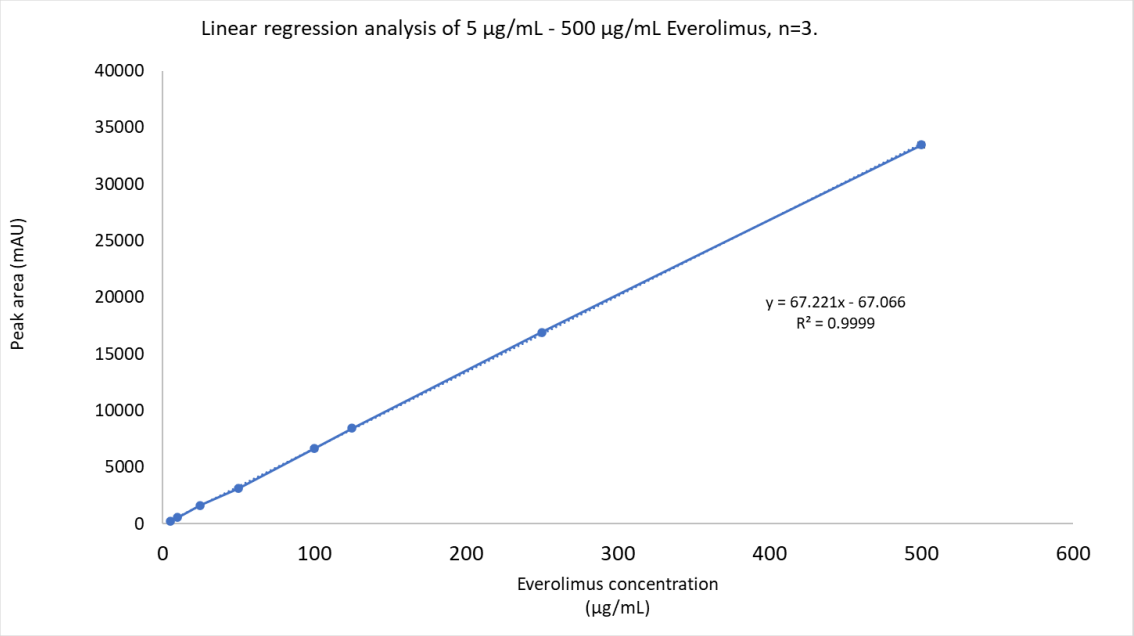


Figure 43:HPLC Method 2 linear regression of everolimus standards in the range 5-500 µg/ mL used for analysis of samples in Study 2. Data represents the average peak area (mAU) and standard deviation of each standard, n=3. Note: the error bars are so small they are not visible.

Table 19: The improvement in LOD and LOQ in HPLC Method 2 in comparison to HPLC Method 1.

Parameter	HPLC Method 1	HPLC Method 2	Difference
LOD	3.01 µg/mL	0.098 µg/mL	2.91 µg/mL
LOQ	9.11 µg/mL	0.30 µg/mL	8.81µg/mL

4.3.2 (Method 2) Quantification of everolimus mass eluted from wet coated discs (0 V) and plasma coated discs (90 V).

In the second coating study, modifications to the formulation method and process parameters were implemented to address the low levels of coating deposition observed in Study 1. The concentration of everolimus in the coating solution was increased from 10 mg/mL (Study 1) to 20 mg/mL. Titanium samples were coated with a 20 mg/mL everolimus solution using different deposition methods: wet deposition with no plasma (0 V), and plasma deposition at 90 V. The impact of adding BHT at 5% and 10% to the everolimus coatings was also investigated. All samples were analysed in triplicate (n=3).

Table 20: Average everolimus mass (µg/ disc) ± standard deviation eluted from discs which were coated with everolimus and various levels of BHT (0%, 5%, 10%), via wet deposition (0 V) and plasma deposition (90 V) *(n=3).*

Everolimus coating solution (20 mg/ mL)	**Average mass calculated (µg/ disc)**	**RSD %**	**Percentage theoretical mass**
0 V	65 ± 13	19%	62% ± 12%
90 V	47 ± 4	8%	45% ± 4%
5% BHT 0 V	37 ± 5	14%	35% ± 5%
5% BHT 90 V	58 ± 4	6%	55% ± 3%
10% BHT 0 V	67 ± 1	3%	64% ± 1%
10% BHT 90 V	59 ± 8	14%	56% ± 7%

The theoretical mass of everolimus deposited per disc was determined to be 105 µg based on deposition rate calculations for the BioDep™ unit (Table 8). The average recovered concentrations of everolimus per disc ranged from 37 ± 5 µg to 67 ± 1 µg. In Figure 44, the theoretical concentration of everolimus deposited (105 µg/disc) is represented by a red line, allowing comparison with the recovered concentrations. Plasma deposition resulted in a decrease in the recovered everolimus concentration, from 65 µg (0 V) to 47 µg (90 V). However, the presence of 10% BHT preserved everolimus, with 58 µg recovered with plasma (90 V) and 67 µg without plasma (0 V). The addition of 5% BHT

also led to a slight increase in recovery to 58 μg for plasma deposited samples. A two-way ANOVA revealed that the voltage (0 V vs 90 V) did not significantly affect the everolimus concentrations recovered ($p = 0.57$). However, the concentration of BHT had a significant effect ($p = 0.006$), and a significant interaction was observed between voltage and BHT concentration ($p = 0.008$). Tukey post-hoc analysis was conducted to explore this interaction further.

The difference in everolimus concentration between the wet deposition at 0% BHT and 5% BHT was significant, with the 5% BHT sample yielding a lower concentration. A significant difference was found between 5% and 10% BHT at 0 V. A significant difference occurred at 5% BHT, where 90 V yielded a higher everolimus concentration. This result was unexpected, as it was hypothesised that BHT would have a positive effect regardless of voltage. It is possible that the 5% BHT sample at 0 V experienced issues with drug loading or elution. Notably, the concentration difference between 0 V and 90 V at 0% BHT was close to the critical value ($q = 4.54$), suggesting that a larger study may help confirm this finding. These results are summarised in Table 33.

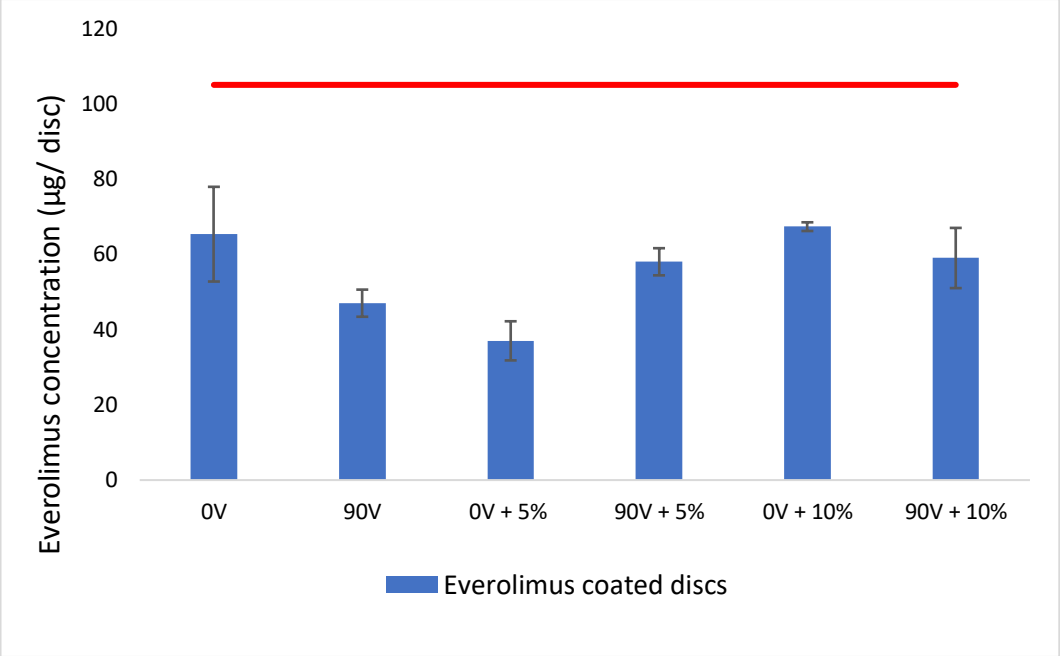


Figure 44: Average everolimus mass eluted (µg/ disc) ± standard deviation, samples coated by (i) wet deposition (0V) (ii) plasma deposition (90 V) and (iii) with the addition of 5% or 10% BHT. The theoretical mass per disc is represented by the red line (105 µg/ disc).

4.3.3 (Method 2) Analysis of everolimus degradation (tautomer peak ratio) eluted from wet coated discs (0 V) and plasma coated discs (90 V).

The extent of everolimus degradation was assessed by evaluating the peak area of the everolimus tautomer peak as a percentage of the total peak area of all other chromatogram peaks. Degradation was defined as a reduction in the tautomer peak area, coupled with an increase in the areas of other peaks or the appearance of new peaks. The average percent tautomer for each sample and standard is presented in Table 21.

Table 21: Average percentage everolimus tautomer peak ± standard deviation, present in various everolimus samples and standards (500 µg/mL).

Sample	Average everolimus tautomer peak ± standard deviation	Relative Standard Deviation between samples
500 µg/mL everolimus standard	98 ± 0.31%	0.31%
500 µg/mL everolimus degraded	95 ± 0.40%	0.43%
20 mg/mL everolimus 0 V	95 ± 0.58%	0.61%
20 mg/mL everolimus 90 V	93 ± 1.16%	1.25%
20 mg/mL everolimus 0 V + 5% BHT	94 ± 0.29%	0.31%
20 mg/mL everolimus 90 V + 5% BHT	94 ± 0.40%	0.43%
20 mg/mL everolimus 0 V + 10% BHT	94 ± 0.40%	0.43%
20 mg/mL everolimus 90 V + 10% BHT	93 ± 0.06%	0.06%

A visual representation of these percentages is shown in Figure 45, where a red line at 98 ± 0.31% indicates the tautomer percentage for the 500 µg/mL everolimus standard, which reflects the 98% purity of the everolimus sample sourced from Kemprotech Ltd (Table 6). In contrast, the blue bars represent the various samples, including the thermally degraded 500 µg/mL control. As depicted in Figure 45, all samples deposited through the BioDep™ system, as well as the 'degraded' control, exhibited a lower everolimus tautomer peak percentage compared to the everolimus standard. However, initial RP-HPLC analysis with HPLC Method 2 (section 4.3.1), suggested that the thermally degraded sample did not undergo significant changes.

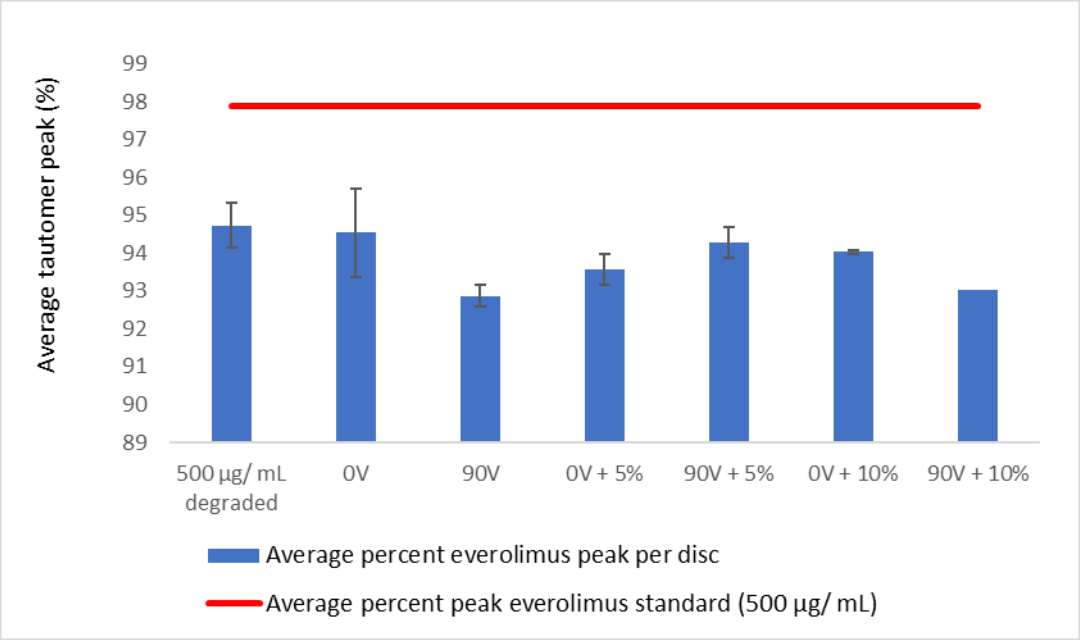


Figure 45: Average everolimus (20 mg/mL) tautomer peak percent ± standard deviation, present in various eluted samples coated by (i) wet deposition (0V) (ii) plasma deposition (90 V) and (iii) with the addition of 5% or 10% BHT. A 500 µg/mL degraded everolimus control is also present, while the average tautomer peak percent in an everolimus standard (500 µg/mL) is represented by the red line.

A paired t-test revealed that forced degradation had a statistically significant effect on the percent tautomer peak compared to the non- degraded 500 µg/mL standard (t-stat = 35.53, t-crit= 2.92). A two-way ANOVA was conducted to assess differences in the percent tautomer peaks among the coated samples. The deposition method (0 V or 90 V) had a statistically significant effect on the percent tautomer ($p = 0.036$), while the BHT concentration did not ($p = 0.546$). However, a significant interaction between voltage and BHT concentration was observed ($p = 0.013$), suggesting that the effect of voltage on the percent tautomer was dependent on the BHT concentration used. Given this interaction, a Tukey post-hoc analysis was performed to examine specific group differences, this data is summarised in

Table *35* (Supplementary information), with no statistically significant difference present.

The degraded sample proved more resistant to degradation than anticipated, indicating that everolimus is more stable than previously thought. No new peaks were observed, nor were any peaks lost in the thermally degraded everolimus sample when compared to the standard, suggesting the everolimus did not undergo measurable degradation, and a new approach to preparing a degraded control is needed.

5 Discussion

The outcomes of this research provide valuable insights into the use of a cold atmospheric plasma (CAP) system for deposition of everolimus coatings onto titanium substrates as well as the evaluation of drug loading. To our knowledge, this is the first ever time that the active pharmaceutical ingredient (API) everolimus has been successfully deposited using a cold atmospheric plasma (CAP) system. Historically, the primary methods for coating drugs like everolimus have been spray coating, dip coating and plasma enhanced chemical vapour deposition (PECVD) (120,121). While PECVD uses a lower temperature, it requires more controlled environments compared to CAP, which can be performed at atmospheric pressure and room temperature (120).

This study successfully demonstrated the deposition of everolimus onto titanium discs using the BioDep^{TM} system, and was characterised using an experimental methodology, which are outlined in Figure 46.

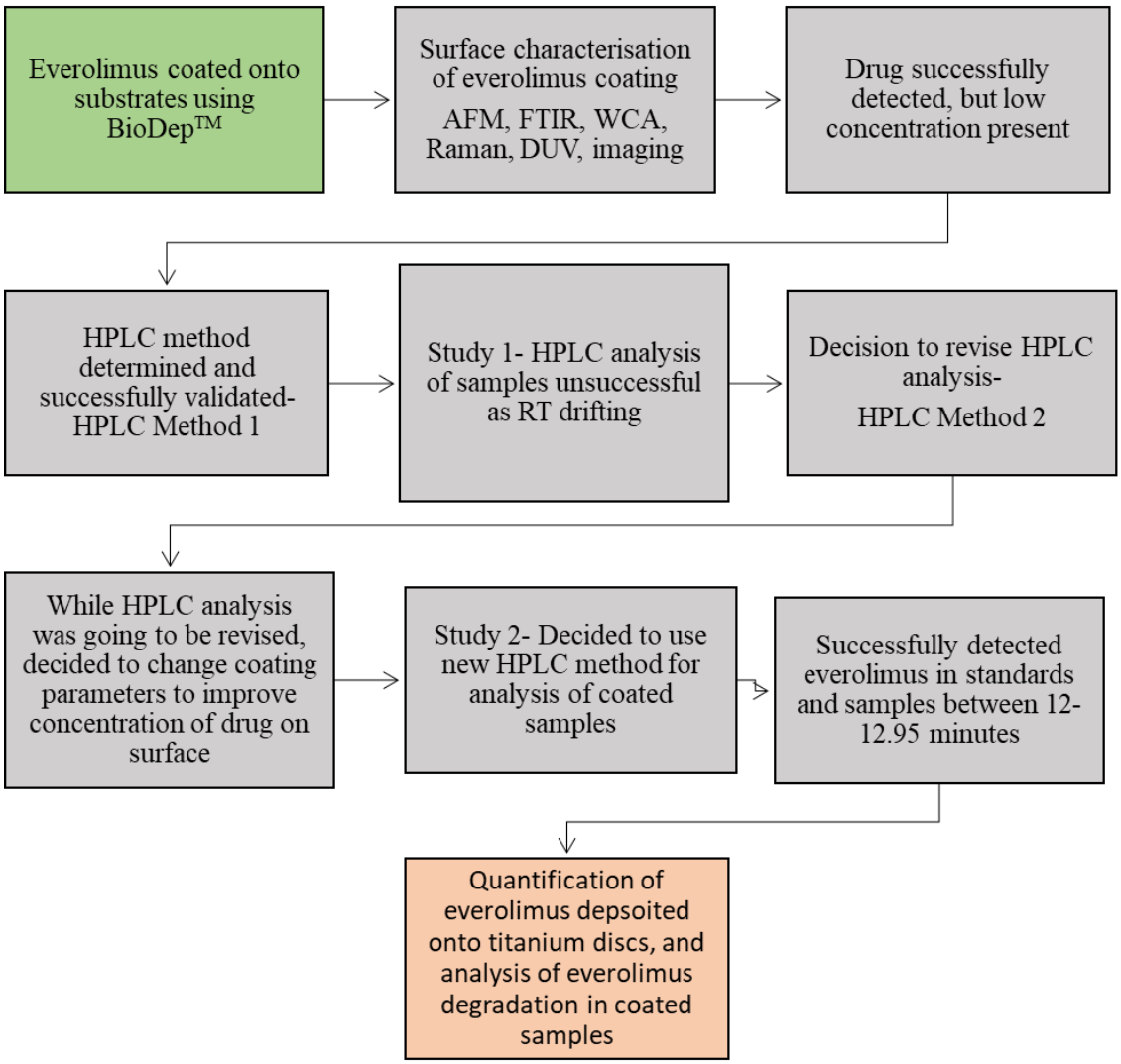


Figure 46: Flow-chart summarising the experimental methodology of this research.

The main aims of this research were achieved: to deposit everolimus using the BioDep™ system, to characterise the coatings using a range of analytical techniques, and to develop an effective HPLC method for quantifying the everolimus coating. The successful deposition of everolimus onto the titanium substrates was shown by coating rings in polarised white light imaging and confocal imaging. Characterisation of the everolimus coatings using AFM, FTIR, Raman, DUV, and WCA provided key insights into the uniformity and efficiency of the coating. Notably, the deposition process used to deposit everolimus did not significantly affect the surface topography of the substrates, AFM

indicated that the surface roughness remained consistent across both wet and plasma deposited everolimus. Water contact angle (WCA) results indicated that the coating procedure altered the titanium surface chemistry and resulting in an overall increase in surface hydrophilicity. Minor differences in WCA were noted between coating procedures and coating with and without BHT, however, these differences may be attributed to the variability in coating coverage observed by chemical image analysis.

Raman spectroscopy and DUV analysis confirmed the successful deposition of everolimus onto the titanium substrates, although lower intensities of the characteristic 1640 cm^{-1} Raman peak suggested a lower concentration of everolimus compared to the pure drug powder, which is expected. DUV mapping confirmed the drugs presence but indicated some variability in deposition efficiency. There were no significant signs of degradation, whether due to plasma exposure or oxidation, as reported in similar studies (122). However, further optimisation is necessary to ensure consistency across samples.

For quantification, a reverse phase HPLC (RP-HPLC) method was validated (Method 1) based on the Ph. Eur. Monograph (106). While the method was stable during validation, issues such as retention time drift led to inaccuracies during sample analysis, suggesting a revision of the RP-HPLC (Method 2). In parallel, it was decided to optimise the coating study to try and increase the amount deposited. Consequently, in order to increase the concentration of everolimus on the disc from 20 μg/disc (Study 1) to 105 μg/disc (Study 2), the concentration of everolimus in the coating solution was doubled and the coating parameters were optimised, leading to the coating research being sub-classified into coating Study 1 and Study 2.

In the RP-HPLC analysis of coated discs (Method 2), everolimus concentrations on the discs ranged from 37 ± 5 to 67.1 μg/disc, with the highest percent recovery of 64%. Statistical analysis revealed that the deposition method (0 V or 90 V) did not significantly impact drug recovery, though the concentration of BHT did (Table 33). Specifically, a significant difference was observed between 0% and 5% BHT at 0 V, where the 5% BHT group had a lower concentration of everolimus. Additionally, at 90 V, the samples with 5% BHT led to a higher drug recovery compared to those at 0 V. The interaction between deposition method and BHT concentration was statistically significant, indicating that their combined effect influences drug recovery. The only statistically significant interactions consisted of the wet deposit (0 V) with 5% BHT. This result was unexpected, as BHT was hypothesised to enhance recovery and not hinder it, especially during wet deposition. These findings suggest potential issues with drug loading or elution efficiency for the 5% BHT wet deposits (0 V) requiring investigation.

Everolimus tautomer peak as a percentage of overall peak area was determined as an indicator of its chemical stability after coating. There were no statistically significant differences in the everolimus tautomer peak percentages between samples, whether deposited with or without plasma, regardless of BHT concentration. This indicates that the plasma deposition process did not alter the everolimus. However, there was a significant difference in everolimus concentration (μg/disc) detected for wet deposition with 5% BHT compared to other groups. Since the tautomer peak percentages were consistent across samples, the concentration variations (0 V, 5% BHT) are likely due to drug loading or elution issues rather than degradation.

It should be noted due to time constraints, RP-HPLC Method 2 for quantifying samples in Study 2 was not validated which is a limitation of the study. Despite this limitation, the

overall characterisation studies provide a strong foundation for future research focused on optimising everolimus deposition and improving drug elution from substrates.

Overall, the findings indicate that while the BioDep™ system can effectively deposit everolimus onto titanium substrates, further optimisation of the deposition process is necessary to improve the consistency of drug loading and recovery. Plasma deposition (90 V) yielded results comparable to wet deposition (0 V), with both methods depositing between 35 μg and 65 μg of everolimus per disc.

These findings position both methods as viable candidates for future research on medical device coatings, such as drug-eluting stents. Future research should focus on optimising the coating method to ensure higher and more consistent drug deposition onto the samples. Investigating liquid flow rate from the syringe pump may help identify potential errors in flow control, while studying evaporation levels could provide insights into how the solution might change during the coating process. Additionally, increasing the concentration of the everolimus solution and further slowing the coating speed could ensure more uniform coverage of the titanium discs. Given the successful deposition of everolimus using the BioDep™ system, there are several avenues for refining the coating process.

The drug recovery study also presents opportunities for optimisation. Future studies could examine:

- The validation of the recovery method through the use of spiked samples,
- Whether any residual drug remains on the discs after elution or possibly on the acrylic tube of the BioDep™ unit after coating,

In parallel, it would be important to investigate the temporal release of everolimus over specific time intervals.

As this research progresses, it could eventually lead to cell culture studies to evaluate the biological effects of the everolimus coating. Cells lines such as HepG2 or HUVEC could be used to investigate cytotoxicity or other relevant biological responses to the coated samples.

6 Conclusions

This study successfully demonstrated the deposition of everolimus onto titanium substrates using the BioDep^{TM} cold atmospheric plasma (CAP) system, marking a significant advancement in drug coating technologies. The deposition was confirmed by Raman spectroscopy, DUV mapping, and RP-HPLC analysis, with results showing comparable drug recovery between wet deposition (0 V) and plasma deposition (90 V). The successful deposition of drug that showed no evidence of degradation highlights the viability of the CAP process for pharmaceutical applications. Despite some variability in drug concentration and recovery, the absence of significant surface morphology changes (as indicated by AFM analysis) support the effectiveness of the plasma deposition. However, further optimisation is required, particularly regarding the drug loading efficiency, and further investigation into the role of BHT in reducing its degradation. These findings provide a strong foundation for future research aimed at enhancing the consistency and efficiency of everolimus coatings, especially in the development of drug eluting stents and other medical devices.

7 Learning outcomes

Throughout this research, I gained extensive knowledge and skills through presentations, training sessions, and on-on-one interactions with lecturers, as well as by presenting my own findings through posters and oral presentations. Working with TheraDep Ltd provided access to state-of-the-art facilities and experts in plasma deposition, enhancing my understanding of the unique systems and techniques employed in this field.

The primary goal of my research was to develop a deposition process for coating everolimus onto titanium discs, conduct comprehensive surface characterisation using advanced analytical techniques, and establish a HPLC method to quantify everolimus loading and elution. The results demonstrated successful deposition and detection of everolimus using RP-HPLC.

During this process, I significantly developed my research and technical skills, particularly in surface characterisation using AFM, FTIR, WCA, RP-HPLC, and interpreting Raman spectroscopy, and DUV mapping. Learning to operate new characterisation equipment broadened my technical expertise and enabled me to interpret data more comprehensively. I also built upon my undergraduate knowledge of HPLC, learning to develop and optimise a method specifically tailored to the detection and quantification of an active pharmaceutical ingredient (API).

My understanding of method validation and optimisation deepened through the challenges associated with developing an effective HPLC method. Additionally, I gained an insight into industry standard methods for coating stents with pharmaceutical agents.

Throughout this research, I demonstrated several key learning outcomes. I enhanced my critical thinking and problem-solving skills by adapting to unforeseen challenges and devising innovative solutions. Meeting strict deadlines required effective time

management, allowing me to balance experimental work with tight schedules. These experiences improved my ability to prioritise tasks, manage workloads, and maintain a high standard of work under pressure.

Overall, this research has strengthened my technical abilities, problem solving, time management, and adaptability. These outcomes not only contributed to the successful completion of my thesis but have also prepared me for future challenges in both research and industry settings.

8 References

1. Bittencourt JA. Fundamentals of Plasma Physics [Internet]. New York, NY: Springer New York; 2004 [cited 2024 Oct 2]. Available from: http://link.springer.com/10.1007/978-1-4757-4030-1

2. Phase | Definition & Facts | Britannica [Internet]. [cited 2023 Apr 6]. Available from: https://www.britannica.com/science/phase-state-of-matter

3. Fridman A, editor. Introduction to Theoretical and Applied Plasma Chemistry. In: Plasma Chemistry [Internet]. Cambridge: Cambridge University Press; 2008 [cited 2023 Mar 1]. p. 1–11. Available from: https://www.cambridge.org/core/books/plasma-chemistry/introduction-to-theoretical-and-applied-plasma-chemistry/AB58BE938A0670916E4B6EB314F648A6

4. Sakudo A, Yagyu Y, Onodera T. Disinfection and Sterilization Using Plasma Technology: Fundamentals and Future Perspectives for Biological Applications. Int J Mol Sci. 2019 Oct 21;20(20):5216.

5. Schram DC. Is plasma unique? The presence of electrons and the importance of charge. Plasma Sources Sci Technol. 2009 Feb 1;18(1):014003.

6. Boenig H. Plasma Science and Technology. Cornell University Press; 2019. 309 p.

7. Rahman Z, Rahman H, Rahman A. Classification and Generation of Atmospheric Pressure Plasma and Its Principle Applications. 2014;2(2).

8. Vacuum Pressure | Understanding Vacuum Cup Products [Internet]. [cited 2023 Apr 6]. Available from: https://www.edcousa.net/vacuum-training/vacuum-pressure

9. Mathew P, George J, Mathews T S, Kurian PJ. Experimental verification of modified Paschen's law in DC glow discharge argon plasma. AIP Adv. 2019 Feb 20;9(2):025215.

10. Neralla S. Chemical Vapor Deposition: Recent Advances and Applications in Optical, Solar Cells and Solid State Devices. BoD – Books on Demand; 2016. 292 p.

11. Subedi DP, Joshi UM, Wong CS. Dielectric Barrier Discharge (DBD) Plasmas and Their Applications. In: Rawat RS, editor. Plasma Science and Technology for Emerging Economies [Internet]. Singapore: Springer Singapore; 2017 [cited 2025 Aug 17]. p. 693–737. Available from: http://link.springer.com/10.1007/978-981-10-4217-1_13

12. Shahbazi Rad Z, Abbasi Davani F. Measurements of the electrical parameters and wound area for investigation on the effect of different non-thermal atmospheric pressure plasma sources on wound healing time. Measurement. 2020 Apr 1;155:107545.

13. Simon AH. Chapter 3 - Sputter processing. In: Schepis D, Seshan K, editors. Handbook of Thin Film Deposition (Fifth Edition) [Internet]. Elsevier; 2025 [cited 2025 Aug 17]. p. 93–140. Available from: https://www.sciencedirect.com/science/article/pii/B9780443135231000119

14. Douroumis D, Onyesom I. Novel Coating Technologies of Drug Eluting Stents. In: Zilberman M, editor. Active Implants and Scaffolds for Tissue Regeneration [Internet]. Berlin, Heidelberg: Springer Berlin Heidelberg; 2011 [cited 2024 Jul 24]. p. 87–125. (Studies in Mechanobiology, Tissue Engineering and Biomaterials; vol. 8). Available from: https://link.springer.com/10.1007/8415_2010_54

15. Tang JZ, Rhodes NP. - Release-Controlled Coatings. In: Biological and Biomedical Coatings Handbook. CRC Press; 2011.

16. Udrițe AS, Burdușel AC, Niculescu AG, Rădulescu M, Grumezescu AM. Coatings for Cardiovascular Stents—An Up-to-Date Review. Int J Mol Sci. 2024 Jan;25(2):1078.

17. Nishi Y, Doering R. Handbook of Semiconductor Manufacturing Technology. CRC Press; 2000. 1186 p.

18. Doll GL, Mensah BA, Mohseni H, Scharf TW. Chemical Vapor Deposition and Atomic Layer Deposition of Coatings for Mechanical Applications. J Therm Spray Technol. 2010 Jan 1;19(1):510–6.

19. Plasma.com [Internet]. [cited 2022 Oct 6]. Vacuum technology. Available from: https://www.plasma.com/en/vacuumtechnology/

20. Vacu um Plasma Overview presented by Plasma Etch, Inc. [Internet]. [cited 2022 Oct 6]. Available from: https://www.plasmaetch.com/vacuum-plasma.php

21. AZoM.com [Internet]. 2001 [cited 2023 Apr 7]. Vacuum Plasma Processing. Available from: https://www.azom.com/article.aspx?ArticleID=912

22. Bárdos L, Baránková H. Plasma processes at atmospheric and low pressures. Vacuum. 2008 Oct 15;83(3):522–7.

23. Corp T. Low Pressure Plasma Systems | Thierry Corporation [Internet]. [cited 2023 Nov 30]. Available from: https://www.thierry-corp.com/low-pressure-plasma-systems

24. Bárdos L, Baránková H. Cold atmospheric plasma: Sources, processes, and applications. Thin Solid Films. 2010 Sep 30;518(23):6705–13.

25. Chang JS, Lawless PA, Yamamoto T. Corona discharge processes. IEEE Trans Plasma Sci. 1991 Dec;19(6):1152–66.

26. OIST Groups [Internet]. 2020 [cited 2023 Apr 12]. Electrocharging Face Masks with Corona Discharge Treatment. Available from: https://groups.oist.jp/nnp/electrocharge-mask

27. Messanelli F, Belan M. A Comparison Between Corona and DBD Plasma Actuators for Separation Control on an Airfoil. In: 55th AIAA Aerospace Sciences Meeting [Internet]. American Institute of Aeronautics and Astronautics; [cited 2024 Oct 2]. Available from: https://arc.aiaa.org/doi/abs/10.2514/6.2017-0395

28. Kogelschatz U. Dielectric-Barrier Discharges: Their History, Discharge Physics, and Industrial Applications. Plasma Chem Plasma Process. 2003;1(23):1–46.

29. ozone-hole-poster_hires_508.pdf [Internet]. [cited 2024 Jun 26]. Available from: https://aura.gsfc.nasa.gov/ozoneholeposter/ozone-hole-poster_hires_508.pdf

30. Production techniques [Internet]. [cited 2024 Jun 26]. Available from: https://www.primozone.com/technology/production-techniques/

31. Inc MP. Matsusada Precision. [cited 2023 Apr 6]. Dielectric Barrier Discharge | Application. Available from: https://www.matsusada.com/application/ps/dielectric_barrier_discharge/

32. Belov I, Paulussen S, Bogaerts A. Pressure as an additional control handle for non-thermal atmospheric plasma processes. Plasma Process Polym. 2017 Nov;14(11):1700046.

33. Arora V. Cold Atmospheric Plasma (CAP) In Dentistry. Dentistry [Internet]. 2013 [cited 2023 Feb 27];04(01). Available from: https://www.omicsonline.org/cold-atmospheric-plasma-cap-in-dentistry-2161-1122.1000189.php?aid=21925

34. Isbary G, Shimizu T, Li YF, Stolz W, Thomas HM, Morfill GE, et al. Cold atmospheric plasma devices for medical issues. Expert Rev Med Devices. 2013 May 1;10(3):367–77.

35. Asimakoulas L, Katsafadou M, Svarnas P, Pachis K, Kostazos N, Gazeli K, et al. Hand-sized dielectric barrier discharge reactor of floating potential electrode for cell model studies. 2015.

36. Iontophoresis [Internet]. Pinnacle Physical Therapy. [cited 2023 Feb 8]. Available from: https://pinnaclephysicaltherapyga.com/iontophoresis/

37. Iontophoresis: MedlinePlus Medical Encyclopedia [Internet]. [cited 2023 Apr 12]. Available from: https://medlineplus.gov/ency/article/007293.htm

38. Arrubla DJ. Applications of iontophoresis in studies investigating microvasculature [Internet]. [cited 2023 Apr 12]. Available from: https://blog.profil.com/blog/applications-of-iontophoresis

39. Fridman G, Brooks AD, Balasubramanian M, Fridman A, Gutsol A, Vasilets VN, et al. Comparison of Direct and Indirect Effects of Non-Thermal Atmospheric-Pressure Plasma on Bacteria. Plasma Process Polym. 2007;4(4):370–5.

40. Roth JR. Industrial Plasma Engineering. In IOP Publishing Ltd; 2001 [cited 2024 Feb 21]. Available from: http://stacks.iop.org/0750308257

41. Donnelly VM, Kornblit A. Plasma etching: Yesterday, today, and tomorrow. J Vac Sci Technol Vac Surf Films [Internet]. 2013 Sep 15 [cited 2024 Feb 21];31(5). Available from: https://www.osti.gov/biblio/22224157

42. Rossnagel SM. Sputter deposition for semiconductor manufacturing. IBM J Res Dev. 1999 Jan;43(1.2):163–79.

43. Hyun J, Lee SG, Hwang J. Application of corona discharge-generated air ions for filtration of aerosolized virus and inactivation of filtered virus. J Aerosol Sci. 2017 May;107:31–40.

44. Wypych G. DEGRADATION BY OTHER FORMS OF RADIATION. In: Wypych G, editor. PVC Degradation and Stabilization (Third Edition) [Internet]. Boston: ChemTec Publishing; 2015 [cited 2024 Feb 1]. p. 215–26. Available from: https://www.sciencedirect.com/science/article/pii/B9781895198850500091

45. Wen TY, Su JL. Corona discharge characteristics of cylindrical electrodes in a two-stage electrostatic precipitator. Heliyon [Internet]. 2020 Feb [cited 2024 Feb 1];6(2). Available from: https://www.ncbi.nlm.nih.gov/pmc/articles/PMC7033520/

46. Chu PK, Chen JY, Wang LP, Huang N. Plasma-surface modification of biomaterials. Mater Sci Eng R Rep. 2002 Mar 29;36(5):143–206.

47. Vancha AR, Govindaraju S, Parsa KV, Jasti M, González-García M, Ballestero RP. Use of polyethyleneimine polymer in cell culture as attachment factor and lipofection enhancer. BMC Biotechnol. 2004 Oct 15;4:23.

48. Suni T, Henttinen K, Suni I, Mäkinen J. Effects of Plasma Activation on Hydrophilic Bonding of Si and SiO2. J Electrochem Soc. 2002 Apr 25;149(6):G348.

49. Ranowsky A. Contact Angle and Surface Tension - A Fascinating Liaison [Internet]. [cited 2022 Oct 6]. Available from: https://www.cscscientific.com/csc-scientific-blog/how-does-contact-angle-relate-to-surface-tension

50. Approaches to design a surface with tunable wettability: a review on surface properties | SpringerLink [Internet]. [cited 2023 Apr 12]. Available from: https://link-springer-com.ucc.idm.oclc.org/article/10.1007/s10853-020-05116-1

51. Contact angle [Internet]. [cited 2024 Feb 1]. Available from: https://www.kruss-scientific.com/en/know-how/glossary/contact-angle

52. Mandal R, Singh A, Pratap Singh A. Recent developments in cold plasma decontamination technology in the food industry. Trends Food Sci Technol. 2018 Oct 1;80:93–103.

53. Bolgeo T, Maconi A, Gardalini M, Gatti D, Di Matteo R, Lapidari M, et al. The Role of Cold Atmospheric Plasma in Wound Healing Processes in Critically Ill Patients. J Pers Med. 2023 Apr 26;13(5):736.

54. Michelmore A, Steele DA, Whittle JD, Bradley JW, Short RD. Nanoscale deposition of chemically functionalised films via plasma polymerisation. RSC Adv. 2013 Jul 30;3(33):13540–57.

55. Friedrich J. Mechanisms of Plasma Polymerization – Reviewed from a Chemical Point of View. Plasma Process Polym. 2011;8(9):783–802.

56. Fotovvati B, Namdari N, Dehghanghadikolaei A. On Coating Techniques for Surface Protection: A Review. J Manuf Mater Process. 2019 Mar;3(1):28.

57. Martinu L, Zabeida O, Klemberg-Sapieha JE. Plasma-Enhanced Chemical Vapor Deposition of Functional Coatings. In: Handbook of Deposition Technologies for Films and Coatings [Internet]. Elsevier; 2010 [cited 2024 Aug 26]. p. 392–465. Available from: https://linkinghub.elsevier.com/retrieve/pii/B9780815520313000090

58. Dabees S, Mirzaei S, Kaspar P, Holcman V, Sobola D. Characterization and Evaluation of Engineered Coating Techniques for Different Cutting Tools—Review. Materials. 2022 Jan;15(16):5633.

59. Amorim M, Savio R, Santiago H, Massi M. Recent Developments on Silicon Carbide Thin Films for Piezoresistive Sensors Applications. In: Mukherjee M, editor. Silicon Carbide -

Materials, Processing and Applications in Electronic Devices [Internet]. InTech; 2011 [cited 2025 Jun 10]. Available from: http://www.intechopen.com/books/silicon-carbide-materials-processing-and-applications-in-electronic-devices/recent-developments-on-silicon-carbide-thin-films-for-piezoresistive-sensors-applications

60. O'Sullivan D, McArdle H, Ng SW, Bourke P, Forster R, O'Neill L. Deposition of Cell Culture Coatings Using a Cold Plasma Deposition Method. Appl Sci. 2020 Jan;10(19):6670.

61. Šimor M, Creyghton Y, Wypkema A, Zemek J. The Influence of Surface DBD Plasma Treatment on the Adhesion of Coatings to High-Tech Textiles. J Adhes Sci Technol. 2010 Jan 1;24(1):77–97.

62. Los A, Ziuzina D, Boehm D, Han L, O'Sullivan D, O'Neill L, et al. Efficacy of Cold Plasma for Direct Deposition of Antibiotics as a Novel Approach for Localized Delivery and Retention of Effect. Front Cell Infect Microbiol [Internet]. 2019 [cited 2023 Nov 28];9. Available from: https://www.frontiersin.org/articles/10.3389/fcimb.2019.00428

63. O'sullivan D, McArdle H, O'Reilly JA, O'Kennedy RJ, Forster R, O'Neill L. Plasma deposition of collagen for cell-culture applications. Plasma Process Polym. 2020;17(3):1900147.

64. O'Sullivan D, O'Neill L, Bourke P. Direct Plasma Deposition of Collagen on 96-Well Polystyrene Plates for Cell Culture. ACS Omega. 2020 Oct 6;5(39):25069–76.

65. O'Neill L, O'Sullivan D, Fourkas M, Tartaglia J. Evaluation of the J-Plasma Electrosurgical Device Combined with Nebulized Collagen for Burn Healing in Rodents. Plasma Med [Internet]. 2018 [cited 2023 Nov 28];8(4). Available from: https://www.dl.begellhouse.com/journals/5a5b4a3d419387fb,1a3e35964d363a91,1a26f4d57b516d57.html

66. O'Neill L, Dobbyn P, Kulkarni M, Pandit A. Wound healing using plasma modified collagen. Clin Plasma Med. 2018 Dec 1;12:23–32.

67. admin. DAIC. 2009 [cited 2024 Aug 28]. Health Canada Approves Abbott's XIENCE V Drug Eluting Stent. Available from: http://www.dicardiology.com/content/health-canada-approves-abbotts-xience-v-drug-eluting-stent

68. Costa MA, Simon DI. Molecular Basis of Restenosis and Drug-Eluting Stents. Circulation. 2005 May 3;111(17):2257–73.

69. Balloon Angioplasty [Internet]. [cited 2023 May 10]. Available from: https://www.vascularsurgeryassociates.net/contents/treatments/balloon-angioplasty

70. Williams DF. Biocompatibility pathways and mechanisms for bioactive materials: The bioactivity zone. Bioact Mater. 2022 Apr 1;10:306–22.

71. Mariani E, Lisignoli G, Borzì RM, Pulsatelli L. Biomaterials: Foreign Bodies or Tuners for the Immune Response? Int J Mol Sci. 2019 Feb 1;20(3):636.

72. Tang L, Eaton JW. Inflammatory Responses to Biomaterials. Am J Clin Pathol. 1995 Apr 1;103(4):466–71.

73. Helmus MN, Gibbons DF, Cebon D. Biocompatibility: Meeting a Key Functional Requirement of Next-Generation Medical Devices. Toxicol Pathol. 2008 Jan 1;36(1):70–80.

74. Biological evaluation of medical devices—Part 1: Evaluation and testing within a risk management process. In: ANSI/AAMI/ISO 10993-1:2018; Biological evaluation of medical devices—Part 1: Evaluation and testing within a risk management process [Internet]. AAMI; 2020 [cited 2025 Jun 18]. Available from: http://array.aami.org/doi/10.2345/9781570207556.ch1

75. Regulation - 2017/745 - EN - Medical Device Regulation - EUR-Lex [Internet]. [cited 2025 Aug 18]. Available from: https://eur-lex.europa.eu/eli/reg/2017/745/oj/eng

76. Advances in mammalian target of rapamycin kinase inhibitors: application to devices used in the treatment of coronary artery disease | Future Medicinal Chemistry [Internet]. [cited 2024 Feb 1]. Available from: https://www.future-science.com/doi/10.4155/fmc-2019-0304

77. The Sirolimus-Eluting Stent | American Journal of Cardiovascular Drugs [Internet]. [cited 2024 Jul 23]. Available from: https://link.springer.com/article/10.2165/00129784-200303030-00007

78. Meredith IT, Worthley S, Whitbourn RJ, Walters DL, Popma J, Cutlip D, et al. The next-generation Endeavor™ Resolute™ stent: 4-month clinical and angiographic results from the Endeavor™ Resolute™ first-in-man trial [Internet]. [cited 2024 Jul 24]. Available from: https://eurointervention.pcronline.com/article/the-next-generation-endeavor-resolute-stent-4-month-clinical-and-angiographic-results-from-the-endeavor-resolute-first-in-man-trial

79. Price MJ, Saito S, Shlofmitz RA, Spriggs DJ, Attubato M, McLaurin B, et al. First Report of the Resolute Onyx 2.0-mm Zotarolimus-Eluting Stent for the Treatment of Coronary Lesions With Very Small Reference Vessel Diameter. JACC Cardiovasc Interv. 2017 Jul 24;10(14):1381–8.

80. Waksman R, Barbash IM, Dvir D, Torguson R, Ben-Dor I, Maluenda G, et al. Safety and Efficacy of the XIENCE V Everolimus-Eluting Stent Compared to First-Generation Drug-Eluting Stents in Contemporary Clinical Practice. Am J Cardiol. 2012 May 1;109(9):1288–94.

81. Ding N (nadine), Pacetti SD, Tang FW, Gada M, Roorda W. XIENCE V™ Stent Design and Rationale. J Intervent Cardiol. 2009;22(s1):S18–27.

82. Dvir D, Kitabata H, Barbash IM, Minha S, Badr S, Loh JP, et al. In vivo evaluation of axial integrity of coronary stents using intravascular ultrasound: Insights on longitudinal stent deformation. Catheter Cardiovasc Interv. 2014;84(3):397–405.

83. Lasala JM, Stone GW, Dawkins KD, Serruys PW, Colombo A, Grube E, et al. An Overview of the TAXUS® Express®, Paclitaxel-Eluting Stent Clinical Trial Program. J Intervent Cardiol. 2006;19(5):422–31.

84. Whitbeck MG, Applegate RJ. Second Generation Drug-Eluting Stents: A Review of the Everolimus-Eluting Platform. Clin Med Insights Cardiol. 2013 Jul 23;7:115–26.

85. Zeller T, Brodmann M, Ansel GM, Scheinert D, Choi D, Tepe G, et al. Paclitaxel-coated balloons for femoropopliteal peripheral arterial disease: final five-year results of the IN.PACT Global Study. EuroIntervention. 2022 Dec 2;18(11):e940–8.

86. Everolimus-Eluting Stent Design, with Fluoropolymer | Abbott [Internet]. [cited 2024 Sep 30]. Available from: https://www.cardiovascular.abbott/us/en/hcp/products/percutaneous-coronary-intervention/xience-family/about/innovative-stent-design.html

87. Yazdani SK, Sheehy A, Pacetti S, Rittlemeyer B, Kolodgie FD, Virmani R. Stent Coating Integrity of Durable and Biodegradable Coated Drug Eluting Stents. J Intervent Cardiol. 2016;29(5):483–90.

88. Livingston M, Tan A. Coating Techniques and Release Kinetics of Drug-Eluting Stents. J Med Devices. 2019 May 4;10(1).

89. PubChem. Everolimus [Internet]. [cited 2023 Apr 27]. Available from: https://pubchem.ncbi.nlm.nih.gov/compound/6442177

90. Everolimus [Internet]. [cited 2023 Apr 27]. Available from: https://go.drugbank.com/drugs/DB01590

91. Klawitter J, Nashan B, Christians U. Everolimus and sirolimus in transplantation-related but different. Expert Opin Drug Saf. 2015 Jul 3;14(7):1055–70.

92. Everolimus (Oral Route) Precautions - Mayo Clinic [Internet]. [cited 2024 Feb 1]. Available from: https://www.mayoclinic.org/drugs-supplements/everolimus-oral-route/precautions/drg-20072842?p=1

93. Kirchner GI, Meier-Wiedenbach I, Manns MP. Clinical Pharmacokinetics of Everolimus. Clin Pharmacokinet. 2004 Feb 1;43(2):83–95.

94. Zanchin C, Ueki Y, Zanchin T, Häner J, Otsuka T, Stortecky S, et al. Everolimus-Eluting Biodegradable Polymer Versus Everolimus-Eluting Durable Polymer Stent for Coronary Revascularization in Routine Clinical Practice. JACC Cardiovasc Interv. 2019 Sep 9;12(17):1665–75.

95. McCarthy JR. On the development of analytical methods for percutaneous transluminal coronary angioplasty catheters and drug eluting stents [Internet] [Thesis]. 2013 [cited 2024 Feb 29]. Available from: https://aran.library.nuigalway.ie/handle/10379/3977

96. Salvadori M. Long-term outcome of everolimus treatment in transplant patients. Transpl Res Risk Manag. 2011 May;77.

97. afinitor-epar-public-assessment-report_en.pdf [Internet]. [cited 2023 May 10]. Available from: https://www.ema.europa.eu/en/documents/assessment-report/afinitor-epar-public-assessment-report_en.pdf

98. Thbayh DK, Fiser B. Computational study of synthetic and natural polymer additives — Antioxidant potential of BHA, TBHQ, BHT, and curcumin. Polym Degrad Stab. 2022 Jul 1;201:109979.

99. Phani Kumar G, Navya K, Ramya EM, Venkataramana M, Anand T, Anilakumar KR. DNA damage protecting and free radical scavenging properties of Terminalia arjuna bark in PC-12 cells and plasmid DNA. Free Radic Antioxid. 2013 Apr;3(1):35–9.

100. Jang SW, Kang MJ. Improved oral absorption and chemical stability of everolimus via preparation of solid dispersion using solvent wetting technique. Int J Pharm. 2014 Oct 1;473(1):187–93.

101. Huo Y, Zhu H, He X. Study of Butylated Hydroxytoluene Inhibiting the Coal Oxidation at Low Temperature: Combining Experiments and Quantum Chemical Calculations. ACS Omega. 2022 May 24;7(22):18552–68.

102. Olmedo R, Ribotta P, Grosso NR. Decrease of chemical and volatile oxidation indicators using oregano essential oil combined with BHT in sunflower oil under accelerated storage conditions. J Food Sci Technol. 2019 May;56(5):2522–35.

103. Gulcin İ, Alwasel SH. Metal Ions, Metal Chelators and Metal Chelating Assay as Antioxidant Method. Processes. 2022 Jan;10(1):132.

104. Olayiwola B, O'Neill F, Frewen C, Kavanagh DF, O'Hara R, O'Neill L. Cold Plasma Deposition of Tobramycin as an Approach to Localized Antibiotic Delivery to Combat Biofilm Formation. Pathogens. 2024 Apr;13(4):326.

105. TVA100 - Contact angle measuring instrument by KRÜSS GmbH | DirectIndustry [Internet]. [cited 2024 Feb 1]. Available from: https://www.directindustry.com/prod/kruess-gmbh/product-14849-815481.html

106. Ph. Eur. 2918 Test for Everolimus Impurity A on Kinetex 2.7 µm C18 (AN-1025) [Internet]. [cited 2024 Mar 15]. Available from: https://www.phenomenex.com/documents/2022/05/20/18/51/ph-eur-2918-test-for-everolimus-impurity-a-on-kinetex-27-m-c18-an1025

107. Anna Chatzi OD. The one-way ANOVA test explained [Internet]. Nurse Researcher; [cited 2024 Oct 3]. Available from: https://journals.rcni.com/nurse-researcher/evidence-and-practice/the-oneway-anova-test-explained-nr.2023.e1885/abs

108. St»hle L, Wold S. Analysis of variance (ANOVA). Chemom Intell Lab Syst. 1989 Nov 1;6(4):259–72.

109. Kim TK. T test as a parametric statistic. Korean J Anesthesiol. 2015 Nov 25;68(6):540–6.

110. Sawyer SF. Analysis of Variance: The Fundamental Concepts. J Man Manip Ther. 2009 Apr 1;17(2):27E-38E.

111. Chinna Babu P, Sundaraganesan N, Dereli Ö, Türkkan E. FT-IR, FT-Raman spectra, density functional computations of the vibrational spectra and molecular geometry of butylated hydroxy toluene. Spectrochim Acta A Mol Biomol Spectrosc. 2011 Aug 1;79(3):562–9.

112. Patil BK and PM. DEVELOPMENT AND VALIDATION OF STABILITY INDICATING ASSAY METHOD OF EVEROLIMUS AND ITS MARKETED FORMULATION. World J Pharm Life Sci [Internet]. [cited 2024 May 1];2021(VOLUME 7, SEPTEMBER ISSUE 9). Available from: https://www.wjpls.org/abstract/2368

113. Informatics NO of D and. Butylated Hydroxytoluene [Internet]. National Institute of Standards and Technology; [cited 2024 Aug 12]. Available from: https://webbook.nist.gov/cgi/cbook.cgi?ID=C128370&Type=IR-SPEC&Index=1

114. Frank O, Zukalova M, Laskova B, Kürti J, Koltai J, Kavan L. Raman spectra of titanium dioxide (anatase, rutile) with identified oxygen isotopes (16, 17, 18). Phys Chem Chem Phys. 2012 Oct 10;14(42):14567–72.

115. Ohsaka T, Izumi F, Fujiki Y. Raman spectrum of anatase, TiO2. J Raman Spectrosc. 1978;7(6):321–4.

116. Ekoi EJ, Stallard C, Reid I, Dowling DP. Tailoring oxide-layer formation on titanium substrates using microwave plasma treatments. Surf Coat Technol. 2017 Sep 25;325:299–307.

117. Zhang Y, Li J, Che S, Yang Z, Tian Y. Chemical leveling mechanism and oxide film properties of additively manufactured Ti–6Al–4V alloy. J Mater Sci. 2019 Nov 1;54(21):13753–66.

118. Adar F. Introduction to Interpretation of Raman Spectra Using Database Searching and Functional Group Detection and Identification. 2016 Jul 1;31:16–23.

119. Grace-Martin K. When Main Effects are Not Significant, But the Interaction Is [Internet]. The Analysis Factor. 2015 [cited 2024 Oct 29]. Available from: https://www.theanalysisfactor.com/interactions-main-effects-not-significant/

120. Sim DS, Jeong MH, Park DS, Kim JH, Lim KS, Bae IH, et al. A novel polymer-free drug-eluting stent coated with everolimus using nitrogen-doped titanium dioxide film deposition in a porcine coronary restenosis model. Int J Cardiol. 2016 Nov 1;222:436–40.

121. Kamberi M, Nayak S, Myo-Min K, Carter TP, Hancock L, Feder D. A novel accelerated in vitro release method for biodegradable coating of drug eluting stents: Insight to the drug release mechanisms. Eur J Pharm Sci. 2009 Jun 28;37(3):217–22.

122. Sharmila D, Rao AL, Kalyani L. Development and Validation of Stability-indicating High Performance Liquid Chromatographic Method for the Estimation of Everolimus in Tablets. Indian J Pharm Sci. 2015;77(5):599–604.

9 Supplementary information.

9.1 Supplementary tables

9.1.1 HPLC Method 1: Inter- day and intra- day precision results.

Table 22: HPLC Method 1-Inter-day precision (n=3) for method validation of the RP- HPLC used in study one, before issues arose with retention time.

Theo Conc. (µg /mL)	Average Peak Area (MAu)	Standard deviation	RSD (%)
1000.0	10696.52612	14.79	0.138
500.0	5088.72942	1.79	0.035
250.0	2571.66507	15.89	0.618
100.0	1095.987497	0.12	0.011
50.0	536.97211	0.51	0.096
25.0	273.3515833	0.17	0.061
10.0	113.1744467	1.70	1.498
5.0	51.66536	0.27	0.528

Table 23: HPLC Method 1-Intra-day precision (n=3) for method validation of the RP- HPLC used in study one, before issues arose with retention time.

Theo Conc. (µg /ml)	Average Peak Area (mAu)	Standard deviation	RSD (%)
1000.0	10878.	216	1.98
500.0	5446	265	4.87
250.0	2618	49	1.88
100.0	1039	41	3.90
50.0	492	33	6.62
25.0	254	15	5.96
10.0	110	6	5.77
5.0	52	5	9.55

9.1.2 HPLC Method 2 results.

Table 24: RP-HPLC analysis of everolimus standards for the construction of a calibration curve

Standard (µg/ mL)	Peak area (mAU)			Average	Standard deviation
	1	2	3		
500	33684.00	33425.04	33237.78	33448.9	224
250	16844.04	16962.66	16927.70	16911.5	61
125	8536.01	8367.97	8425.24	8443.1	85
100	6835.90	6514.08	6559.59	6636.5	174
50	3143.57	3131.21	3116.50	3130.4	14
25	1705.31	1556.85	1681.60	1647.9	80
10	552.42	592.52	597.93	581.0	25
5	256.43	254.87	252.58	254.6	2

Table 25: Linear regression analysis, calculation of estimated concentrations, standard deviation, RSD and percent accuracy.

Theo Conc.	Run	Measured Conc.	Mean	STD	%RSD	Accuracy	Mean	STD
	1	235.1022				94.04		
250.00	2	237.6501	239.387	5.368	2.24	95.06	95.75	2.15
	3	245.4085				98.16		
	1	99.7686				99.77		
100.0	2	91.4111	94.575	4.5336	4.79	91.41	94.57	4.53
	3	92.5444				92.54		
	1	48.5016				97.00		
50.0	2	41.6295	44.361	3.6465	8.22	83.26	88.72	7.29
	3	42.9512				85.90		
	1	24.3251				97.30		
25.00	2	20.9338	22.559	1.700	7.54	83.74	90.24	6.80
	3	22.4179				89.67		
	1	9.6354				96.35		
10.0	2	8.5750	9.373	0.7046	7.52	85.75	93.73	7.05
	3	9.9091				99.09		
	1	3.9944				79.89		
5.00	2	3.5823	4.001	0.422	10.55	71.65	80.02	8.44
	3	4.4264				88.53		

9.1.3 Statistical analysis

Table 26: One-way ANOVA test carried out on AFM surface roughness of blank titanium discs, everolimus coated discs without plasma (0V) and with plasma (90V) with a significance level of 0.05- study one.

Source of variation	***SS***	***df***	***MS***	***F***	***P- value***	***F crit***
Between groups	520.186	2	260.093	2.986	0.126	5.143

Table 27: Two- way- ANOVA analysis of WCA results to assess the effect of deposition type, and use of BHT on WCA results of everolimus coated discs- study one.

ANOVA						
Source of Variation	*SS*	*df*	*MS*	*F*	*P-value*	*F crit*
Sample	264.70088	1	264.7009	7.923877	0.012452	4.493998
Columns	203.522	1	203.522	6.092474	0.025231	4.493998
Interaction	53.00768	1	53.00768	1.586796	0.22585	4.493998
Within	534.48764	16	33.40548			
Total	1055.7182	19				

Table 28: Two- way ANOVA carried out to analyse the effect of deposition type and use of BHT on average everolimus concentration found (µg/ disc)- study one.

ANOVA						
Source of Variation	*SS*	*df*	*MS*	*F*	*P-value*	*F crit*
Sample	28.37556	1	28.37556	2.821648	0.118826	4.747225
Columns	13.01941	2	6.509706	0.647321	0.540789	3.885294
Interaction	92.59214	2	46.29607	4.603653	0.032823	3.885294
Within	120.6765	12	10.05638			
Total	254.6636	17				

Table 29: Tukey statistical test; Everolimus concentration recovered from samples coated by wet deposition (0 V), plasma deposition (90 V) and with various concentrations of BHT (0%, 5% 10%). Tukey critical value = 4.75 (k=6, df=12).

Group 1	Group 2	q	Significance
0 V, 0% BHT	0 V, 5% BHT	2.42	Not SSD
0 V, 0% BHT	0 V, 10% BHT	1.46	Not SSD
0 V, 5% BHT	0 V , 10% BHT	3.87	Not SSD
90 V, 0% BHT	90 V, 5% BHT	2.08	Not SSD
90 V, 0% BHT	90V, 10% BHT	0.27	Not SSD
90 V, 5% BHT	90 V, 10% BHT	1.81	Not SSD
0% BHT 0 V	0% BHT 90 V	0.25	Not SSD
5% BHT 0 V	5% BHT 90 V	4.74	Not SSD
10% BHT 0 V	10% BHT 90 V	0.94	Not SSD

Table 30: Two- way ANOVA carried out to analyse the effect of deposition type and use of BHT on average everolimus concentration found (µg/ disc)- study two.

ANOVA						
Source of Variation	*SS*	*df*	*MS*	*F*	*P-value*	*F crit*
Sample	16.05556	1	16.05556	0.348193	0.566084	4.747225
Columns	739.1111	2	369.5556	8.014458	0.006158	3.885294
Interaction	1253.778	2	626.8889	13.59518	0.000824	3.885294
Within	553.3333	12	46.11111			
Total	2562.278	17				

Table 31: One- way- ANOVA carried out to analyse the effect of degradation on the average percent tautomer peak (%) of an everolimus standard (500 µg/ mL)- study two.

ANOVA						
Source of Variation	*SS*	*df*	*MS*	*F*	*P-value*	*F crit*
Between Groups	14.72666667	1	14.72667	114.7532	0.00043	7.708647
Within Groups	0.513333333	4	0.128333			
Total	15.24	5				

Table 32: Two- way ANOVA carried out to analyse the effect of deposition type and use of BHT on average percent tautomer peak of everolimus samples (%)- study two.

ANOVA						
Source of Variation	*SS*	*df*	*MS*	*F*	*P-value*	*F crit*
Sample	1.933889	1	1.933889	5.551834	0.036299	4.747225
Columns	0.443333	2	0.221667	0.636364	0.546168	3.885294
Interaction	4.467778	2	2.233889	6.413078	0.012754	3.885294
Within	4.18	12	0.348333			
Total	11.025	17				

Table 33: Tukey statistical test: Everolimus mass (µg/ disc) recovered from samples coated by wet deposition (0 V), plasma deposition (90 V) and with various concentrations of BHT (0%, 5% 10%). Tukey critical value = 4.75 (k=6, df=12), Table 29.

Group 1	**Group 2**	**q**	**Significance**
0 V, 0% BHT	0 V, 5% BHT	7.10	SSD
0 V, 0% BHT	0 V, 10% BHT	0.48	Not SSD
0 V, 5% BHT	0 V , 10% BHT	7.56	SSD
90 V, 0% BHT	90 V, 5% BHT	2.71	Not SSD
90 V, 0% BHT	90V, 10% BHT	2.92	Not SSD
90 V, 5% BHT	90 V, 10% BHT	0.21	Not SSD
0% BHT 0 V	0% BHT 90 V	4.54	Not SSD
5% BHT 0 V	5% BHT 90 V	5.27	SSD
10% BHT 0 V	10% BHT 90 V	2.10	Not SSD

Table 34: One-way- ANOVA test carried out on the everolimus standard (1 mg/ mL) and degraded everolimus standard (1 mg/ mL) analysing average peak tautomer- study two.

ANOVA						
Source of Variation	*SS*	*df*	*MS*	*F*	*P-value*	*F crit*
Between Groups	520.186	2	260.0929861	2.985862	0.125888	5.143253
Within Groups	522.6491	6	87.10817811			
Total	1042.835	8				

Table 35: Tukey statistical test; Everolimus tautomer peak detected from samples coated by wet deposition (0 V), plasma deposition (90 V) and with various concentrations of BHT (0%, 5% 10%). Tukey critical value = 4.75 (k=6, df=12).

Group 1	**Group 2**	**q**	**Significance**
0 V, 0% BHT	0 V, 5% BHT	2.64	Not SSD
0 V, 0% BHT	0 V, 10% BHT	1.47	Not SSD
0 V, 5% BHT	0 V , 10% BHT	1.17	Not SSD
90 V, 0% BHT	90 V, 5% BHT	4.11	Not SSD
90 V, 0% BHT	90V, 10% BHT	0.29	Not SSD
90 V, 5% BHT	90 V, 10% BHT	3.81	Not SSD
0% BHT 0 V	0% BHT 90 V	4.69	Not SSD
5% BHT 0 V	5% BHT 90 V	2.05	Not SSD
10% BHT 0 V	10% BHT 90 V	2.93	Not SSD

9.2 Extended data and results

9.2.1 Quantum cascade laser analysis (QCL)

The QCL analysis spectra is shown in Figure 47, for both the wet deposited everolimus and plasma deposited everolimus, which indicates that both coatings are similar. This analysis shows no obvious changes between the drug coatings with and without the use of plasma. The most dominant peak demonstrated by both the wet and plasma deposited everolimus is indicated between 1590 cm^{-1} to 1650 cm^{-1}. Since QCL is IR absorption similar to FTIR, peaks within this range are indicative of C=C stretching (111).

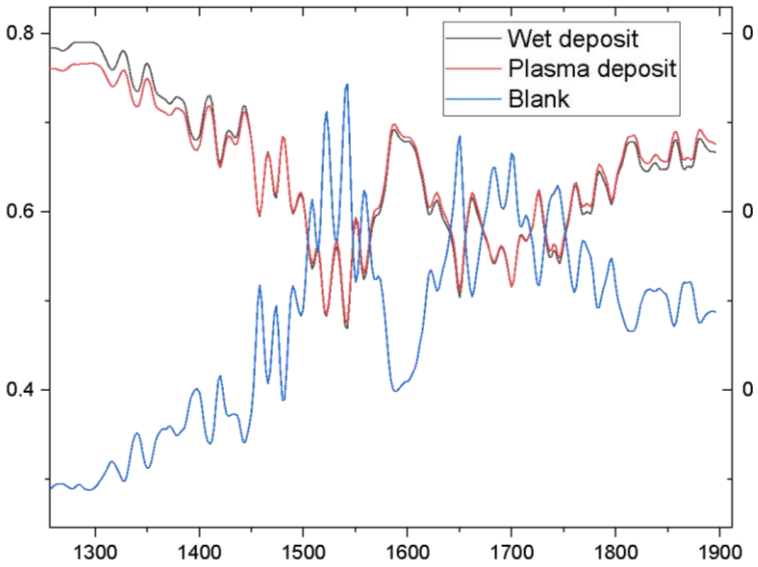


Figure 47: QCL Spectral response of everolimus wet deposited (0 V) and Everolimus plasma deposited (90 V).

Figure 48 shows the QCL images of everolimus coatings deposited on titanium discs by both the plasma (90 V) and the wet chemical process (0 V). The red colour represents the background from the disc, while the yellow spots are indicative of the everolimus drug coating. From the comparison, it is evident there is no huge variation or changes between samples when plasma was introduced. This is summarised previously in the spectral response in Figure 47.

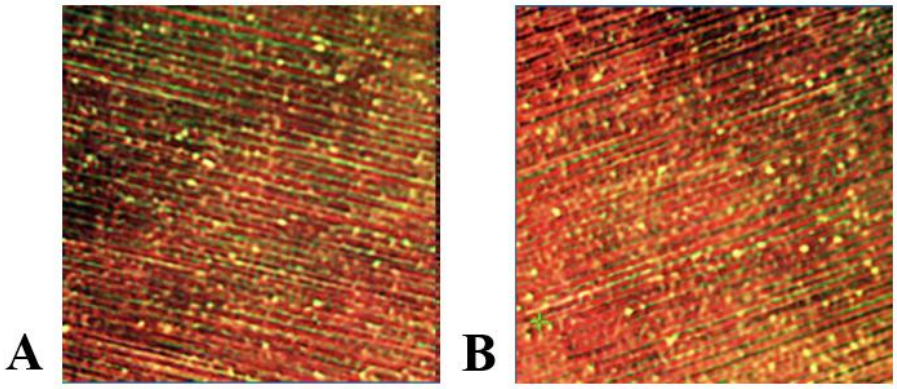


Figure 48: QCL image of everolimus deposited by (A) plasma 90 V and (B) wet deposition 0 V.

9.2.2 HPLC Method 2- Representative chromatograms for everolimus standards- study two.

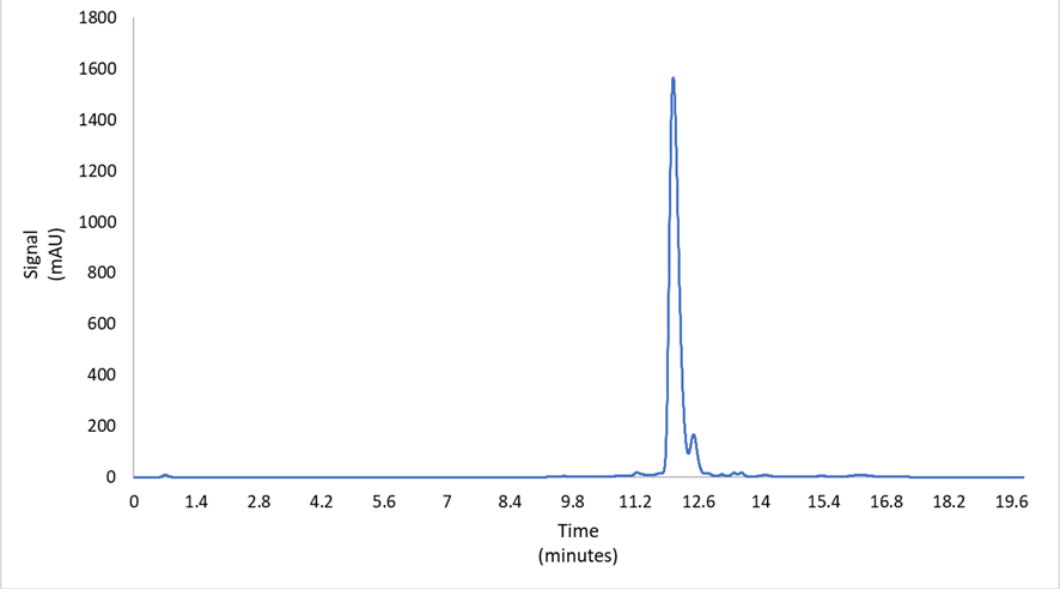


Figure 49: Representative chromatogram for the 500 µg/ mL everolimus standard run at the end of sequence to confirm retention time had not shifted, and also for comparison to 'degraded' everolimus.

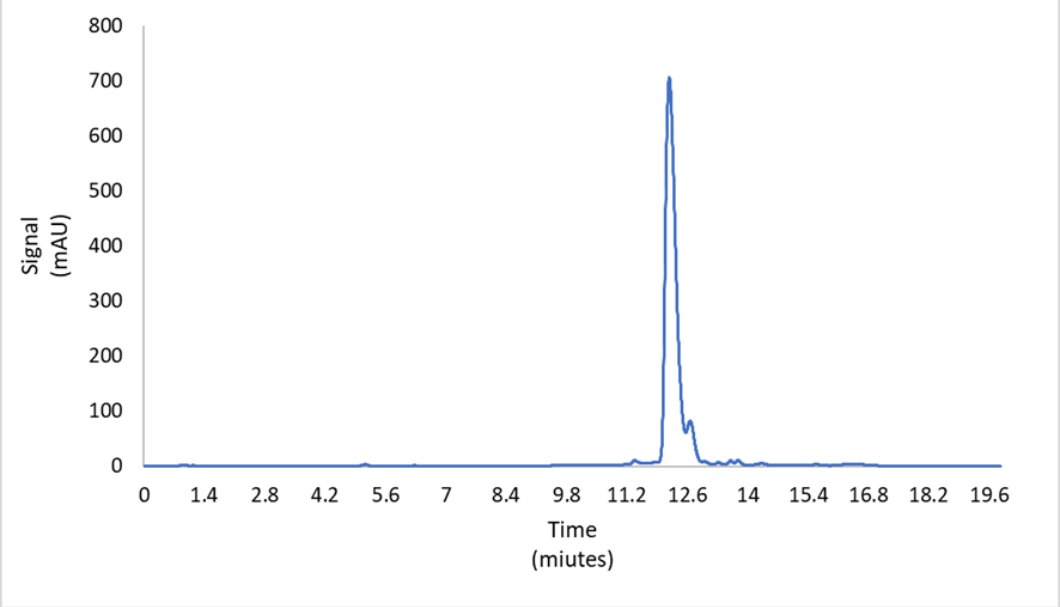


Figure 50: Representative chromatogram for the 250 µg/ mL everolimus standard run at the end of sequence to confirm retention time had not shifted.

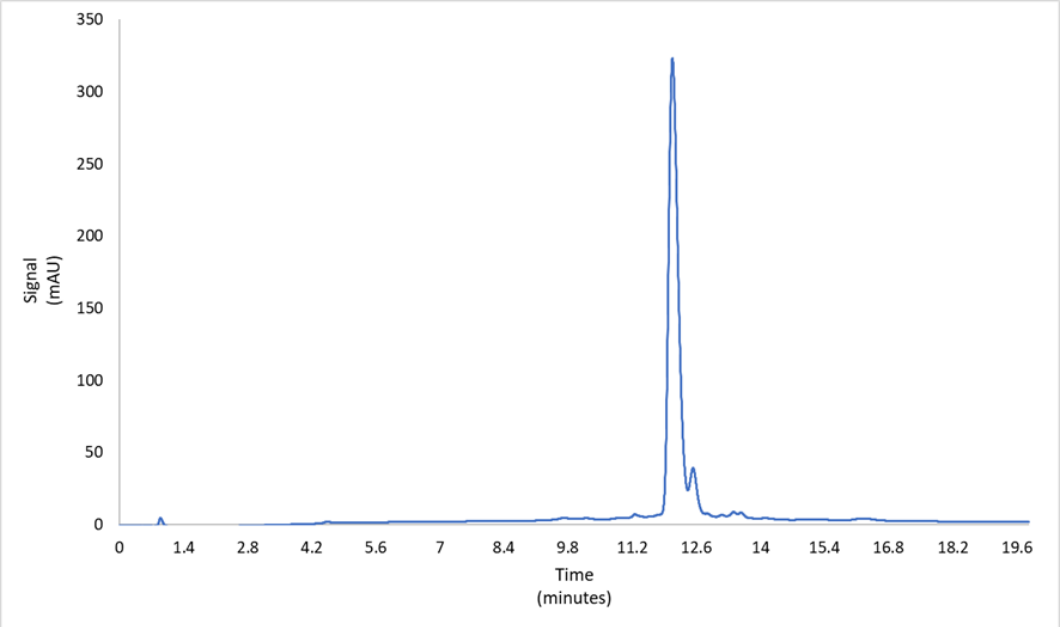


Figure 51: Representative chromatogram for the 100 µg/ mL everolimus standard run at the end of sequence to confirm retention time had not shifted.

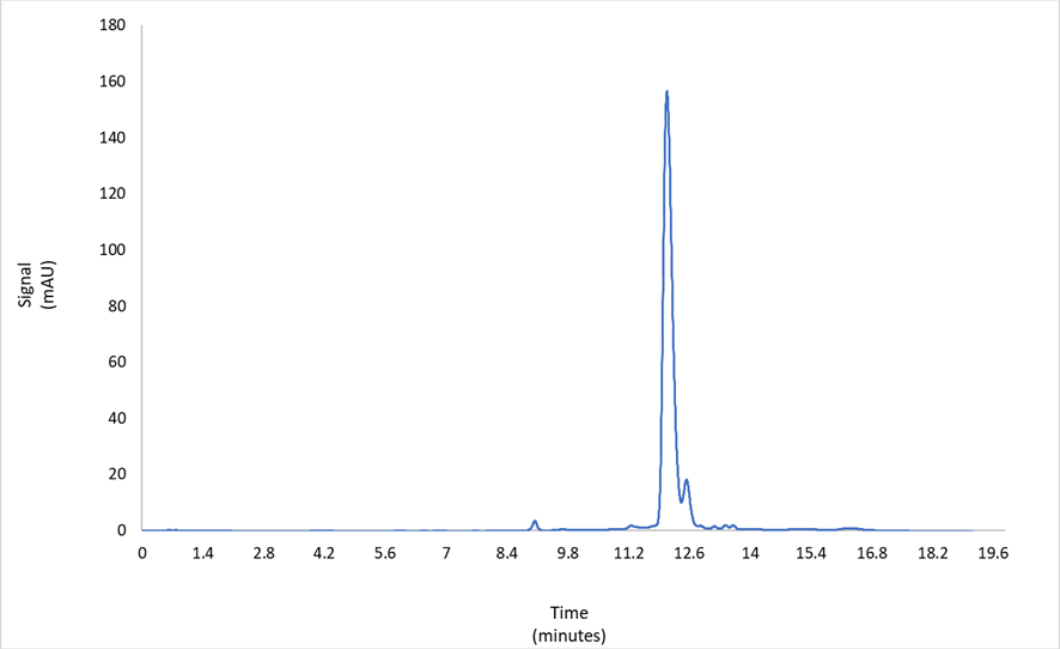


Figure 52: Representative chromatogram for the 50 µg/ mL everolimus standard run at the end of sequence to confirm retention time had not shifted.

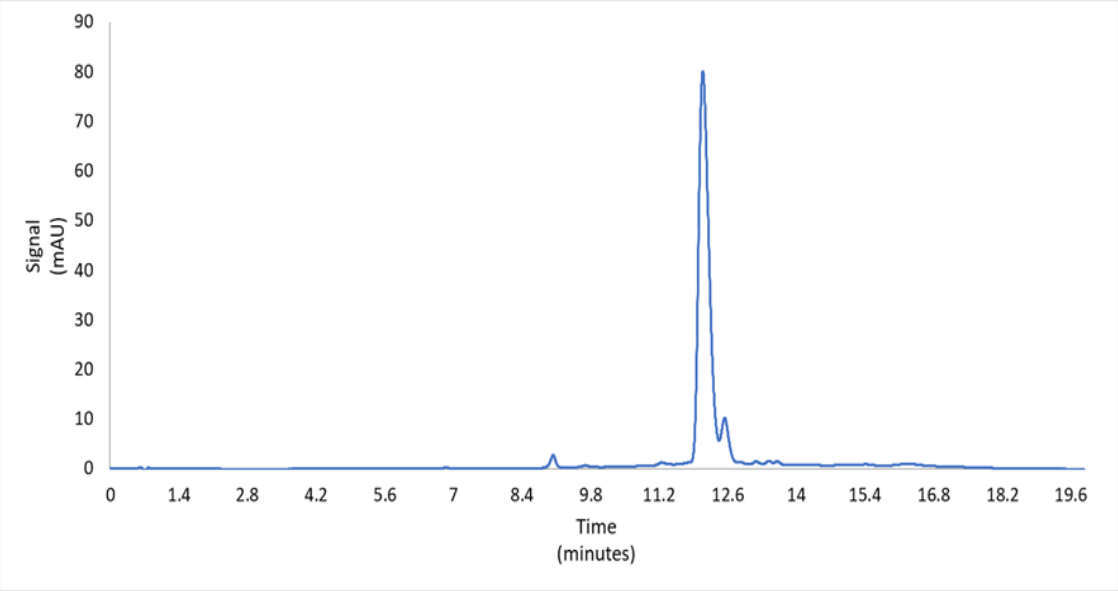


Figure 53: Representative chromatogram for the 25 µg/ mL everolimus standard run at the end of sequence to confirm retention time had not shifted.

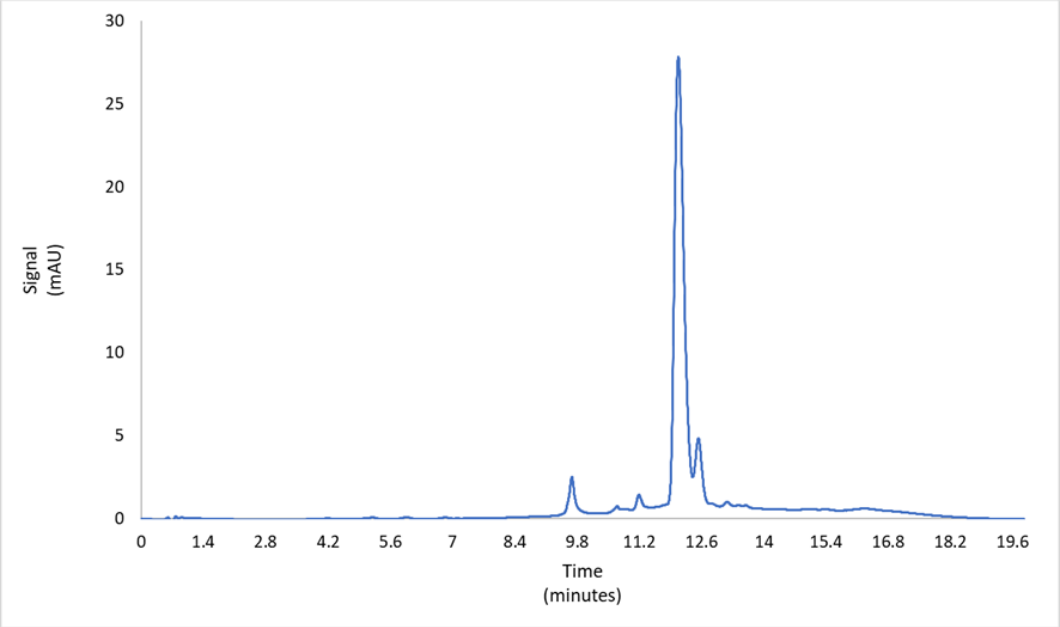


Figure 54: Representative chromatogram for the 10 µg/ mL everolimus standard run at the end of sequence to confirm retention time had not shifted.

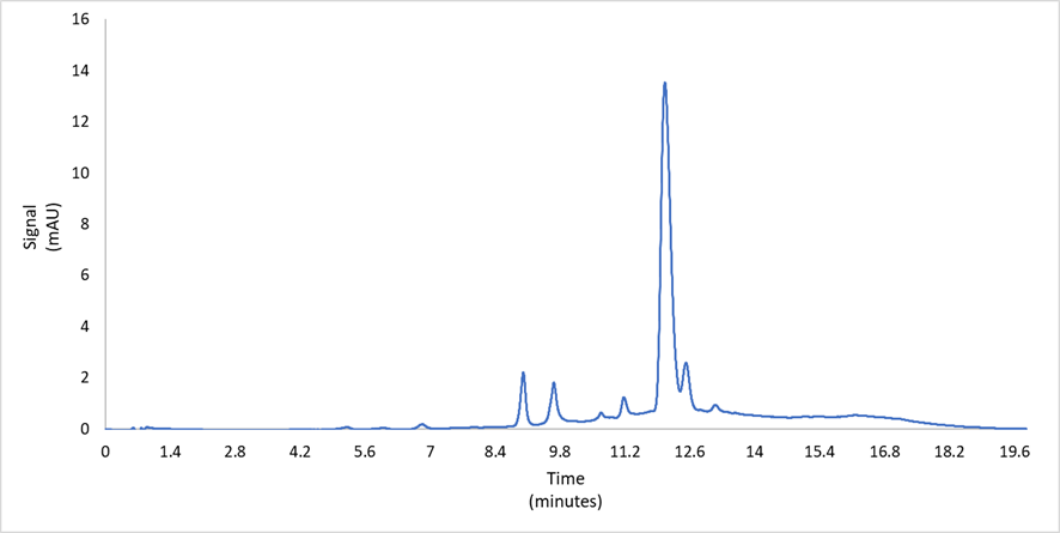


Figure 55: Representative chromatogram for the 5 µg/ mL everolimus standard run at the end of sequence to confirm retention time had not shifted.

9.2.3 HPLC Method 2- Representative chromatograms for everolimus coated samples- study two.

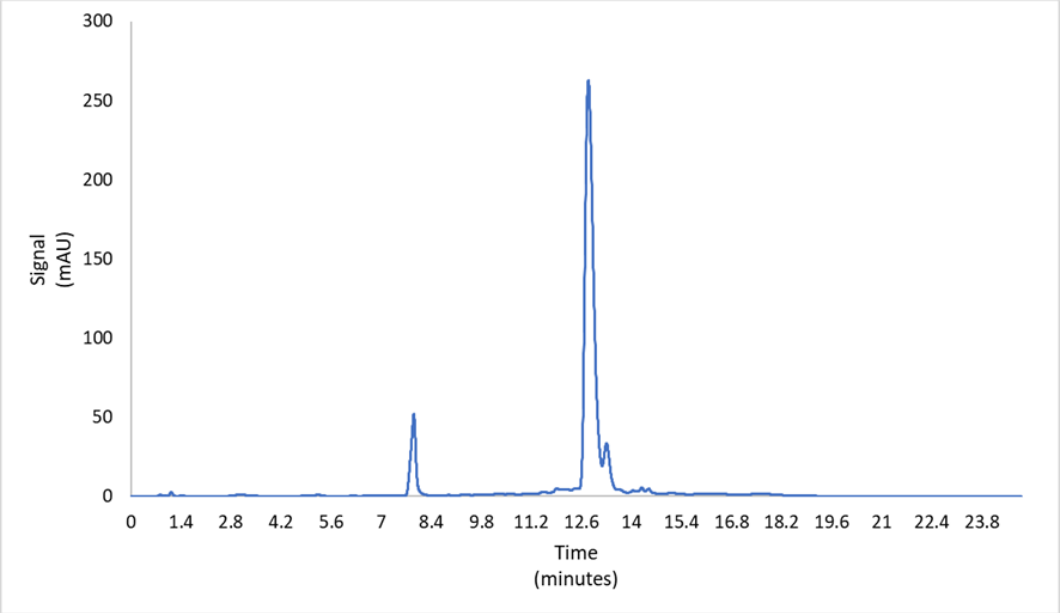


Figure 56: Representative chromatogram for everolimus 0V coated sample, eluted after 2 hr in acetonitrile. Note, peak at 7 minutes was determined to be contamination due to polystyrene and acetonitrile interaction.

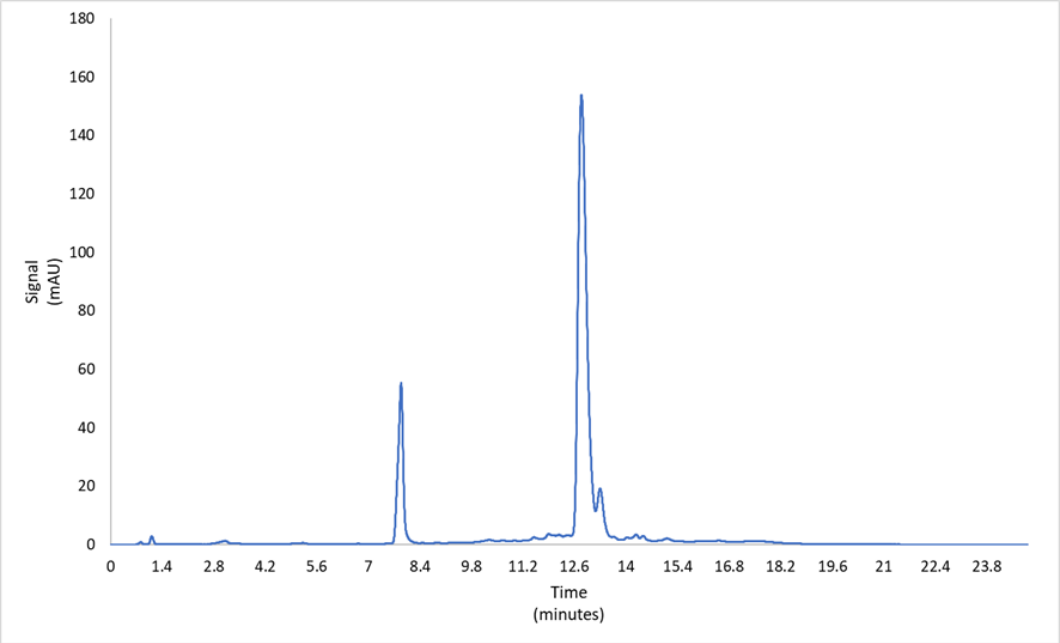


Figure 57: Representative chromatogram for everolimus 90 V coated sample, eluted after 2 hr in acetonitrile. Note, peak at 7 minutes was determined to be contamination due to polystyrene and acetonitrile interaction.

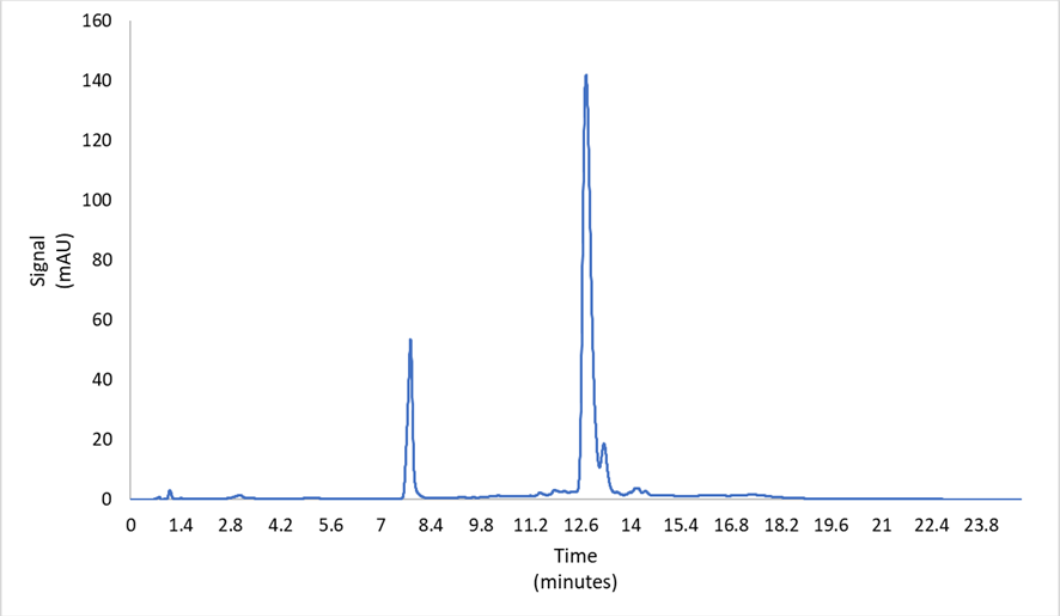


Figure 58: Representative chromatogram for everolimus 0 V + 5% BHT coated sample, eluted after 2 hr in acetonitrile. Note, peak at 7 minutes was determined to be contamination due to polystyrene and acetonitrile interaction.

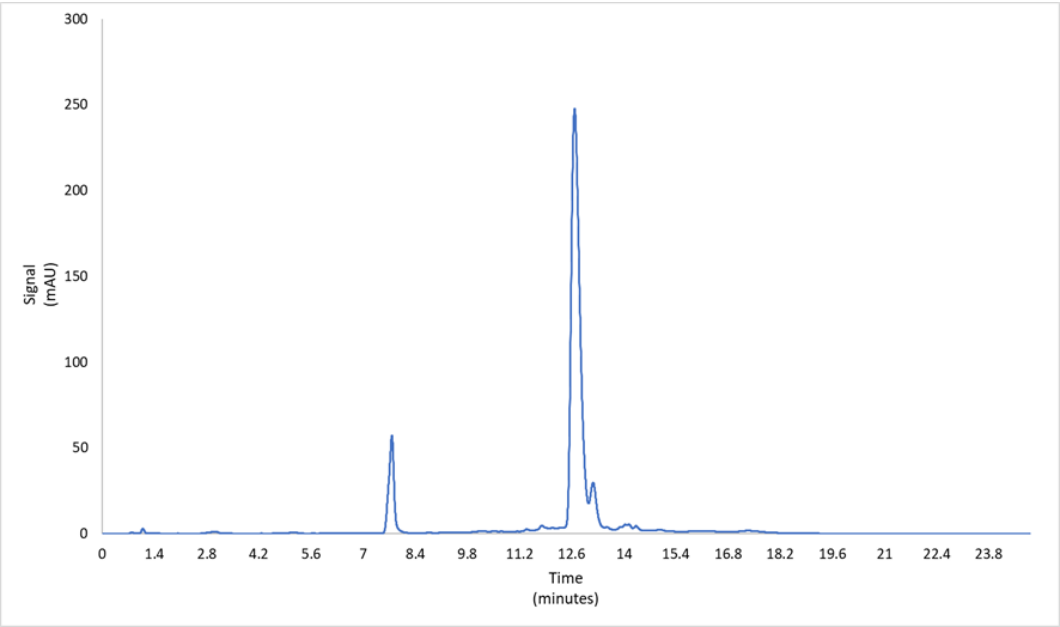


Figure 59: Representative chromatogram for everolimus 90 V + 5% BHT coated sample, eluted after 2 hr in acetonitrile. Note, peak at 7 minutes was determined to be contamination due to polystyrene and acetonitrile interaction.

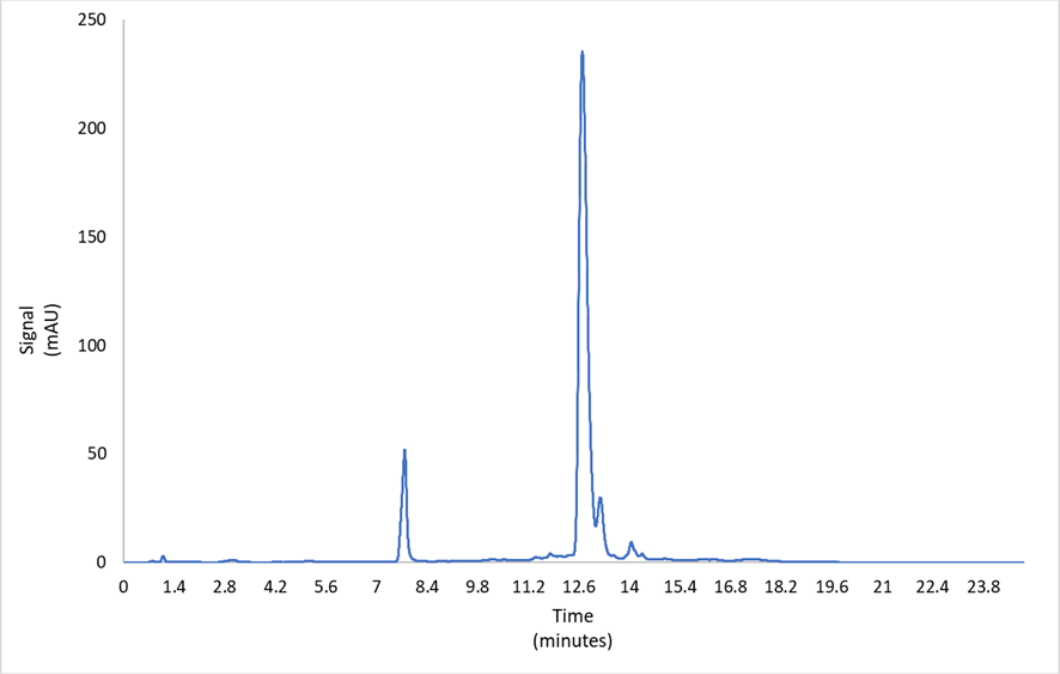


Figure 60: Representative chromatogram for everolimus 0 V + 10% BHT coated sample, eluted after 2 hr in acetonitrile. Note, peak at 7 minutes was determined to be contamination due to polystyrene and acetonitrile interaction.

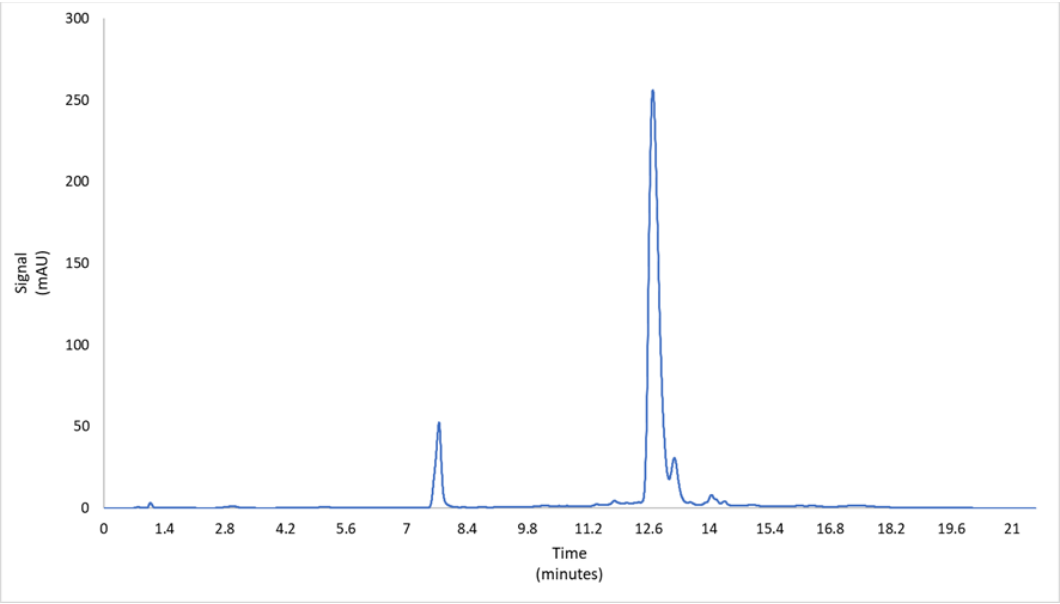


Figure 61: Representative chromatogram for everolimus 90 V + 10% BHT coated sample, eluted after 2 hr in acetonitrile. Note, peak at 7 minutes was determined to be contamination due to polystyrene and acetonitrile interaction.

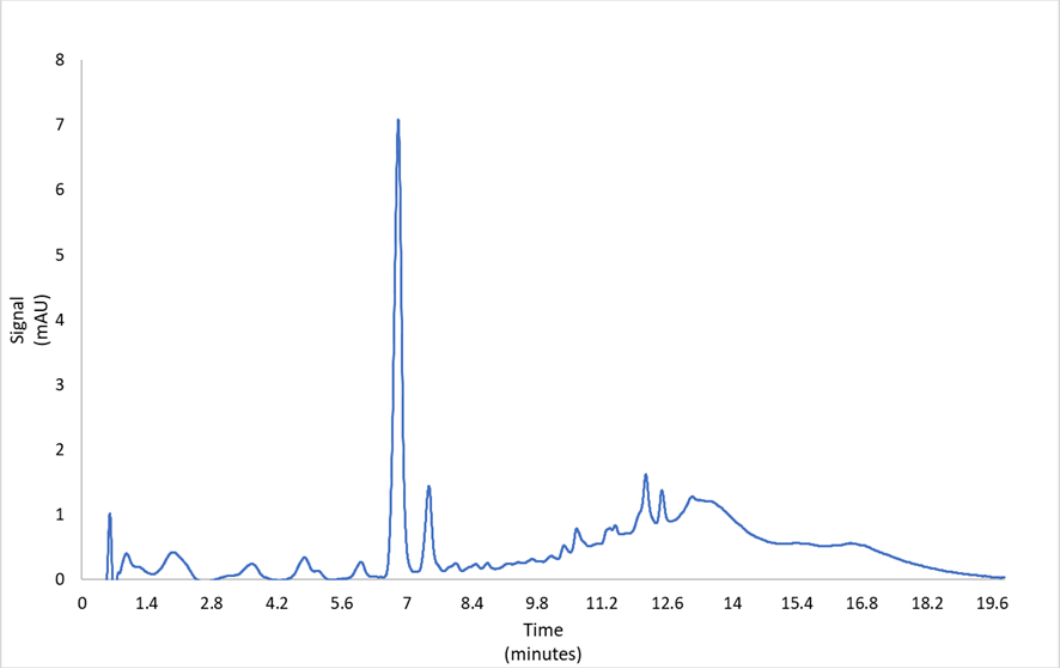


Figure 62: Representative chromatogram for acetonitrile left in a 6- -well plate. Note, peak at 7 minutes which was also observed in all coated samples which were eluted at 2 hours in a 6-well plate.

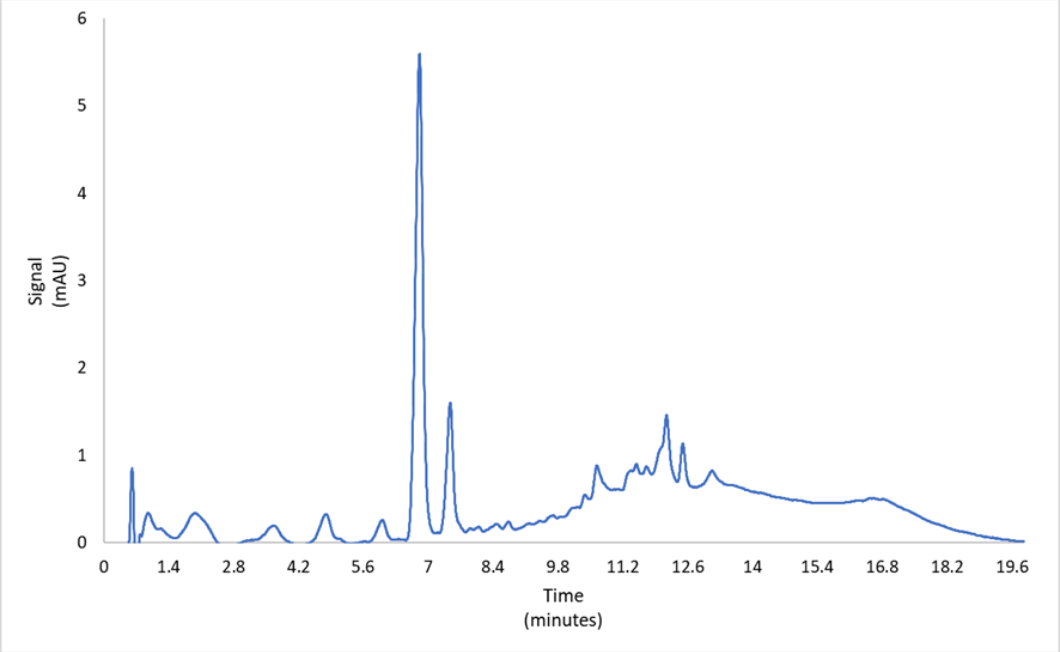


Figure 63: Representative chromatogram for acetonitrile left in a 6-well plate with a blank/ uncoated titanium disc. Note, peak at 7 minutes which was also observed in all coated samples which were eluted at 2 hours in a 6-well plate. It was confirmed that all coated samples eluted at 2 hours in 6- well plates had contamination form the interaction between the polystyrene plate and acetonitrile.

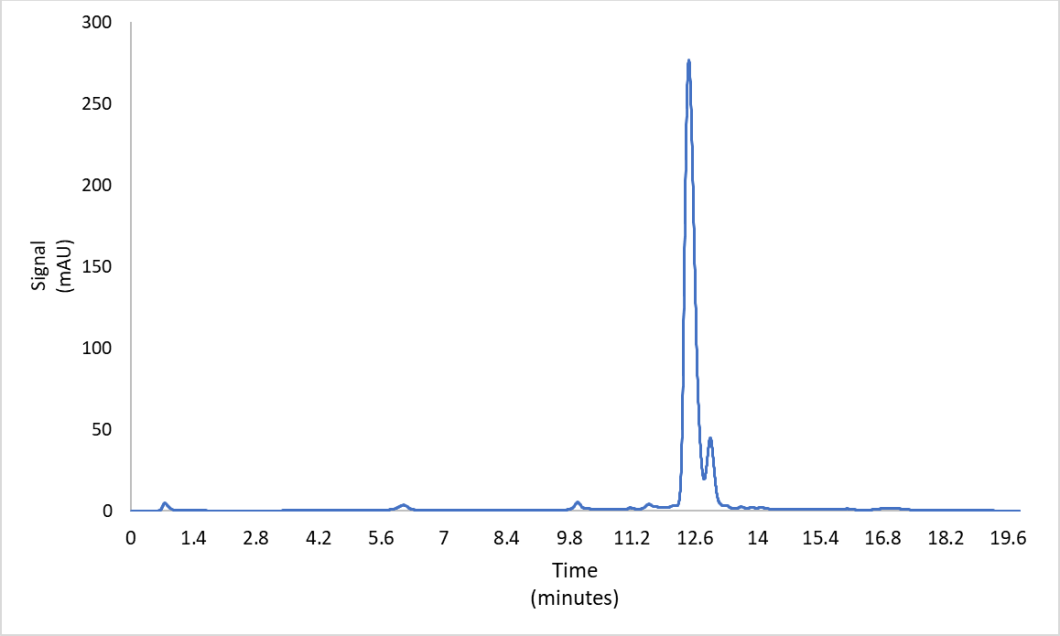


Figure 64: Representative chromatogram for everolimus coated disc, deposited with no plasma (0V).

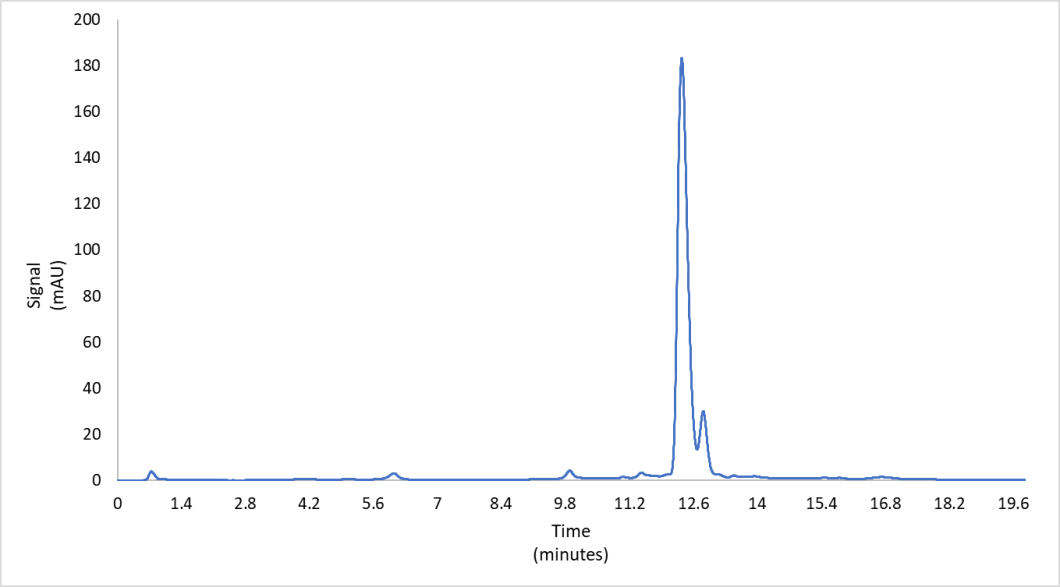


Figure 65: Representative chromatogram for everolimus coated disc, deposited with no plasma (90V).

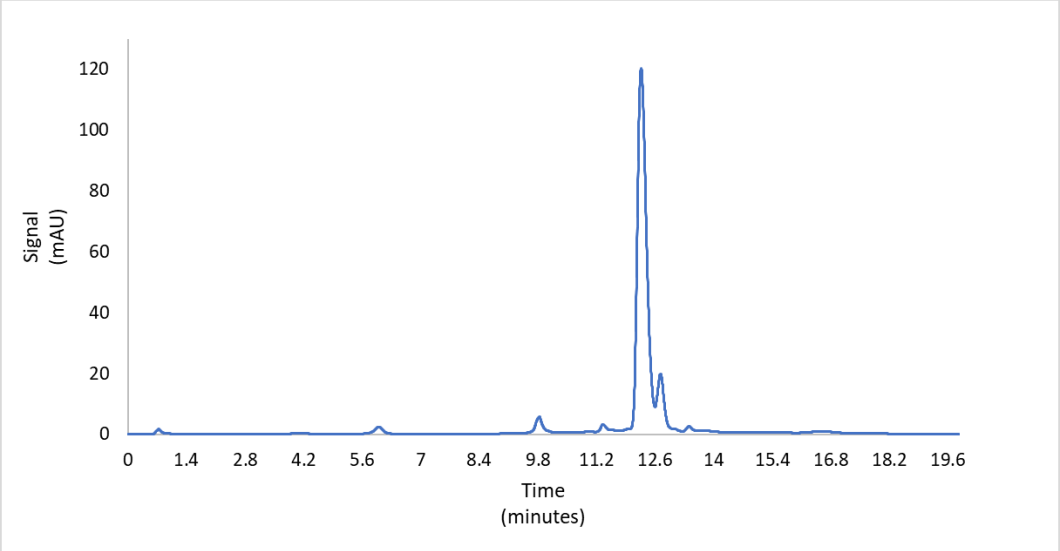


Figure 66: Representative chromatogram for everolimus coated disc with 5% BHT present, deposited with no plasma (0V).

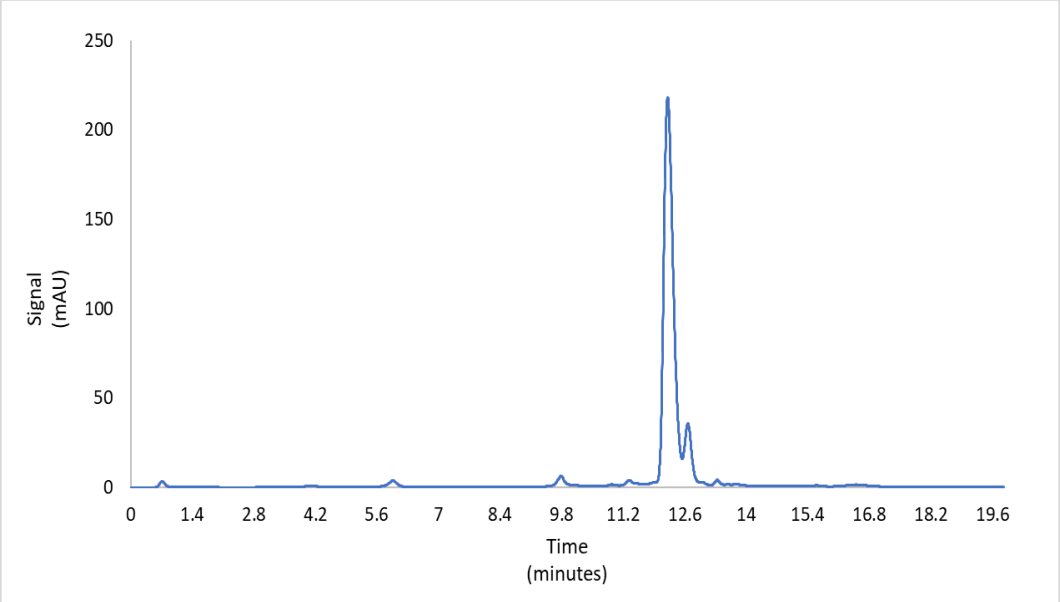


Figure 67: Representative chromatogram for everolimus coated disc with 5% BHT present, deposited with no plasma (90V).

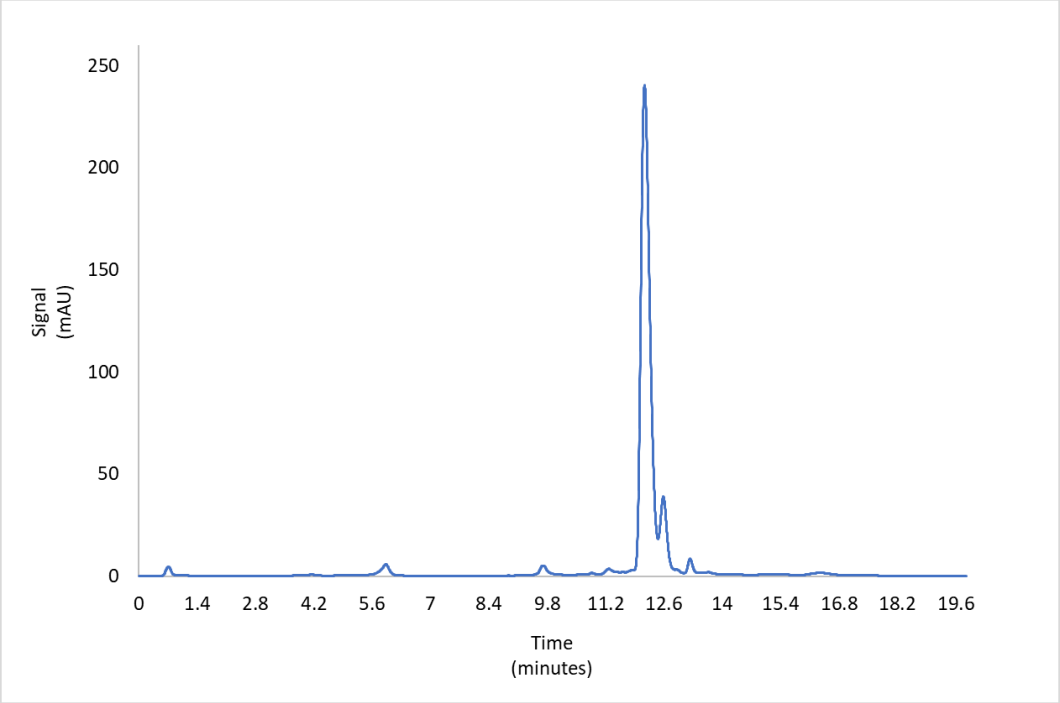


Figure 68: Representative chromatogram for everolimus coated disc with 10% BHT present, deposited with no plasma (0V).

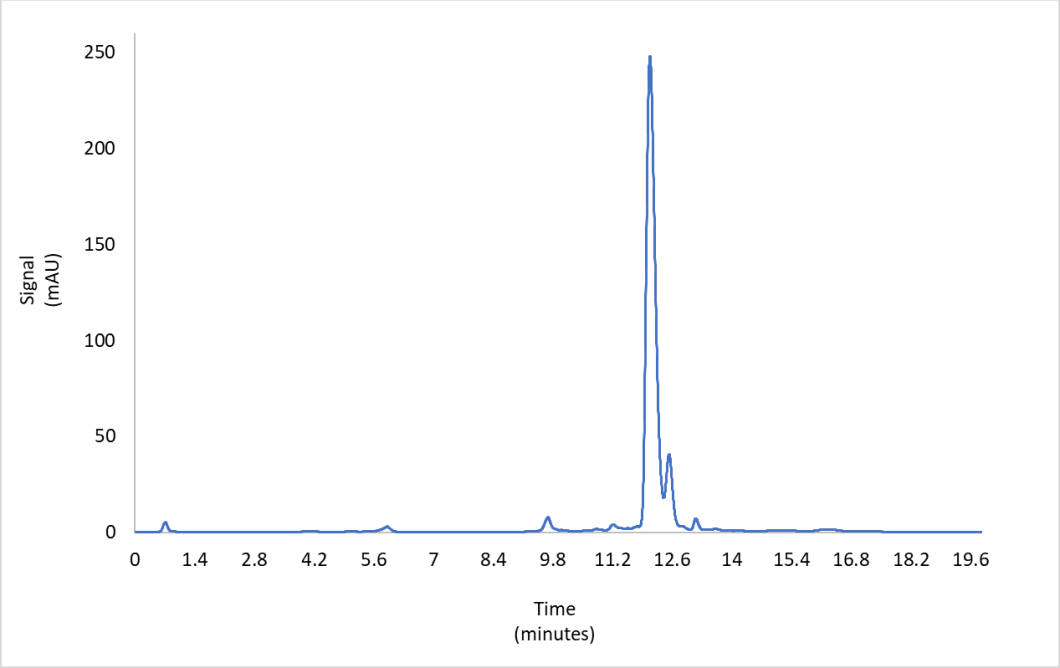


Figure 69: Representative chromatogram for everolimus coated disc with 10% BHT present, deposited with no plasma (90V).